UNIVERSITÁ DEGLI STUDI DI MILANO
Ph.D. IN ORAL SCIENCES
XXXI° CYCLE

DEPARTMENT OF BIOMEDICAL, SURGICAL AND DENTAL SCIENCES

PH.D. DISSERTATION

DEVELOPMENT OF MOUSE MODELS OF ORAL SQUAMOUS CELL CARCINOMA (OSCC) METASTASIS FOR THE EVALUATION OF EMERGING ANTI-METASTATIC NANOMEDICINE DRUGS

MED/28

Ph.D. Candidate:
Sabrina Marcazzan
Matricola R11206

:
Prof. Giovanni Lodi
Co-tutor:
Dr. Mauro Ferrari

Ph.D. Coordinator:
Prof. Massimo Del Fabbro

Academic Year 2017-2018

Contents

Chapter 1

Introduction

1.1 Oral Squamous Cell Carcinoma

1.1.1 Epidemiology, incidence, and risk factors

Oral Squamous Cell Carcinoma (OSCC) is included in the large group of Head and Neck Squamous Cell Carcinoma (HNSCC), which is the sixth most frequent type of cancer worldwide[1]. In the oral cavity, SCC is diagnosed in 95% of cases and it is 3-4% of all human cancers[2, 3]. Indeed, more than 300'000 new cases of lip/oral cavity SCC (age-standardized to the world population or ASR[W]: 4.0 x 100'000) were reported in 2012 with an estimated mortality-ASR[W] of 2.7 per 100'000 worldwide[4].

In the US and in Europe, the most common tumor locations in the oral cavity are the tongue and the floor of the mouth, while other locations such as the buccal mucosa, gingiva, and hard palate are reported less frequently[4]. In the past decades, a higher incidence of oral cavity SCC was reported in men than in women, due to the greater exposure to the main risk factors. However, this trend has declined from 5:1 in the 60s to less than 2:1 in 2002[3].

Tobacco and alcohol consumption are the most known major risk factors for OSCC[3, 4]. The carcinogenic effect of tobacco is dose-dependent and studies conducted in Europe and America have revealed a synergy between tobacco and a heavy consumption of alcohol[4, 5]. In the Asian countries, tobacco is commonly mixed with the betel quid, formed by slaked lime, betel leaf, and areca nut, which is also a known carcinogen. The interaction between tobacco, alcohol and betel quid chewing has proven to increase the risk for oral cavity SCC[4].

Recently, the human papillomavirus (HPV) has been recognized as an important emergent risk factor for HNSCC, particularly for oropharyngeal

SCC. In the oral cavity SCC, a contribution of HPV is estimated only in 7-16% of cases, compared to 40% -60% of oropharyngeal SCC cases reported worldwide[3, 4]. In addition, an interaction between HPV, tobacco, and alcohol is currently under investigation[4]. Other factors that may contribute to the emerging of oral cavity and oropharyngeal SCC include a low socio-economical status, the oral microbiome, dietary factors (e.g. vegetables may have a protective effect), HIV infection or organ transplantation due to immunosuppression, certain heritable conditions, and exposure to heavy metals or solvents[3, 4, 5].

1.1.2 Clinical stages and current therapeutic approaches

Oral cancerogenesis is a complex multifactorial process. In the oral cavity, common potentially malignant lesions include leukoplakia and erythroplakia. Leukoplakia is defined as "a white patch or plaque that cannot be characterized clinically or pathologically as any other disease" and its malignant potential is well known [4]. In addition, an uncommon variant of leukoplakia (proliferative verrucous leukoplakia/PVL) has been reported, especially in patients which do not present the common risk factors for oral cavity SCC. PVL may progress to oral cavity SCC or a verrucous carcinoma, a certain well-differentiated subtype of oral cavity SCC. Other risk factors for verrucous carcinoma include tobacco chewing and dry snuff[4]. Erythroplakia is defined as "a fiery red patch that cannot be characterized clinically or pathologically as any other definable disease"[4]. In contrast to leukoplakia, histological analysis of erythroplakias may show high-grade dysplasia, carcinoma *in situ*, or invasive SCC[4].

Table 1.1 shows the current therapies adopted for each stage of oral cavity SCC (TNM Clinical Classification or **c**TNM) . Despite efforts in improving the therapeutic approach, the prognosis of patients with oral cavity SCC remains poor, with a 5-year survival rate of around 50% worldwide. In the US, the 5-year survival rate of OSCC is 63%. In addition, death rates did not improve significantly between 2002 and 2012 [4, 6].

Traditionally, early-stage primary OSCC (I-II) has been treated with a radical surgery, whose complete response (CR) has been reported in 60%-80% of cases. CR is achieved when the histological examination reveals negative surgical margins (surgical margin free of tumor) and two different examinations separated by an interval > 4 weeks do not show evidence of tumor [7, 8]. A large study on 200 patients with oral cavity or oropharyngeal SCC reported an overall survival (OS) of 60% in the patients with negative margins at 5 years, while 16% died free of SCC[7]. In contrast, patients with close (tumor within 5 mm of margins) or involved margins (evidence of tumor at the margins) had an OS of 36% and 11% respectively[7]. This

Table 1.1: Standard treatments for oral cavity SCC[9, 113, 114]

Stage	**cTNM Classification**	**Treatment**
I II	T1 N0 M0 T2 N0 M0	radical surgery of the primary tumor with 1-2 cm margins ± ipsilateral/bilateral neck dissection/sentinel lymph node biopsy
III	T3 N0 M0 T1 N1 M0 T2 N1 M0 T3 N1 M0	surgical treatment + ipsilateral or bilateral neck dissection + chemoradiation or radiotherapy
IV a	T4a N0 M0 T4a N1 M0 T1 N2 M0 T2 N2 M0 T3 N2 M0 T4a N2 M0	surgery of the primary tumor + ipsilateral/bilateral neck dissection followed by concurrent chemoradiotherapy; chemoradiotherapy followed by neck dissection (if surgery was not an option);
IV b	T4b Any N M0 Any T N3 M0	immunotherapy for metastatic cancer if progression on or after chemotherapy
IV c	Any T Any N M1	chemoradiotherapy only (if surgery is not an option); immunotherapy for metastatic cancer if progression on or after chemotherapy

result was mainly attributed to the aggressive behavior of the disease, which also presents a higher risk for local (55% in patients with close margins) and regional recurrence (22% in patients with close margins). In such cases, the use of adjuvant radiotherapy has been effective in the local control of the disease, but not in improving the long-term survival[7].

Advanced-stage oral cavity SCC has been traditionally treated with surgery and radiotherapy, despite substantial adverse effects may occur [3, 2]. The addition of postoperative adjuvant chemotherapy to radiotherapy has improved the OS by up to 16%. For instance, concomitant chemoradiotherapy reported an improvement in OS of 10-22% compared with radiotherapy alone in patients with unresectable tumors[3]. In contrast, the use of induction chemotherapy has not shown benefits in improving the OS compared to locoregional treatment alone[3]. However, a reduction of locoregional recurrence may be achieved in the oral cavity SCC patients undergoing induction chemotherapy[3, 4]. Finally, the combination of radiotherapy and chemotherapy may result in a substantial increase in toxicity per patient treated[3].

Chemotherapy is the administration of anticancer or "cytotoxic" drugs, whose mechanism of action consists in altering the life cycle of cancer cells. Since different types of chemotherapeutic agents target different stages of the life cycle of tumor cells, it is common to combine two or three different drugs into a chemotherapeutic regimen. In OSCC, the common standard chemotherapeutic regimen for 20 years has been the combination of cisplatin and 5-fluorouracil (5-FU)[3]. Indeed, an alkylating agent such as cisplatin interferes with the cellular divisions, inducing a cross-linking of DNA and activating cell apoptosis. 5-FU is classified in the antimetabolites and inhibits the synthesis of thymidylate, an enzyme essential for DNA replication[10, 87].

Other widely used chemotherapeutic agents include carboplatin, oxaliplatin (alkylating agents), methotrexate (antimetabolite), docetaxel, and paclitaxel [3, 12, 13]. These last two agents are classified in the taxanes and inhibit the replication of the tumor cells by altering the microtubule function. They were added to chemotherapeutic regimens for OSCC treatment in 2007 and their combination with cisplatin and 5-FU demonstrated to be superior to cisplatin and 5-FU alone,[3, 14]. More in detail, a decrease in toxic deaths and an increase in OS (70.6 months vs 30.1 months) were achieved combining docetaxel with cisplatin and 5-FU compared with cisplatin and 5-FU alone[14].

The efficacy of chemotherapy in OSCC is currently reduced by the consistent adverse effects and multi-drug resistance (MDR). For instance, cisplatin may cause nephrotoxicity, neurotoxicity, gastrointestinal toxicity, hematological toxicity, and ototoxicity, while 5-FU has toxic effects on bone marrow-[10, 87]. Other adverse effects of chemotherapy may consist in anemia, tiredness, nausea/ vomiting, diarrhea or constipation, hair loss, mucositis, and susceptibility to infections. Adverse effects are the result of the non-specific

distribution of chemotherapeutic agents within the body, which target the normal cells in addition to the tumor ones[10, 15]. The type and the grade of collateral events depend on the type of agent, the dosage used, the duration of the treatment, and the patient [3, 10, 15].

Several mechanisms of MDR contribute to the collateral effects of chemotherapy, resulting in an exposure of healthy cells to high levels of expelled chemotherapeutic agent[13, 15]. The most known mechanism of MDR which occurs also in OSCC is the overexpression of multi-drug transporters [e.g. MDR1 or P-gp, ATP binding cassette (ABC)C1, ABCG2], which promote the efflux of drugs from the tumor cells. As a consequence, the intracellular concentration of the drug decreases along with the drug efficacy. Studies on cell lines resistant to cisplatin and 5-FU and in recurrent OSCC have reported an overexpression of ABCC1, P-gp, and ABCG2. In addition, P-gp positive OSCC cells may become resistant to the taxanes and its expression can be induced by chemotherapy (acquired resistance)[13]. In contrast, an overexpression of MRP1 has been found in OSCC cell lines treated with cisplatin, while the over expression of ABCG2 has been associated with cancer stem cell properties and a MDR to cisplatin and 5-FU[13].

Other mechanisms of MDR reported in OSCC include the dysfunction of apoptosis (e.g. up regulation of Bcl-2 and Bcl-xL), the enhancement of DNA repair, which is crucial for platinum-based chemotherapy, epithelial mesenchymal transition (EMT), the dysregulation of miRNAs, and autophagy. However, further investigation is necessary in order to elucidate the exact molecular mechanisms of MDR in OSCC[13].

Recently, molecular-targeted agents are also being developed to enhance the efficacy of the treatment for OSCC[6]. Indeed, these new agents have the capability to target molecular changes highly specific to OSCC, reducing the toxic effects on the normal cells. For instance, several monoclonal antibodies (mAb) against the epidermal growth factor receptor (EGFR) such as cetuximab, panitumumab, and nimotuzumab have been developed for OSCC[6, 14]. Indeed, EGFR is overexpressed in 80%-90% of HNSCC and its expression has been correlated with a poor outcome[2, 6].

Clinical studies using anti-EGFR mAb in combination with standard therapies have reported an increase in the OS and locoregional control of patients, most affected by oropharyngeal cancer, compared with standard treatments alone[6]. In addition, a retrospective study reported a CR rate of 33.3% in patients with locally advanced or recurrent/metastatic OSCC[2]. However, the administration of cetuximab has been associated with severe

collateral effects such as infusion reactions, skin toxicity, rash, neutropenia, and interstitial pneumonia in rare cases[2, 6].

Other targeted therapies like bevacizumab and vandetanib (anti-VEGF therapies), and immunotherapy have also been explored[6, 8, 13].

1.1.3 Causes of death in patients affected by HNSCC

Death caused by HNSCC has been reported in 29-64% of patients. Indeed, several studies have shown that patients affected by HNSCC may frequently die also from a cause other than HNSCC[16]. In these cases, the onset of secondary carcinomas is considered the leading cause of death (27%-54%)[16, 17]. In such cases, lung cancer and bronchus cancer are the most common type of second cancer reported with a 50% prevalence followed by esophageal (10%) and colorectal cancer (5%)[17, 18]. Cardiovascular disease also exerts a significant impact on the patient's survival: death from cardiovascular diseases is reported in 21-28%. Other frequent causes of death other than HNSCC include chronic obstructive pulmonary disease, pneumonia, and influenza[17].

Among the OSCC-related deaths, the most frequent causes of death are local recurrence and metastases[16, 19]. In a study, locoregional recurrence represented 80% of the OSCC-related deaths[16]. Recurrence occurred mainly in the sublingual sulcus, tongue, and the floor of the mouth. Interestingly, distant metastases (DMs) were present in almost 41% of the patients with locoregional recurrence, while DMs alone were attributed to the remaining 20% of the OSCC-related deaths. Interestingly, the locoregional control rate of the disease reported was around 80% in patients with stage T2-T4 resectable tumors without DMs (TNM classification 7th Edition) undergoing preoperative radiochemotherapy. After 5-6 weeks, radical locoregional surgery was performed in all patients, including lymph node resection according to N stage[16].

Another study reported an improvement of locoregional control in HNSCC patients treated with the combination of chemotherapy and radiation compared with radiation alone. However, the incidence of DMs was not significantly different between the two groups (21% chemotherapy plus radiation vs 25%radiation alone)[20]. In addition, more cases with DMs have recently been diagnosed, due to the improvement achieved by the multimodality treatment[21]. After the failure of platinum-containing chemotherapy, there are currently few therapeutic options for patients with DMs and the use of cetuximab is restricted by severe adverse effects that may often occur[2, 20].

Regional and distant metastases in OSCC

Regional metastases in lymph nodes are a common finding in patients with OSCC. Indeed 40% of OSCC may metastasize to the regional lymph nodes, especially advanced stages of the disease[22]. In presence of lymph node metastases, patients undergo a neck dissection, which is currently recommended also for the management of clinical lymph-node negative (cN0) tumors (see Table 1.1)[9] . Despite T1 and T2 tumors (TNM classification 7th Edition) have a low risk to develop lymph node metastases (10-30% respectively), it has been demonstrated that occult lymph node metastases may occur in T1 (6-25%) and T2 lesions (20-32%)[4, 22]. In order to detect the occult metastases, sentinel lymph node biopsy is also performed and may constitute an alternative to neck dissection in patients affected by T1 and T2 oral cavity SCC according to TNM classification 7th Edition[113]. In the oral cavity, the tongue is the most frequent site of OSCC which is prone to invade the regional lymph node, compared with the floor of the mouth[4, 23].

It is well known that the presence of lymph node metastases constitutes an important prognostic indicator for OSCC and correlates with a poor prognosis. Indeed, the 5-year survival rate of patients with lymph node metastases is only 25-40% compared with 90% of those without lymph node metastases. In the US, an increase of the 5-year survival rate was achieved between 2005 and 2015 (from around 50% to 60%) in patients with invasion of lymph node and\or surrounding tissues [24]. Size of the primary tumor, site, T stage, grade, depth of invasion, biological tumor markers, perineural invasion, and patient compliance are reported to affect the development of lymph node metastases. However, the mechanisms of metastasis are still poorly understood [22, 23, 25].

When single versus multiple lymph node metastases are detected outside the sentinel node area, the patients have also a higher risk of DMs (41-43%)[23]. In the case of DMs, the prognosis is poor and the control over them remains low. In the US, the 5-year survival rate of patients with DMs was around 30% in 2005 and increased by 35% in 2015. In addition, the incidence of DMs increased from 10% of cases diagnosed in 2005 to 18% in 2015[23, 24].

DMs are found more frequently in oropharyngeal SCC cases than in oral cavity SCC ones. Indeed, a recent study reported that 60% of DMs derived from the pharynx SCC, followed by the tongue one (50-53%)[26]. Another study also reported a metastasis rate of 6.6% and 4.1% from upper gingiva SCC and tongue SCC respectively[26, 27]. This finding was also confirmed by another study[27]. A larger study on 502 patients with oral cavity SCC

reported DMs in 54 patients (10.8%) from 1 month to 76 months after radical surgery[28]. More than half of the patients (29\54 53.7%) also presented locoregional recurrence and their prognosis was better than those without local recurrence. The lung was the most frequent site of DMs (44\54 81.5%), followed by the bone (25\54 46.3%), mediastinum (10\54 18.5%), and liver (9\54 16.6%). Less common locations were kidney (3\54), brain (2\54), spleen (2\54), and adrenal gland (2\54)[28]. Other studies confirmed the lung as the most frequent distant site of DMs in HNSCC patients[2, 26, 27]. Some studies reported also metastases in mediastinal, parapharyngeal lymph nodes, heart and, peritoneum[2, 21, 26].

The median OS of patients with DMs is 3-8 months[2, 21, 28]. In particular, the presence of lung and bone metastases is significantly associated with a poorer survival than patients without lung and bone metastases. In a study by Takahashi et al.[28], the histological grade and the presence of lymph node metastases were the most significant prognostic factors for the development of lung and bone metastases, respectively. The presence of bone metastases resulted in the lowest median OS (1.80-2.32 months), which is also shorter than those of patients with bone metastases from other cancers (e.g. breast and prostatic cancer)[21, 28]. For these reasons and for the increasing incidence of DMs, further studies are needed to investigate the basic mechanism of DMs in OSCC.

1.1.4 Animal models of OSCC metastasis

As reported in 1.1.3, it is necessary to fully understand the metastatic process of OSCC, especially the development of DMs. In OSCC research, animal models have contributed to the understanding of the molecular mechanism of lymph node metastases, elucidating the role of VEGF-C and VEGF-D in lymphangiogenesis. These factors have recently received clinical relevance[25].

However, reproducing metastases in animal models is difficult, due to the recapitulation of all steps of the metastatic dissemination: tumor proliferation, local invasion, intravasation, extravasation, colonization in the metastatic site, and proliferation[29]. In addition, the interaction of the cancer cells with the tumor microenvironment, tumor-associated immune cells, and stromal cells may contribute to metastases[29, 30]. The animal models used to resemble cancer metastases are Drosophila, zebrafish, mice, rats and less frequently rabbits, companion pets, and monkeys. The most used animal in cancer research has been the laboratory mouse, which has been genetically modified over the years[29].

In cancer research, the most used mouse models consist in the transplantation of murine cell lines into another mouse recipient of the same genetic

background (syngeneic model) or in transplantation of human cell lines into an immunodeficient mouse host (xenograft model). In such models, metastases have been obtained by the direct injection of the tumor cells into the systemic circulation (e.g. tumor cells injected into the tail vein to produce lung metastases) or by the injection of tumor cells in the site of origin of the primary tumor (orthotopic model). On one side, important drawbacks of the first type of metastatic model are the lack of the primary tumor and the reproduction only of the late phases of the metastatic dissemination. On the other side, the orthotopic model requires a long period for the development of metastases. Other mouse models frequently used to reproduce metastases of certain types of cancers (breast, prostate, and lung cancer) are the genetically engineered mice (GEM). These models have been developed by engineering mice to express (transgene) or not express (knockout) a gene of interest. This has allowed researchers to humanize mice through the replacement of murine genes with their human counterparts[29].

Several animal models of OSCC have been developed, but only a few of them have shown the development of metastases, especially DMs[31, 32]. A list of the mouse models of OSCC metastasis is reported in Table 1.2, with a specific focus on DMs. The xenograft models have the advantage of using human cell lines to establish the tumor, but the lack of a complete immune response does not permit to evaluate the role of immunity in the metastatic process and in the response to treatment. In such cases, a syngeneic immunocompetent model is more realistic and appropriate[31]. In the literature, both xenograft and syngeneic mouse models of OSCC metastasis have been published. In such studies (Table 1.2), lymph node metastases were present in almost all the cases and some of the models presented also a high prevalence of lung metastases[32, 50, 52].

Regarding the transplantation of OSCC cells, several authors have reported the inadequacy of the subcutaneous (SC) models of OSCC. Indeed, they do not mimic the metastatic process observed in human OSCC and the tumor microenvironment of their growth is different from the one of the orthotopic site. In addition, SC models do not resemble the response to treatments observed in clinical trials.[31, 32, 58]. In a study published by Myers et al.[48], a greater tumorigenicity of OSCC cells was reported in the orthotopic site than the SC one[48]. Indeed, most of the published mouse models of OSCC metastasis are orthotopic and some of them developed DMs also in other sites such as the liver and bone[32, 50].

There are also few articles which reported the tail vein injection of OSCC cells[56, 92]. Indeed, important limitations of this model are the lack of the primary tumor and the high number of cells required, whereas only few

tumor cells are involved in the metastatic dissemination of OSCC[31, 55]. In such models, the lung metastasis rate is higher than some orthotopic models, but they lack lymph node metastases compared with the orthotopic ones.

Table 1.2: Mouse models of OSCC metastasis

Model	**Cell derivation**	**Procedure**	**Metastasis rate**	**Ref.**
syngeneic	lung metastases from OP carcinoma HPV +	SC implantation of the cells	draining LN metastases (22-100%) lung metastases (77-100%)	[33, 34]
syngeneic	HNSCC	cell implantation in the LN and ear	lung metastases (100%)	[35]
xenograft	tongue SCC	SC implantation and PCR analysis	draining LN metastases (40-45%) lung metastases (20-30%)	[39]
xenograft	tongue SCC	SC cell implantation; SC tumor fragments then implanted in the cheek	LN metastases (42.8%)	[37, 38]
xenograft	recurrent OC carcinoma	implantation in the tongue	LN metastases (90%; NR in[32]) sublingual tissue, mandible, liver intestine, lung, kidney, and bone (100%)	[32, 36]
xenograft	cervical LN metastases from tongue SCC	implantation in the tongue	LN metastases (36-100%) lung metastases (NR)	[40, 41] [42, 43]
xenograft	tongue SCC and LN metastases	implantation in the tongue	LN metastases (30-90%) lung metastases (10% in [44])	[44, 45, 46]
xenograft	hypopharyngeal carcinoma	transcervical injection in the mouth floor	LN metastases (66%)	[47]
xenograft	patient-derived adenoid cystic carcinoma (ACC), SCC	implantation in the tongue	LN metastases (20-50%ACC;33-90%SCC) lung metastases (10%ACC)	[45]
xenograft	oral cavity SCC	SC and orthotopic injection	LN metastases (30% ortho) lung metastases (20% ortho)	[48]
xenograft	several HNSCC cells	injection in the tongue	LN metastases (10-88%)	[49]

Model	**Cell derivation**	**Procedure**	**Metastasis rate**	**Ref.**
xenograft	LN metastases from OSCC	injection in the tongue	LN metastases (100%) lung metastases (83%) liver metastases (67%)	[50]
xenograft	CD44+, CD44- cells from OSCC cells	injection in the tongue	LN metastases (30% CD44-; 80% CD44+) lung metastases (NR)	[51]
syngeneic	OSCC and HPV16 E7 expressing OSCC	implantation in the floor of the mouth	lung metastases (42%; NR in [53]) LN metastases (90%)	[52, 53]
syngeneic	LN metastases from OSCC	implantation in the floor of the mouth	lung metastases (32%)	[54]
xenograft	several HNSCC cells	injection into the tail vein	lung metastases (5-100%)	[55]
syngeneic	OSCC	injection into the tail vein	lung metastases	[56]
xenograft	OSCC	injection into the tail vein	lung metastases (100%)	[92]

Legend: OP= oropharyngeal; LN = lymph node; SC = subcutaneous; NR = not reported.

Finally, the use of GEM in OSCC research is rare and they do not metastasize frequently. A 25% of lymph node metastases in the para-tracheo-pharyngeal-esophageal regions was reported in L2D1+/p53+ mice, which developed cancer in the anterior and posterior tongue, the cheek mucosa, the upper, and lower esophagus. In contrast, chemically-induced OSCC animal models such as the dimethyl-1,2, benzanthracene (DMBA)-induced cheek pouch tumors in the hamster and the 4NQO-induced oral cavity SCC in the rat have been frequently used. However, the tumor formation requires several months and the metastasis rate is low[31].

In conclusion, the development of animal models of OSCC metastasis is necessary not only to investigate the metastatic process of OSCC but also to evaluate new emergent therapies, such as nanomedicine-based ones[59].

1.2 The advent of nanomedicine for cancer therapy

In recent times, the field known as nanomedicine has emerged from the union between nanotechnology, medicine, physics, mathematics, and biology. Goals of this new field are to design new platforms to enhance the efficacy and the specificity of the existing therapies and support the diagnosis of several diseases with few toxic effects. These results are being partially achieved thanks to the development of nanoparticles (NPs)[60].

NPs are particles which exist on a nanometer scale (i.e., below 100 nm in at least one dimension)[60, 111]. They have been applied not only as anticancer drugs, but also as ultrasound contrast agents, vaccines, anesthetics, fungal treatments, anemia, macular degeneration therapies, and imaging tools. In addition, other applications such as gene therapies, therapies for bacterial infections, inflammation (arthritis), and graft versus host disease (GVHD) are currently under investigation[61]. Indeed, NPs are suitable carriers of several compounds such as chemotherapeutic agents, anticancer drugs, nucleic acids, contrast agents for imaging applications, and natural compounds[5, 61, 62].

In oncology, NPs have achieved a great relevance and their application includes not only the treatment of several types of cancer but also cancer imaging and thermal ablation of tumors[61]. There are several advantages of using NPs instead of the free drugs alone. Indeed, such systems may increase the solubility and chemical stability of the drugs, protect the same drugs from the degradation and the immune cells, and increase the circulation time. As a consequence, the half-life of the compounds increases together with the therapeutic effect. In addition, the specific accumulation of NPs in tumors results in a further increase of the efficacy[60, 61, 62].

Therapeutic and diagnostic NPs are classified into two categories: inorganic and organic particles. Inorganic particles consist of materials like gold, silver, silica, iron oxide and they have been clinically approved for imaging applications. In contrast, organic particles have been clinically approved for cancer therapy and they are made of polymers or lipids (liposomes or micelles)[61, 62]. Most of the NPs clinically approved for cancer treatment are liposomes and are reported in Table 1.3.

1.2.1 Generations of the nanomedicine platforms

First generation

Liposomes consist of a semisolid phospholipid layer and have been widely used in cancer treatment due to their reduced toxicity and their tumor specificity[63]. They are considered the first-generation nanomedicine drugs due to their passive accumulation in the tumor. This is owed to the fact that tumor vessels have larger endothelial fenestrations (between 100 nm and 780 nm of size) than normal endothelium. This phenomenon is known as the enhanced permeability and retention (EPR) effect and allows NPs to extravasate and enter the tumor interstitial space[61, 62, 64]. All of the NPs currently approved for cancer therapy belong to the first-generation nanomedicine drugs[61, 62]. However, passive targeting alone has some limitations. Indeed, it has been reported a heterogeneity of EPR within and between tumor types due to tumor location, macrophage infiltration, and site (primary vs metastatic). In addition, the treatment with NPs does not always result in a significant increase of OS[64]. For these reasons, second-generation nanomedicine drugs have been developed.

Second generation

The second-generation of NPs is characterized by the addition of components for active targeting or by stimuli-responsive systems. In the preclinical setting, actively targeted NPs have shown an enhanced tumor specificity and drug retention in tumors thanks to the ligand-receptor binding[61, 62]. The early clinical results of some of these systems are promising, but none of these are clinically approved. In addition, the ligand used for active targeting (e.g. monoclonal antibodies) may result in an increase of the NPs uptake by the cells of the mononuclear phagocyte system (MPS), reducing the concentration of NPs in the tumor and therefore the efficacy[15, 61, 62].

Stimuli-responsive systems are principally inorganic NPs. For instance, gold NPs have the capability to convert the electromagnetic radiation from a light source (external stimulus) into heath[65]. Other examples of stimuli-responsive systems are those capable to release the compound in response to changes in pH, reductive agents or temperature (internal stimulus), which occur in the tumor microenvironment. Additionally, some of these systems are currently being investigated in several clinical trials[61, 62].

Table 1.3: Clinically approved nanomedicine systems for cancer therapy

Name	**Type**	**Approved application**	**Country**
Doxil/Caelyx	liposomal doxorubicin	secondary treatment for ovarian cancer, HIV-associated Kaposi′s sarcoma, and multiple mieloma	EU,US
Myocet	liposomal doxorubicin	primary treatment for metastatic breast cancer	EU
DaunoXome	liposomal doxorubicin	primary treatment for HIV associated Kaposi′s sarcoma	US
Marqibo	liposomal vincristine	tertiary treatment for ALL FAB type L1	US
MEPACT	liposomal mifamurtide	primary postoperative treatment for osteosarcoma	EU
Onivyde MM-398	liposomal irinotecan	secondary treatment for metastatic pancreatic cancer	US
Abraxane	albumin-particle bound paclitaxel	primary treatment for metastatic pancreatic cancer; secondary treatment for metastatic breast cancer; advanced NSCLC if surgery or radiotherapy not an option	EU, US

Legend: ALL FAB type L1 = Philadelphia chromosome-negative acute lymphoblastic leukemia; NSCLC = non-small cell lung cancer.

Third generation

The third-generation of NPs platforms has been developed to sequentially overcome the biological barriers, which reduce the efficacy of the NPs systems injected intravenously. The first barrier is represented by the cells of the MPS, which contribute to the non-specific accumulation of NPs in organs such as liver and spleen. In the blood vessels, the fluid dynamics influences the flow of the NPs and is therefore considered another important barrier. Depending on the geometry of the NPs, their interaction with the endothelium may decrease or increase (e.g. spheric vs discoidal geometry). In addition, the intratumoral pressure can strongly decrease the extravasation of NPs by the EPR effect. At the intracellular level, endosomal compartmentalization and MDR may limit the NPs-based drug delivery[15, 60, 66].

The third-generation nanomedicine platform multistage nanovector (MSV) has shown advantages over the NPs of the previous generations, thanks to the activation of several components in a sequential manner. It is characterized by a discoidal first-stage mesoporous silicon particle (S1MP) in the micrometer range carrying a second-stage NPs (S2NPs) embedded within the nanopores[60, 67]. Following intravenous (IV) injection, this system is able to protect the S2NPs from the cells of the MPS within the circulation, adhere to tumor endothelium and release the S2NPs directly into the tumor interstitial space[60, 68, 69]. Thanks to the geometry and the size of the S1MPs, MSVs may accumulate preferentially in metastatic sites such as the lungs, compared to other conventional NPs systems[66, 68, 69]. This peculiarity results in an efficacy also against lung metastases, obtained in animal models of different types of cancer. For instance, a down-regulation of ki67 and CD31 was obtained in an orthotopic mouse model of ovarian cancer with the administration of MSVs with liposomes containing EphA2-specific siRNA embedded within the nanopores. Similarly, lung metastases significantly decreased in mice bearing A375SM-Luc melanoma lung metastases treated with MSVs loaded with liposomes containing siRNA and polymeric NPs with docetaxel compared with the administration of the two types of NPs alone[60, 68, 69].

Beyond the third generation

Moreover, a more elaborate NP system has been recently published by Xu et al.[66]. The system includes an injectable NP Generator (iNPG) loaded with a polymeric doxorubicin (pDox). The iNPG consists of a mesoporous silicon particle packaged with doxorubicin binding to poly (L-glutamic acid) through a ph-sensitive linkage (pDox). Once iNPG-pDox accumulates into the site of interest due to innate tropism and adheres to the tumor endothelium, pDox self-assembles into NPs *in situ* and enters tumor interstitial

space. Intratumorally, pDox is internalized by the tumor cells and doxorubicin is released in the perinuclear region, thanks to the cleaving of the pH-sensitive linker, overcoming the MDR efflux pumps. The use of iNPG-pDox resulted in an anti-metastatic efficacy and a significant increase of the survival time (233 d) in an orthotopic mouse model of breast cancer lung metastases compared with free doxorubicin (98 d) and Doxil (124 d)[66].

In conclusion, several NPs systems are emerging for cancer therapy and they can be rationally designed to overcome sequential barriers and to target specifically metastatic sites. For these reasons, they are promising systems also for OSCC therapy. Some clinical and preclinical studies have been published on the use of different NPs systems in OSCC[59].

1.2.2 Nanomedicine for HNSCC therapy

Clinical studies

The NP system Doxil/Caelix clinically approved for other types of cancer has been also evaluated as adjuvant chemotherapy on patients with advanced and\or metastatic HNSCC[63, 70, 71, 72]. The phase 1 evaluation in 24 patients with recurrent (21 patients) and metastatic HNSCC (3 patients) showed an overall response rate of 33% with few adverse effects (skin toxicity, stomatitis, neutropenia). Oral cavity was the site of the primary tumor in 10\24 patients[63]. In phase II clinical trial, Doxil was used as induction chemotherapy prior radiotherapy in 20 patients with locally advanced unresectable HNSCC. In this study, no cardiotoxicity and no grade 3\4 hematological toxicity were reported. A partial response (PR) to Doxil was also achieved in 20% of lymph node metastases. However, only four patients were affected by oral cavity SCC[70]. In addition, a larger study on 74 patients with locoregional recurrent and\or metastatic HNSCC did not report any significant difference in survival and overall response rate between patients treated with paclitaxel plus Doxil (36 patients) and those treated with paclitaxel plus gemcitabine (38 patients)[72].

In another study, Faivre et al.[71] administrated Doxil to patients with locoregional relapse of HNSCC in irradiated areas (17\26 patients) and/or with DMs (12 patients). Most of the patients included presented oropharyngeal (15), oral cavity (5) or hypopharynx (4) SCC. This phase I-II study confirmed the low toxicity of Doxil reported by phase I study. However, a moderate response (17%) was obtained and no response was achieved in patients with DMs[71].

Other clinical studies were performed using a liposomal formulation of cisplatin, one of the most used chemotherapeutic agent in OSCC (see 1.1.2). A phase I study was first conducted by Rosenthal et al.[73] on 20 patients

with stage IVa\b HNSCC treated with liposomal cisplatin concurrent with radiotherapy. No ototoxicity, neurotoxicity, and nephrotoxicity of the treatment with liposomal cisplatin were reported. Eight patients experienced a CR. However, further dose escalation was stopped by the sponsor because the liposomal cisplatin was not able to reach a high concentration within the tumor, resulting in a limited clinical efficacy [73]. More recent studies were performed with another liposomal cisplatin (lipoplatin) by Jehn et al.[74, 75]. In this phase III study, 25 and 21 patients with stage IV HNSCC were treated with lipoplatin plus 5-FU and cisplatin plus 5-FU respectively. Less renal toxicity, neurotoxicity, hematoxicity, and mucositis were reported in the group treated with lipoplatin than the one treated with cisplatin. However, patients treated with lipoplatin experienced more grade III anemia and grade IV neuropathy. At the therapeutic level, less stable disease (50% vs 64%) and more PR cases (38.8% vs 19%) were observed in the cisplatin group than in the lipoplatin one[74]. One of the reasons for this difference may be a different pharmacokinetics between the two compounds. Indeed, another study reported a higher total platinum plasma concentration, a shorter half-life and a higher plasma clearance of lipoplatin than cisplatin[75].

Paclitaxel-albumin NPs were administered intraarterially in 31 patients with advanced HNSCC[76]. In this study, the toxicity of paclitaxel NPs was acceptable and CR and PR were observed in 10.34% and 65.51% of cases respectively[76].

Only one study included only patients (n=23) affected by tongue SCC. All patients were treated intraarterially with paclitaxel NPs. The administration of the paclitaxel NPs resulted in 8.6% of hematoxicity and neurotoxicity cases. The overall response rate was 76.5-83.3%[77].

Another type of NPs encapsulating paclitaxel (cationic liposomes) was used in one small clinical study by Strieth et al.[78]. In contrast to conventional liposomes and paclitaxel, cationic liposomes are capable of targeting the tumor endothelial cells, resulting in an anti-vascular effect within the tumor. The preliminary results of this first study revealed a good safety profile of the cationic liposomes loaded with paclitaxel[78].

Finally, another recent study[79] administered NPs albumin-bound paclitaxel combined with cetuximab, cisplatin, and 5-FU followed by cisplatin and radiotherapy in 30 patients, most with oropharyngeal (n=18) or laryngeal (n=9) SCC. The majority of the patients had a large primary tumor (T3, T4) and lymph node metastases. Seventeen patients had HPV+ oropharyngeal SCC. Severe adverse effects occurred in 30% of the patients, while a complete clinical response of the primary tumor site was obtained

in 63% of the patients with oropharyngeal SCC (14 patients) after 2 cycles of paclitaxel NPs plus cetuximab. In addition, a CR of 30% and a PR of 48% were obtained at the site of lymph node metastasis[79].

The clinical studies performed on nanomedicine drugs and others currently underway indicate the emerging of these systems as possible therapeutic strategies for OSCC therapy[112]. In the clinical studies reported[63, 76, 77], NPs demonstrated few collateral effects and were easier to handle than free drugs. However, most of the clinical trials reported the use of first-generation nanomedicine drugs, which are not able to accumulate in high concentrations within the tumor (lipoplatin) or to target metastatic sites (Doxil and lipoplatin). Further clinical trials with more sophisticated platforms are needed in order to achieve more therapeutic efficacy against metastatic sites.

Preclinical studies

In contrast to clinical studies, several preclinical studies have been published for OSCC therapy. Despite most of these studies evaluated the NPs systems only *in vitro*, some of them used more sophisticated platforms with active targeting or stimuli-responsive components[59].

In addition to the published clinical trials [63, 70, 71, 72], different nanoformulations of doxorubicin were also evaluated on HNSCC cells and *in vivo*. These formulations consisted of the combination of doxorubicin with resveratrol[80], methotrexate [81, 82, 83] or an autophagy inhibitor[84]. *In vitro*, the drug combination was more effective than the free form and nanoformulation of the single drug, resulting in an increase of chemosensitivity[84]. *In vivo*, the administration of liposomes loaded with doxorubicin and methotrexate decreased the expression of VEGF and Matrix Metalloproteinases (MMPs) in a NQO-induced oral cavity SCC rat model[81, 82, 83]. Regarding cisplatin, ligand-decorated cancer-targeted polymeric NPs loaded with cisplatin were more cytotoxic in oral cavity SCC cells than non-targeted NPs and free cisplatin, due to a higher uptake[85]. In contrast, cisplatin was more cytotoxic than polymeric micelles loaded with cisplatin (NC-6004) in another study by Endo et al.[86]. In a SC xenograft model, the NC-6004 demonstrated less renal toxicity than free cisplatin, while NC-6004 was more effective against lymph node metastases in an orthotopic xenograft mouse model of OSCC metastasis[86]. Finally, 5-FU was encapsulated in self-assembled nucleoside NPs by Zhao et al.[87]. The system exhibited low toxic effects on normal human oral cells. In addition, the NP formulation presented a long-term effect and less toxicity *in vivo* than free 5-FU[87].

The stimuli-responsive properties of magnetic NPs have also been explored in the preclinical setting. An *in vivo* study[88] reported that gold NPs with

laser had more antitumor efficacy than gold NPs alone in a DMBA-induced oral cavity SCC hamster model. Melancon et al.[89] targeted gold nanoshells for EGFR through the addition of cetuximab. *In vitro*, the application of near-infrared (NIR) light activated the gold nanoshells, reducing significantly the cell viability compared with the nanoshells alone. In addition, the cellular uptake of the targeted NPs was higher than non-targeted NPs. Other types of magnetic[90, 91] and polymeric NPs[92] coupled with photothermal/photodynamic therapy (PDT) had similar results. Another system consisting of a stimuli-responsive titanium dioxide NPs targeted against EGFR was tested *in vivo* by Lucki et al.[93]. The system plus laser treatment exerted a high antitumor effect compared with NPs alone and a low toxicity on a SC model of OSCC. Another study[94] reported similar results *in vivo* using photocatalytic titanium dioxide NPs combined with high intensity focused ultrasound (HIFU). Finally, novel hybrid NPs were developed by Sathapaty et al.[95] to kill OSCC stem cells. *In vitro*, the NPs were able to disrupt OSCC spheroids and to induce apoptosis also of the cancer stem cells, characterized by a high self-renewal capability. *In vivo*, a high anti-angiogenic effect of the NPs was observed in a Chick Chorioallantoic Membrane (CAM) model[95].

Gene therapy with lipid-based NPs has also been reported in OSCC with promising results. In a study by Miao et al.[96] PEI-modified $Fe_3\ O_4$ NPs were used to deliver human TNF-related apoptosis-inducing ligand (TRAIL) gene with an hTERT tumor-specific promoter (pACTERT-TRAIL). More *in vitro* cytotoxicity and a higher transfection efficacy were obtained than conventional PEI\lipofectamine. The platform obtained positive results also in a SC model of OSCC[96]. Two more recent studies[97, 98] reported the use of lipid-calcium-phosphate (LCP)- NPs loaded with HIF1α or VEGF siRNA combined with photosan-mediated PDT. Photosan has been used as a photosensitizer drug and is locally administered after the laser treatment. To increase the efficiency of PDT, which usually requires multiple treatments, LCP-NPs were also actively targeted against σ receptors[97, 98], expressed by HNSCC. A higher cytotoxic activity and cellular uptake were obtained using targeted NPs compared with non-targeted NPs. *In vivo*, HIF1α lipid NPs plus PDT reported more efficacy than scrambled siRNA LCP plus PDT in a SC model of OSCC[98]. A similar *in vivo* efficacy was also reported by Lecaros et al.[97] who used σR-targeted LCP-NPs to deliver VEGF-A siRNA with and without PDT compared with scrambled siRNA with and without PDT.

Finally, NPs with natural plant compounds have been also developed for OSCC. Indeed, plant products are rich in flavonoids and stilbenes, which exert antitumor effects[5]. NPs can overcome the poor solubility and bioavail-

ability showed by these compounds in the clinic[5]. In OSCC, NPs encapsulating curcumin, naringenin, genistein, and salvianolic acid B were tested *in vitro* and *in vivo*. The nanoformulation of curcumin decreased chemoresistance in a cisplatin-resistant cell line and increased the cellular uptake compared with the free form[98]. Stimuli-responsive nanocarriers with curcumin were also used in combination with a laser[100] or ultrasonography[101], resulting in a lower cell viability and a higher down-regulation of VEGF, MMP-9, and NF-κB than free curcumin and nanocarriers alone[100, 101]. In addition, Mazzarino et al.[102] prepared mucoadhesive polycaprolactone (PCL) NPs loaded with curcumin and a chitosan-coating for the local treatment of OSCC. The platform was able to induce apoptosis in tongue cancer cells[102]. Similar efficacy was obtained by Gavin et al.[103] with the mucoadhesive NPs loaded with genistein compared with aqueous nanoemulsions of genistein. In addition, the malignant transformation of oral cells was prevented in the group treated with NPs encapsulating genistein compared to controls and free genistein group in a DMBA-induced model of OSCC[104]. This effect is known as chemoprevention. Finally, a nanoformulation of salvianolic acid was able to decrease the cell growth in oral precancerous and OSCC cell lines compared with the free form[105].

In conclusion, advanced and/or metastatic OSCC is still a fatal disease with a poor survival rate, especially when DMs occur. Recently, nanomedicine has changed the cancer treatment, contributing in some cases to an increase of OS and the quality of life[61, 62]. Despite the few toxic effects reported compared with the free form of anticancer drugs, the first-generation nanomedicine drugs report some limitations not only in targeting the primary tumor site but also metastatic ones[71, 73]. These findings are observed in patients affected by HNSCC.

In the preclinical setting, there are several published studies on the use of second-generation nanomedicine compounds for OSCC therapy. However, most of them reported only an *in vitro* evaluation, which may not reflect the *in vivo* one, particularly in the case of metastases[29]. In addition, the majority of the study used a SC xenograft model of OSCC, which does not resemble the behavior and clinical response of OSCC[31]. Orthotopic models were used in a few cases. Only the study by Endo et al.[86] reported an anti-metastatic effect of a nanoformulation of cisplatin against lymph node metastases. Therefore, more efforts are warranted in order to develop and to evaluate novel nanomedicine platforms in more appropriate animal models of OSCC, including also models of OSCC metastasis.

1.3 Aim of the dissertation

The aim of the work reported in the present dissertation was to establish mouse models of OSCC metastasis that may be then used to evaluate innovative and promising anti-metastatic platforms such as iNPG-pDox. Indeed, iNPG-pDox presented a promising efficacy against lung metastases, the most frequent DMs reported in OSCC(see 1.1.3). In addition, iNPG-pDox is a third-generation nanomedicine drug, which has never been reported for OSCC therapy.

In a first experiment, the efficacy of the platform was evaluated *in vitro* on an OSCC cell line (HSC-3). This cell line was chosen because of its derivation from a tongue SCC with a high metastatic potential. For these studies, only the pDox NPs, without iNPG, were used due to the capability of iNPG to target lung metastases *in vivo* only by natural tropism. In addition, pDox NPs were reported to enter the tumor interstitial space, after being generated *in situ*[66]. This cell line was treated with pDox NPs and the free form of doxorubicin and the viability was evaluated after 72 and 96 h of treatment. After that, qualitative uptake studies were performed at different time points in order to evaluate the internalization of pDox NPs in the HSC-3 cell line compared to doxorubicin.

After proving the capability of pDox NPs to kill the HSC-3 cells, pilot studies were conducted to establish an orthotopic model of OSCC lung metastasis. Indeed, the orthotopic model of OSCC is still considered the most similar to human OSCC. In addition, the majority of the orthotopic models of OSCC metastasis presents a low rate of lung metastasis (see Table 1.2). In this experiment, the primary tumor and/or the lung metastases were evaluated by *in vivo* and *ex vivo* imaging techniques, as well as histology and immunohistochemistry (IHC). Both sexes of athymic nude mice were used to establish the model and promising results were obtained using male mice, in which a high prevalence of lung metastases was observed.

In addition, a second model of OSCC metastasis was established through IV injection. Indeed, this model is widely used to establish lung metastases of several types of cancer and presents a rapid growth and a high reproducibility. In addition, this model has not been frequently used in OSCC research and no serial transplantations have been reported (see Table 1.2). Indeed, the first experiment with IV injection of HSC-3 cells resulted in the growth of large lung metastases in one mouse. From these lung metastases, a new cell line (HSC-3 M1) was isolated and was injected IV in other 5 athymic nude mice. In this model, a high rate of lung metastases was obtained. HSC-3 M1 cell line was also treated with pDox and doxorubicin and

the results did not significantly differ from those obtained on the parental cell line, suggesting a potential efficacy of pDox NPs also against tumor cells isolated from lung metastases.

Chapter 2

Viability assay and pDox uptake in OSCC cells

2.1 Materials and Methods

Cell line Human HSC-3 cell line was obtained from the Japanese Collection of Research Bioresources Cell Bank (n°JCRB0623). HSC-3 cells derives from a tongue SCC with a high metastatic potential. Cells were cultured in DMEM with 10% fetal bovine serum (FBS) plus 1% penicillin-streptomycin (PS) at 37°C in a humidified atmosphere of 5% CO_2 and 95% air.

Synthesis of pDox nanoparticles pDox was synthesized by Guodong Zhang according to Xu et al.[65]. Briefly, a conjugation with hydrazide groups to glutamic acid side chains of poly(L-glutamic acid) was performed through an acid anhydride reaction as the following: isobutyl chlorformate was dropwise added at 4°C to a DMF solution of poly(L-glutamic acid) and N-morphylmorline. After 15 minutes, carbazic acidtert-butyl ester in DMF was added to the solution. The reaction occurred initially for 30 minutes at 4°C. Then the solution was placed at 25°C for 2 h. The polymer was synthesized dissolving poly(L-glutamic acid hydrazide)-co-poly(L-glutamic acid) in anhydrous methanol with the addition of trifluoro-acetic acid. After that, doxorubicin hydrochloride was added and the final product was allowed to stir at 25°C for 2 days under Argon gas. pDox was then concentrated, dialyzed in methanol and purified by using Spehadex-LH20 (Amersham Pharmacia Biotech Co).

Preparation of pDox nanoparticles and measurement of size pDox NPs were obtained by suspending pDox in DMF at a concentration of 10 mg/ml. The pDox DMF solution was then resuspended in PBS. The size of pDox NPs was measured in PBS using Zetasizer Nano-ZS (Malvern Instruments Ltd).

MTS Assay HSC-3 cells were plated in a 96-well plate (4 x 10^3 cells per well) and incubated for 24 h to allow cell adhesion. HSC-3 cells were then treated with different concentrations of free doxorubicin. Equimolar amounts of doxorubicin in polymeric form were used. After 72 and 96 h, cells viability was evaluated through MTS assay (Promega) according to the manufacturer′s protocol. The absorbance of the samples was measured at 490 nm using a Synergy H4 hybrid reader.

Uptake studies of pDox nanoparticles and free doxorubicin For uptake studies, HSC-3 cells (2 x 10^4 cells per chamber) were seeded on 4-well chamber slides (BD Falcon) and incubated for 24 h. Cells were then treated with 5 μM of free doxorubicin and equimolar amounts of pDox NPs for 1, 6 and 24 h. The cells were then washed three times with PBS and fixed in paraformaldehyde for 20 minutes. Actin cytoskeletal microfilaments were stained with Alexa Fluor 488 phalloidin (Invitrogen, 1:200; excitation\emission:495\518 nm) and DAPI (4 μg/ml; incubation time of 3 minutes) was used to stain the nucleus. Finally, cells were washed three times with PBS and slides were mounted with ProLong Gold Antifade Mountant (Invitrogen). Z-stack images were then collected using a confocal microscope (Nikon A1 Confocal Imaging system) at 0.51 (treatment groups) or 1.10 μm intervals (control group). Doxorubicin was detected in the groups treated with free and pDox NPs using the propidium iodide (PI) channel (excitation\emission: 543\619 nm). The images were further elaborated with ImageJ software.

Statistical analysis Statistical analyses were performed using one-way or two-way analysis of variance (ANOVA) with the GraphPad Prism software. Differences at $p < 0.05$ were considered to be statistically significant.

2.2 Results

As stated in the 1.3, the present *in vitro* study performed on HSC-3 cells consisted of a viability assay and a qualitative uptake study. The viability assay after the treatment with different concentrations of doxorubicin permitted to confirm that HSC-3 cells were sensitive to doxorubicin. After that, the effect of pDox NPs on the cells viability was investigated. The treatment with the highest concentration of pDox NPs resulted in a cell viability below 40%, proving that also pDox NPs were able to kill HSC-3 cell line. The internalization of pDox NPs was then confirmed by confocal microscopy, although it was delayed compared to the free form of doxorubicin. This difference in uptake between doxorubicin and pDox NPs may explain the one observed in cytotoxicity.

2.2.1 Viability assay for HSC-3 cells after treatment with doxorubicin and pDox NPs

Results obtained from MTS assay of HSC-3 cells treated with 0, 0.0001, 0.001, 0.1, 0.5, and 1 μM of doxorubicin hydrochloride are summarized in Fig. 2.1. The cell viability of HSC-3 cells significantly decreased after the treatment with the highest concentrations of doxorubicin (0.1, 0.5 and 1 μM) at both time points. In addition to a dose-dependent effect, doxorubicin exerted a time-dependent effect on cell viability. Indeed the cells treated for 96 h had a lower viability than those of cells treated for 72 h. However, this difference was not statistically significant.

The procedure of making pDox NPs is reported in the Material and Methods. In Table 2.1, different measurements of the size of pDox NPs are reported. Measurements were performed using intensity average. The average size of pDox NPs was 111.85 $\pm$ 4.36 nm. Results are reported as mean $\pm$ SD.

Fig. 2.2 represents the cellular viability assay performed after 72 and 96 h of treatment with doxorubicin and pDox NPs (Fig. 2.2 a, b). In contrast with the free form of doxorubicin, only the treatment with the two highest concentration of pDox NPs (0.5 and 1 μM) resulted in a significantly lower cell viability than controls at both time points (Fig. 2.2 a, b). Indeed, pDox NPs were significantly less cytotoxic than the free form of doxorubicin. However, this difference in cytotoxicity decreased after 96 h of treatment with 0.5 and 1 μM of pDox NPs (Fig. 2.2 b), proving that both pDox NPs and free form of doxorubicin were able to effectively kill HSC-3 cells. As the free form of doxorubicin, the effect of pDox NPs on cell viability was dose- and time-dependent (Fig. 2.2 a, b).

Table 2.1: pDox NPs size measurement

Dispersant	pDox Z-Ave (d.nm)	PdI
PBS	111.9 ± 1.305	0.097 ± 0.045
PBS	113.7 ±1.266	0.138 ± 0.017
PBS	103.9 ± 2.650	0.136 ± 0.017
PBS	117.9 ± 2.196	0.084 ± 0.046
PBS	112.3 ± 1.888	0.109 ± 0.018
PBS	109.3 ± 0.854	0.089 ± 0.028
PBS	113.9 ± 0.838	0.122 ± 0.017

Legend: Z-Ave = z-average size; PdI= polydispersity index

2.2.2 Cellular uptake study of pDox NPs and free doxorubicin in HSC-3 cells

The cellular uptake study reported in Figg. 2.3-2.4 reveals that pDox NPs presented a delayed entry into HSC-3 cells compared with the free form of doxorubicin after 1, 6 and 24 h of treatment. In the group treated with pDox NPs, doxorubicin localized within the nucleus after 6 and 24 h of treatment (Fig. 2.3 b and Fig. 2.4). In contrast, doxorubicin was already observed within the nucleus of HSC-3 cells after 1 h of treatment with the free form of doxorubicin (Fig. 2.3 a).

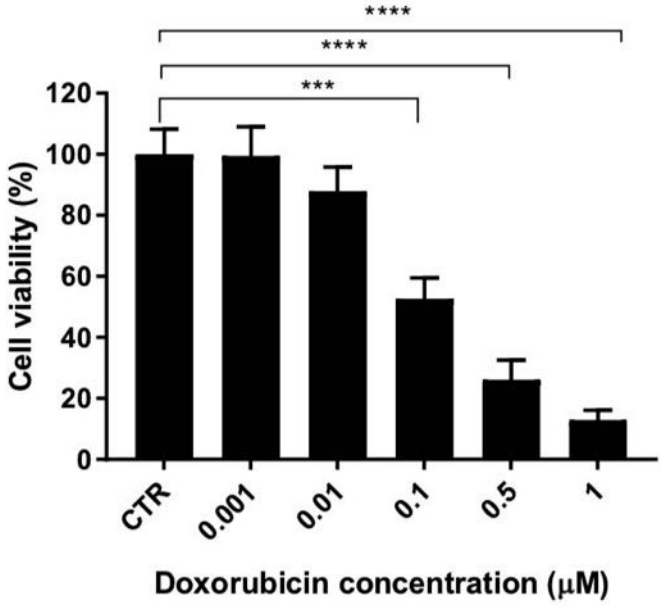

(a)

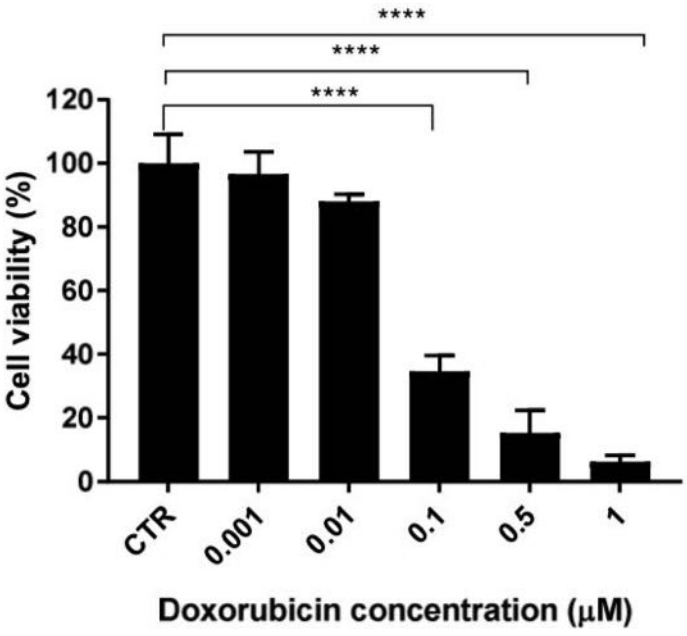

(b)

Figure 2.1: Viability assay results for HSC-3 cell line after 72 (a) and 96 h (b) of treatment with different concentrations of doxorubicin. Data are expressed as the mean ± SEM of at least three experiments. *** P $\leq$0.001, ****P $\leq$ 0.0001 by one-way ANOVA statistical analysis and Dunnet′s multiple comparisons test.

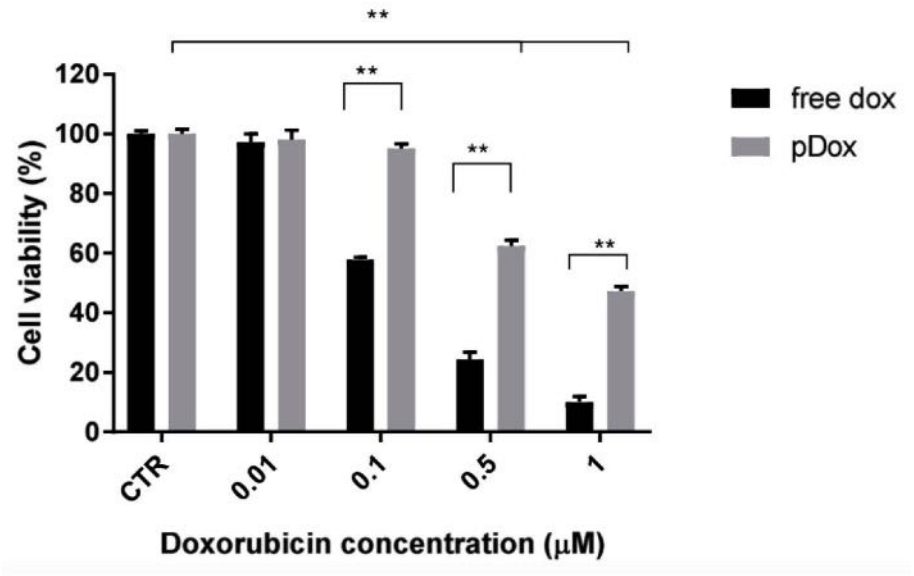

(a)

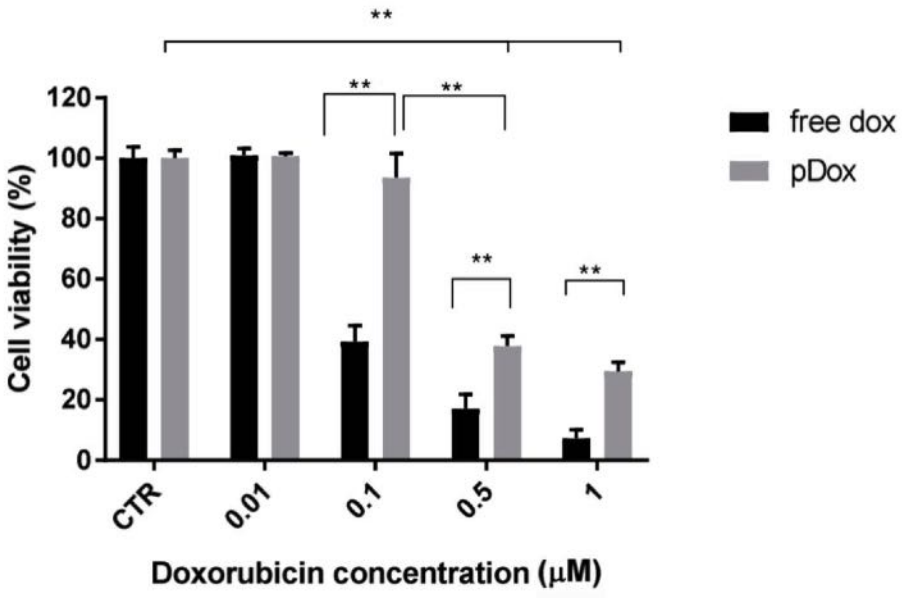

(b)

Figure 2.2: Viability assay results for HSC-3 cell line after 72 (a) and 96 h (b) of treatment with different concentrations of pDox NPs and the free form of doxorubicin. Data are expressed as the mean ± SEM of at least three experiments. ** P $\leq$0.01 by one-way ANOVA statistical analysis and *post hoc* Tukey test.

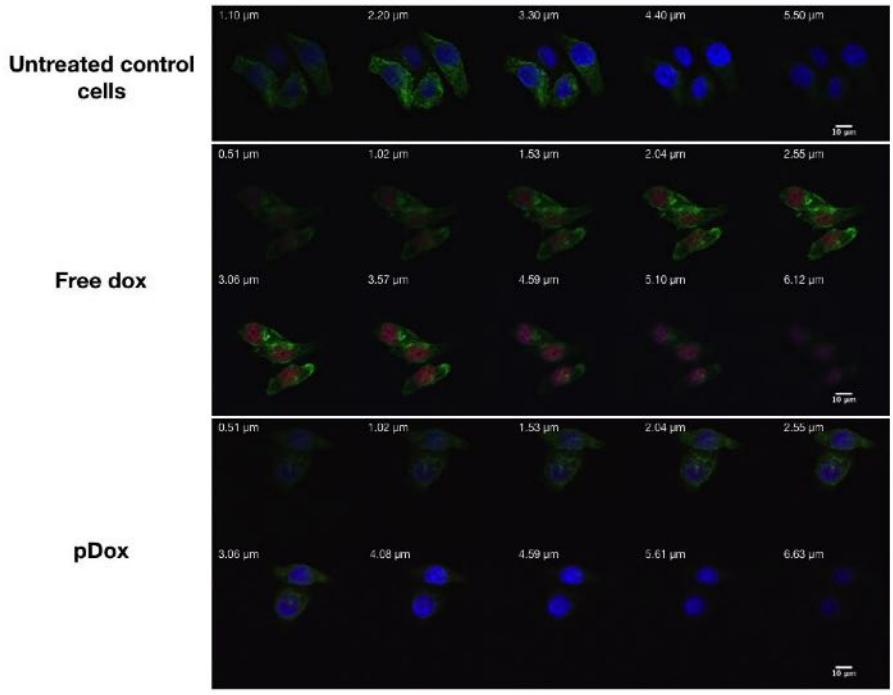

(a)

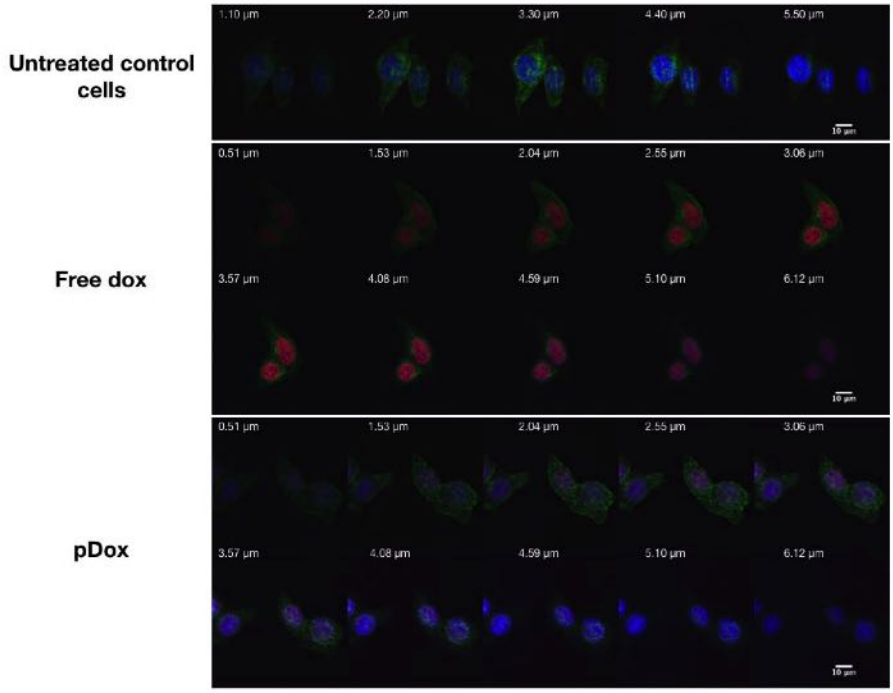

(b)

Figure 2.3: Z-stack confocal images after 1 (a) and 6 h (b) of treatment with doxorubicin (free dox) and pDox NPs. Alexa Fluor 488® phalloidin (green fluorescence) was used to stain the cytoskeleton. DAPI (blue fluorescence) was used to stain the nuclei. Propidium iodide channel (red fluorescence) was used to detect doxorubicin in the free and polymeric form. The pink/purple fluorescence indicates doxorubicin localized within the nucleus. Scale bar represents 10 μm.

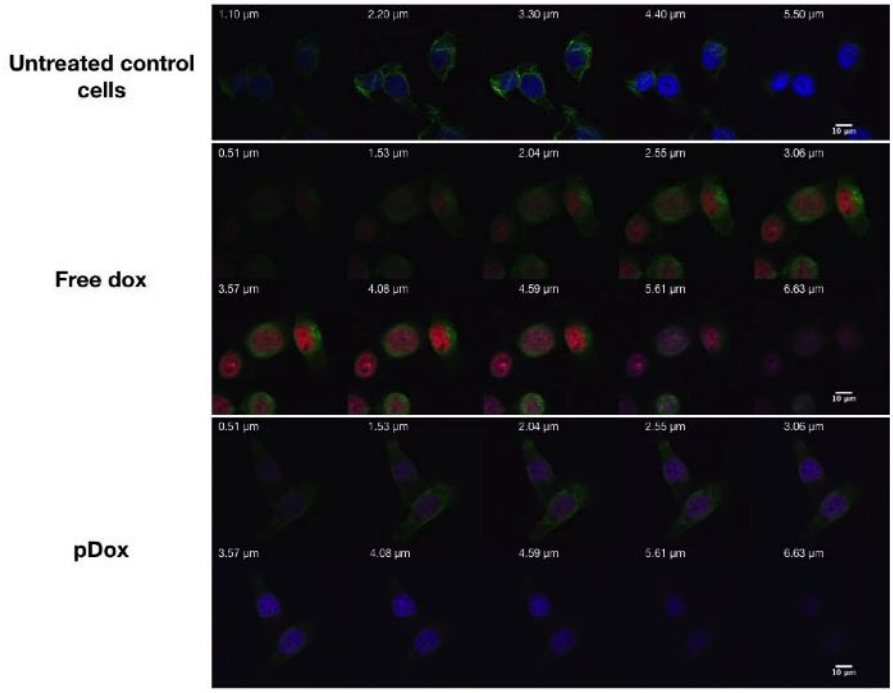

Figure 2.4: Z-stack confocal images after 24 h of treatment with doxorubicin (free dox) and pDox NPs. Alexa Fluor 488® phalloidin (green fluorescence) was used to stain the cytoskeleton. DAPI (blue fluorescence) was used to stain the nuclei. Propidium iodide channel (red fluorescence) was used to detect doxorubicin in the free and polymeric form. The pink/purple fluorescence indicates doxorubicin localized within the nucleus. Scale bar represents 10 μm.

Chapter 3

An orthotopic model of OSCC metastasis

3.1 Materials and Methods

HSC-3 cell line transfection A stable HSC-3 cell line expressing luciferase (Luc) and GFP was generated using a lentivirus carrying both genes. Briefly, HSC-3 cells were plated in a 6-well plate (72 x 10^3cells per well). After 24 hours, 500 μl of new media without antibiotics with polybrene (2x) and 500 μl of lentivirus were added. After an incubation time of 15 hours, the media was changed. The selection of transfected cells was initially performed by treating transfected and control cells with 0.5 μg/ml of puromycin, to which transfected cells were resistant. Non-transfected cells served as controls. After 6 days of treatment, the cells were allowed to grow in normal media (DMEM 10% FBS plus 1% PS) and GFP expression was evaluated by an inverted digital fluorescence microscope (EVOS FL^{TM}, American Microscope Group).

Cell sorting and evaluation of luciferase expression HSC-3 GFP/Luc cells were selected for GFP expression by Fluorescence Activated Cell Sorting (FACS) using BD FACSAria II Cell Sorter. Before sorting, the cell suspension was filtered using a 40 μm cell strainer (Fisherbrand^{TM}). Sorted HSC-3 GFP/Luc cells were then cultured in DMEM 10% FBS plus 2% PS for the first 5 days. After that, the cells were cultured in normal media.

The expression of Luc was confirmed as follows: different concentrations of HSC-3 GFP cells were plated in a 96-well plate in 100 μL of media and 50 μL of D-luciferin (15 mg/ml) were added to each well. DMEM media was used as a negative control. The Luc expression was then evaluated by IVIS Spectrum In-Vivo Imaging System (Perkin Elmer Inc., Waltham, MA).

Orthotopic mouse model All animal experiments were performed with a protocol approved by the Institutional Animal Care and Use Committee (IACUC) at the Houston Methodist Research Institute and in accordance with the National Institutes of Health Guide for the Care and Use of Laboratory Animals.

For this experiment, athymic nude-Foxn1nu mice (Envigo), male (n = 5) and female (n = 10), 5-6 weeks old (male weight 25.30 ± 2.20; female weight 21.35 ± 1.03) were used. The animals were maintained in individually ventilated cages (Tecniplast) with controlled air flow in light controlled rooms (12 hours of light). After the transplantation of tumor cells, the mice were fed with water and soft food *ad libitum*. The soft food diet consisted of moistened pellet and DietGel (ClearH2O).

For the orthotopic mouse model, HSC-3 GFP/Luc cells were trypsinized and suspended in PBS. Thirty minutes before the procedure, analgesia was provided to the animals by a SC injection of buprenorphine SR (1 mg/kg). The animals were induced with 3% isoflurane and maintained with 2.5% isoflurane. The tongue was exposed using a 10 cm forceps (Robox Surgical) and 5 x 10^4 HSC-3 GFP/Luc cells suspended in 20 μl of PBS were slowly injected into the left side of the tongue submucosally using an insulin syringe with 28G $^1/_2$ needle. After the procedure, the experimental animals were monitored and weighed periodically. The animals were humanely sacrificed before the endpoint of the experiment (6 weeks and 11 weeks after injection for females and males respectively) when they presented 20% of weight loss, severe dehydration, inappetence, facial deformation, and/or malocclusion.

Evaluation of the growth of the primary tumor and distant metastases The growth of the primary tumor and lung metastasis were periodically visualized using IVIS Spectrum In-Vivo Imaging System (Perkin Elmer Inc., Waltham, MA). Briefly, 200 μl of D-luciferin (15 mg/kg) were administered to each mouse intraperitoneally 10 minutes before the imaging. Mice were induced with 3% isoflurane in 100% oxygen and then maintained under 2% isoflurane. In order to visualize the lung metastases, the primary tumors were covered with a black sheet.

The growth of the primary tumor was then quantified defining the bioluminescence region of interest (ROI). Data were reported as p/s/cm^2/sr/(μW/cm^2) as per the instructions (PerkinElmer, USA).

Mice sacrifice, harvesting of tissues and staining Eight and eleven weeks after the injection, female and male mice were humanely sacrificed respectively through an overdose of isoflurane followed by cervical dislocation

to confirm the death. At necropsy, the tongue, the mandibular lymph nodes with the salivary glands, the lungs, the liver, and the spleen were collected from each mouse. The presence of the tumor and metastases was evaluated by IVIS of the mice organs.

After the imaging, the organs were fixed in Bouin′s solution for 12 hours (lungs) or in 10% buffered formalin for 48 hours (all the other tissues). The tissues were then embedded in paraffin and processed for hematoxylin and eosin (H&E) staining (two sections per organ). Pictures of the tongue tumor, lymph node and/or lung metastasis were captured using an upright microscope system (Nikon Eclipse 80i). Oral cancer metastases (two sections per organ) were further confirmed through immunohistochemistry (IHC) for anti-human mouse monoclonal pan-cytokeratin (pan-CK) antibody (Dako).

Statistical analysis Survival analysis was performed by the Kaplan-Meier method and a comparison between survival curves was performed using the log-rank test.

3.2 Results

The present *in vivo* pilot study consisted of the establishment of an orthotopic model of OSCC in both sexes of athymic nude mice. Indeed, it is well known that this model resembles the metastatic potential and tumor growth of human OSCC. For these experiments, the HSC-3 GFP/Luc cell line was used in order to investigate a possible development of lymph node and lung metastases. As a result, regional lymph node metastases were present in more than 50% of the animals which developed the primary tumor. Interestingly, the presence of lung metastases was observed by *ex vivo* IVIS in 60% of male mice, one of which presented large metastatic nodules. However, only 20% of the female mice developed small lung metastases. Histology and IHC for pan-CK were also performed to confirm the metastases in the lungs and in the lymph nodes.

3.2.1 Generation of a stable HSC-3 cell line expressing GFP and luciferase

Images of transfected HSC-3 cells selected with puromycin and control cells are reported in Fig 3.1 a. However, only 1% of transfected HSC-3 cells presented a good expression of GFP at the sorting (Fig. 3.1 b). The expression of Luc of sorted HSC-3 GFP cells was also evaluated using In Vivo Imaging Spectrum (IVIS) (Fig 3.1 b). As expected, sorted HSC-3 GFP cells expressed also Luc and the intensity of the bioluminescent signal correlated with the cellular concentration.

3.2.2 Mice survival

All males (n = 5) survived after the tongue injection and all of them developed the tongue tumor. The weight of the mice did not decrease after the procedure. Two male mice (508, 512) who presented weight loss, poor BCS and dehydration were sacrificed 43 and 54 days after the injection. Another male mouse (510) died 60 days after the injection due to the lung metastases. The other two mice (507, 509) were sacrificed 11 weeks after the injection.

All females (n =10) survived after the procedure without any complications. Two mice (030, 089) did not develop the primary tumor. The mouse 081 was sacrificed for head tilt and left circling due to a bacterial infection (*B. Gladioli*) 41 days after the injection. Five mice with weight loss and poor BCS were sacrificed on day 32 (094), day 34 (095), day 36 (090, 097), and day 44 (083). The last two mice (080,096) were sacrificed 8 weeks after the injection.

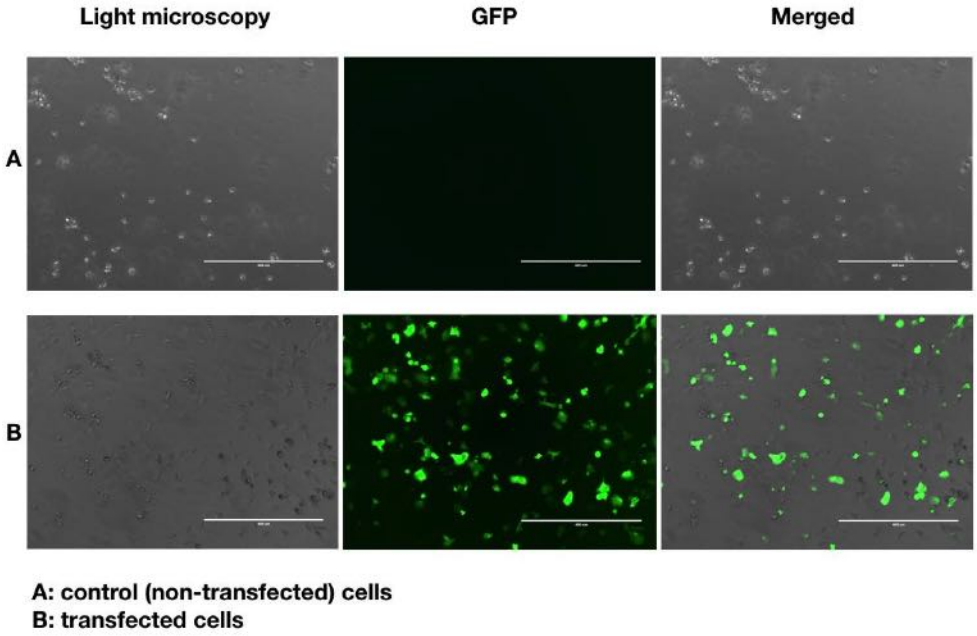

(a)

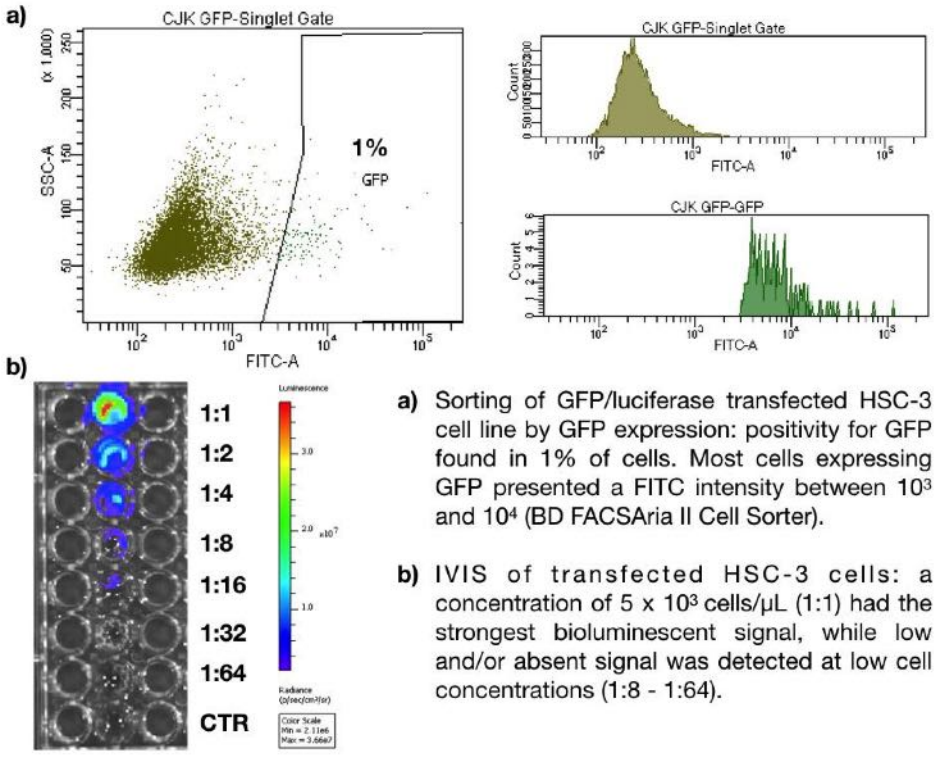

(b)

Figure 3.1: Fluorescence microscopy and FACS of transfected HSC-3 cells. a) Control and transfected HSC-3 cells, fluorescence microscope. Scale bar represents 400 μm. b) Flow cytometry analysis for GFP expression and IVIS.

The median survival of male mice was 60 days, in contrast with female mice, whose median survival was 43.5 days (Fig. 3.2). However, this difference was not statistically significant.

3.2.3 Development of the primary tumor

The growth of the primary tumor was periodically evaluated by IVIS (Fig. 3.3 a, b) in all the animals injected. However, a difference in tumor growth was observed among the animals (Fig. 3.3 and 3.5). Indeed, 4 male mice developed the tongue tumor 30 days after the injection, while the mouse 510 began to develop the tumor 43 days after the injection (Fig. 3.3 a). This finding is more evident in the graph of Fig. 3.4, which represents the average radiance of the signal of each tumor. In addition, only two mice (508, 512) presented a large tumor (> 7.5 x 10^6 p\s\cm^2\sr) and the mouse 512 had also large lymph node metastases. The signal grew progressively in 3 mice, while it seemed to be irregular in the mice 507 and 509, whose peaks of growth were at day 64 and 50, respectively. After that day, the signal decreased in both mice.

Regarding the females, 2 of 10 mice (030, 089) did not develop the primary tumor 31 days after injection (Fig. 3.3 b and 3.5). The tumor seemed to regress completely in the mouse 096 between 43 and 50 days after the injection and partially in the mouse 080 between day 37 and 43 (Fig. 3.3 b). Despite this irregular growth, the quantification data in Fig 3.4 show a homogenous signal of the tongue tumor until day 50 (> 7.5 x 10^6 p\s\cm^2\sr) .

3.2.4 Presence of lung and lymph node metastases

The first signal of lung metastases was observed 30 days after the injection only in one male mouse (Fig. 3.6 a). From day 50 the bioluminescent signal from the lungs was visible together with the primary tumor. The metastases continued to grow until the death of the animal, which occurred 60 days after the injection. Interestingly, the primary tumor was very small at the time of the first evidence of lung metastases (Fig. 3.4 and Fig. 3.6) and its growth was relatively slow until day 50 (Fig. 3.3 a). No evident lung metastases were observed in the surviving two mice (Fig. 3.6 a). In contrast to the male mice, lung metastases did not become evident in female nude mice (Fig. 3.6 b).

Regarding the lymph node metastases, they were observed as a separate signal only in few male nude mice: the mouse 512 developed regional lymph node metastasis from 22 days after the injection, while a small signal was observed in the mouse 509 43 days after the injection. However, the signal

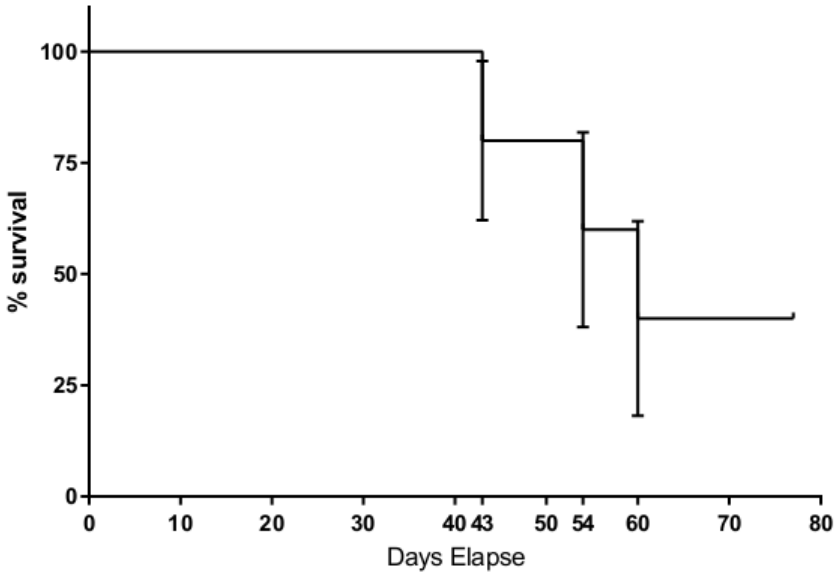

(a)

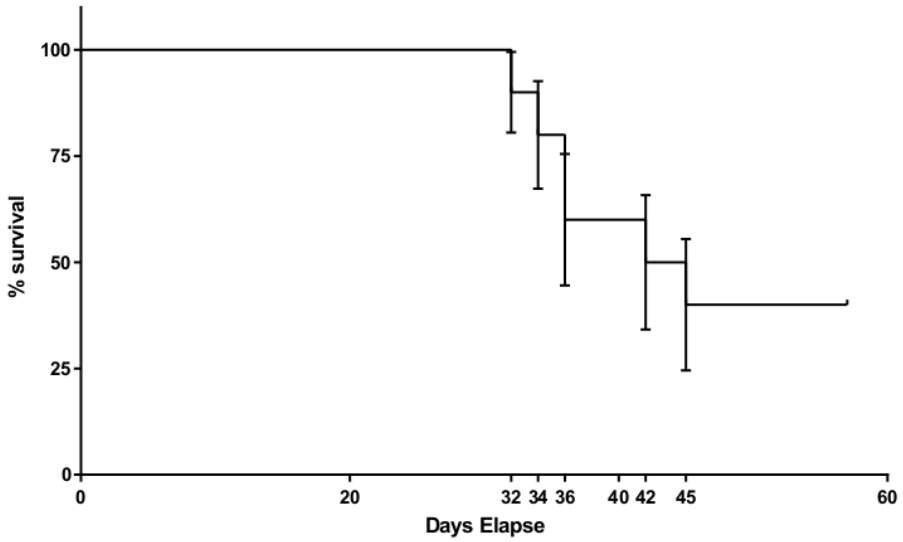

(b)

Figure 3.2: Results of the animal study: survival of the male (a) and female nude mice (b) by Kaplan-Meyer analysis.

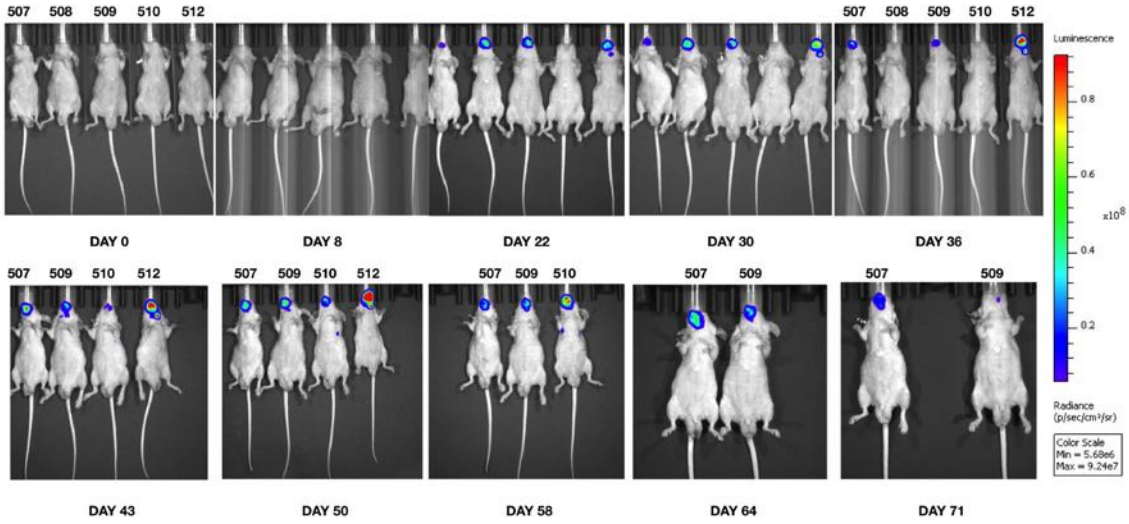

(a)

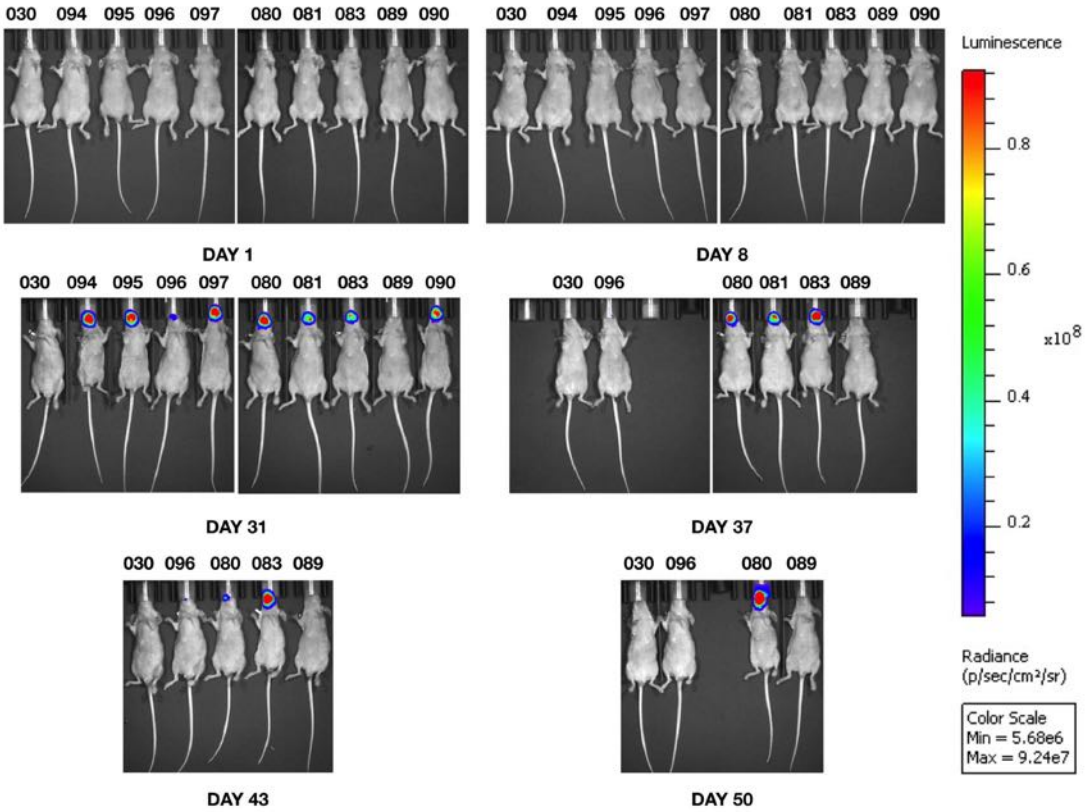

(b)

Figure 3.3: IVIS of the tongue tumor in male (a) and female (b) athymic nude mice: the growth of the primary tumor was observed in male and female athymic nude mice 22 days and 31 days after the injection respectively. The presence of regional lymph node metastases was observed in two male mice.

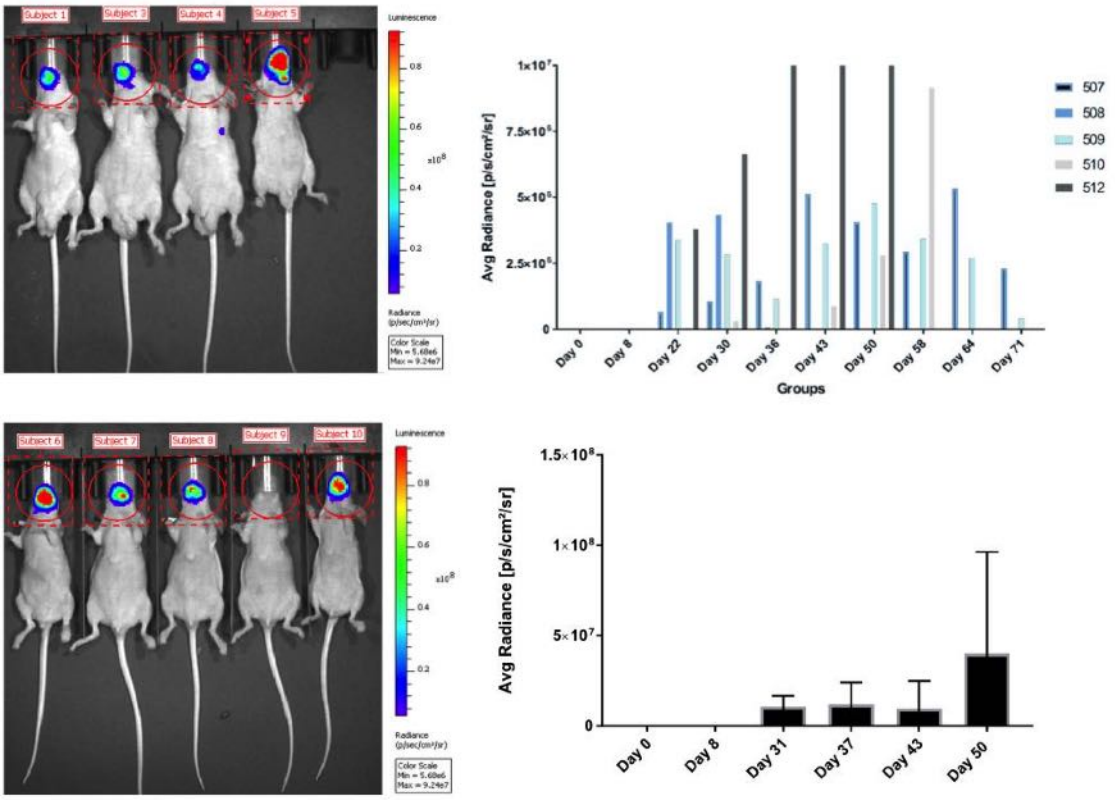

Figure 3.4: IVIS of the tongue tumor and quantification of the bioluminescence signal in males (graphs above). Quantification data for each mouse are reported. The graphs below report the signal and the quantification in females. Data are expressed as the mean±SD. The rectangle delimitates the region of each subject. The red circle represents the ROI for the tongue tumor.

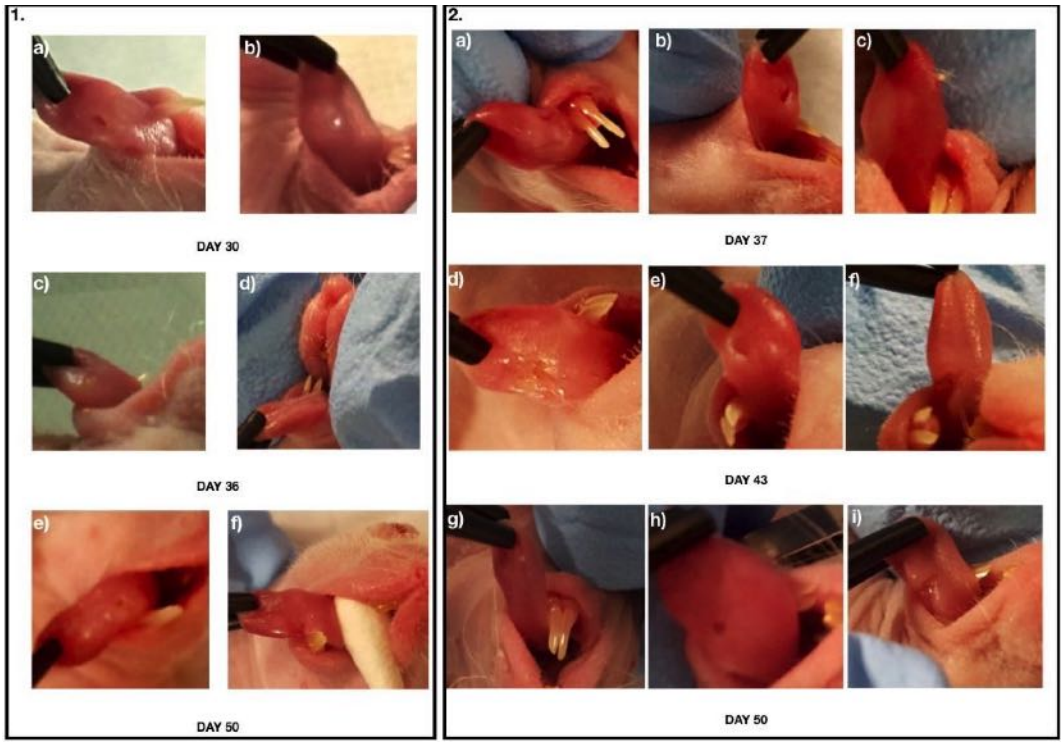

Figure 3.5: Representative pictures of the primary tongue tumor in nude male (1) and female mice (2) at different time points. The left middle portion of the tongue appeared enlarged in most animals. Fig. g) represents a mouse without the primary tumor. The tumor was identified by the discoloration of the tongue. Ulcerations of different dimensions were also present in some cases (1: a, e; 2: b, h). In a mouse, the ulceration occupied part of the left margin of the tongue(Fig f, i).

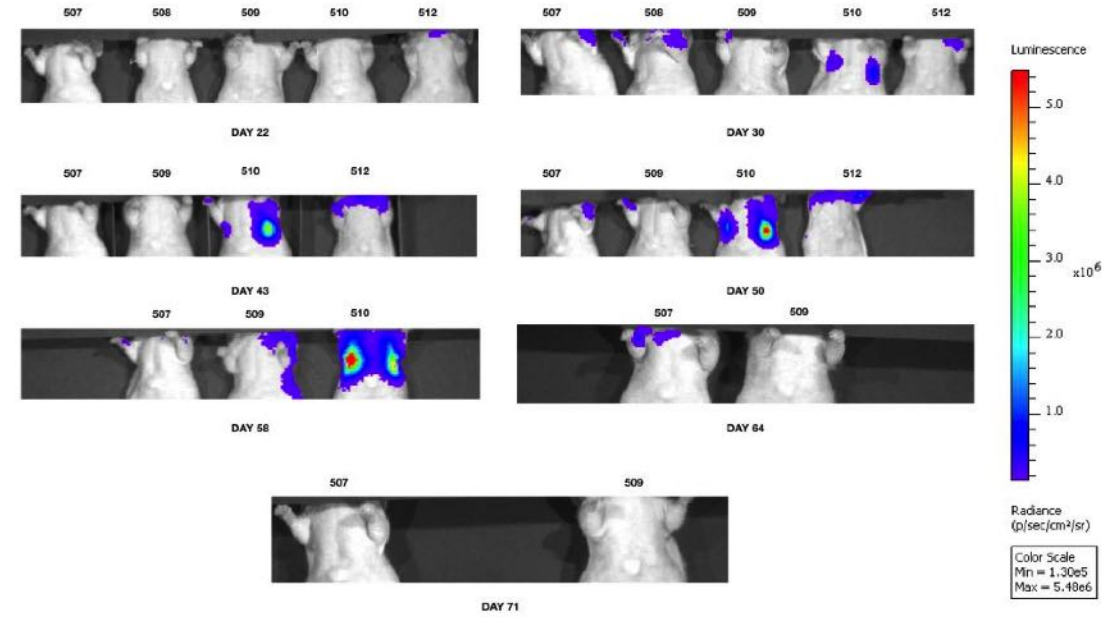

(a)

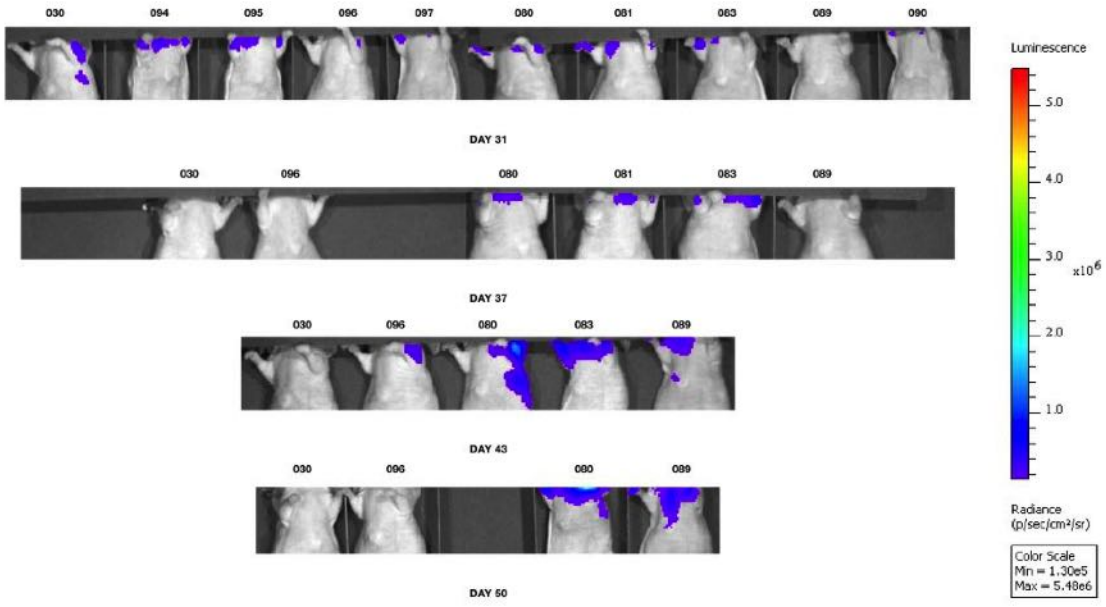

(b)

Figure 3.6: IVIS for lung metastases in male (a) and female athymic nude mice (b): the mouse 510 presented large lung metastases 30 days after the injection. Lung metastases were not detected in females from 31 to 50 days after the injection.

decreased after day 58 (Fig. 3.3 a). As mentioned previously, the primary tumor of these two mice had different dimensions and a different growth (Fig. 3.4). No clear signal from regional lymph node metastases was observed in females (Fig. 3.3 b).

3.2.5 Necropsy and *ex vivo* IVIS of mice organs

Representative pictures of the tongue tumor, lymph node metastases, and lungs at necropsy are reported in Figg. 3.7 - 3.8. The tongue tumor was mainly located on the left side of the tongue, but in several cases, the right side was also involved, especially in females (Fig. 3.8). The tumor presented as a medium-large yellowish-whitish mass with undefined margins in the middle and anterior portion of the tongue. In a few cases, ulcerations were present (small arrows). Lung metastases were not clearly macroscopically observed, except for the mouse 510. Indeed, this mouse presented several coalescent large white metastatic nodules in the lungs 60 days after the injection (Fig. 3.7). Lymph node metastases were macroscopically evident in some animals as yellow masses with undefined margins (small arrows).

Ex vivo IVIS of the tongue, regional lymph nodes, lung, spleen, and liver was also performed to show the presence of tumor and metastases (Figg. 3.7 - 3.8). The tongue tumor was evident in all the 4 nude male mice. Interestingly, the mice 508 and 512 sacrificed at early time points (43-55 days after the injection) presented larger tongue tumors than those of the animals 507 and 509, sacrificed 77 days after the injection (Fig. 3.7). In addition, the mice 508 and 512 in which lung metastases were not observed at IVIS (Fig. 3.6 a), presented metastatic nodules in the lungs. In addition, lymph node metastases were detected in 3/4 mice by *ex vivo* IVIS. Interestingly, the mice with lung metastases (508 and 512) presented large lymph node metastases, in contrast to the mouse 507 which had a small one. The metastases involved principally the left regional lymph nodes. In the mouse 512, some tumor cells were visible also in the right regional lymph node (Fig. 3.7).

In female nude mice, large tongue tumors were observed 32-34 days (Fig. 3.8, mice 094, 095) and 56 days after the injection (Fig. 3.8, mouse 080). No tongue tumor was detected in mice 030, 089 and 096. Lung metastases were observed only in two mice (Fig. 3.8, mice 094 and 080) and they were smaller than the ones in male mice (Fig. 3.7, mice 512 and 508). Also in females, the mice with lung metastases had lymph node metastases, one of which was bilateral (Fig. 3.8, mouse 080). Four more female mice presented lymph node metastases, while no metastases were detected in the mice without the primary tumor.

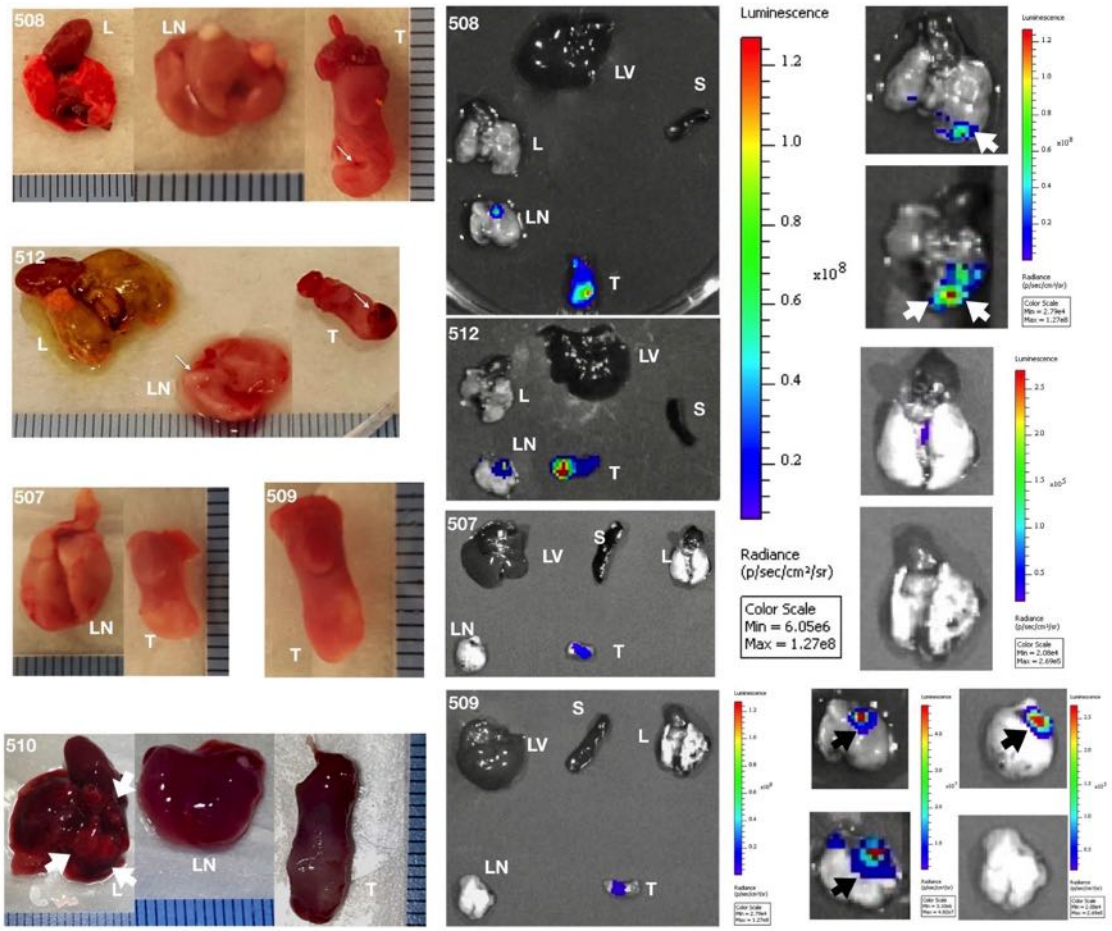

Figure 3.7: Necropsy and *ex vivo* IVIS of male mice tumor and organs. Representative pictures of the tongue (T), regional lymph nodes with salivary glands (LN) and lungs (L) of all 5 mice (507-510, 512). Large lung metastases observed in mouse 510 (arrows). *Ex vivo* IVIS of the tongue (T), lymph node (LN), lungs (L), liver (LV), and spleen (S) of 4 mice. Black and white arrows indicate the presence of lymph node and lung metastases respectively. Lung and lymph node metastases were observed macroscopically or by IVIS in 3/5 mice. No liver metastases were observed.

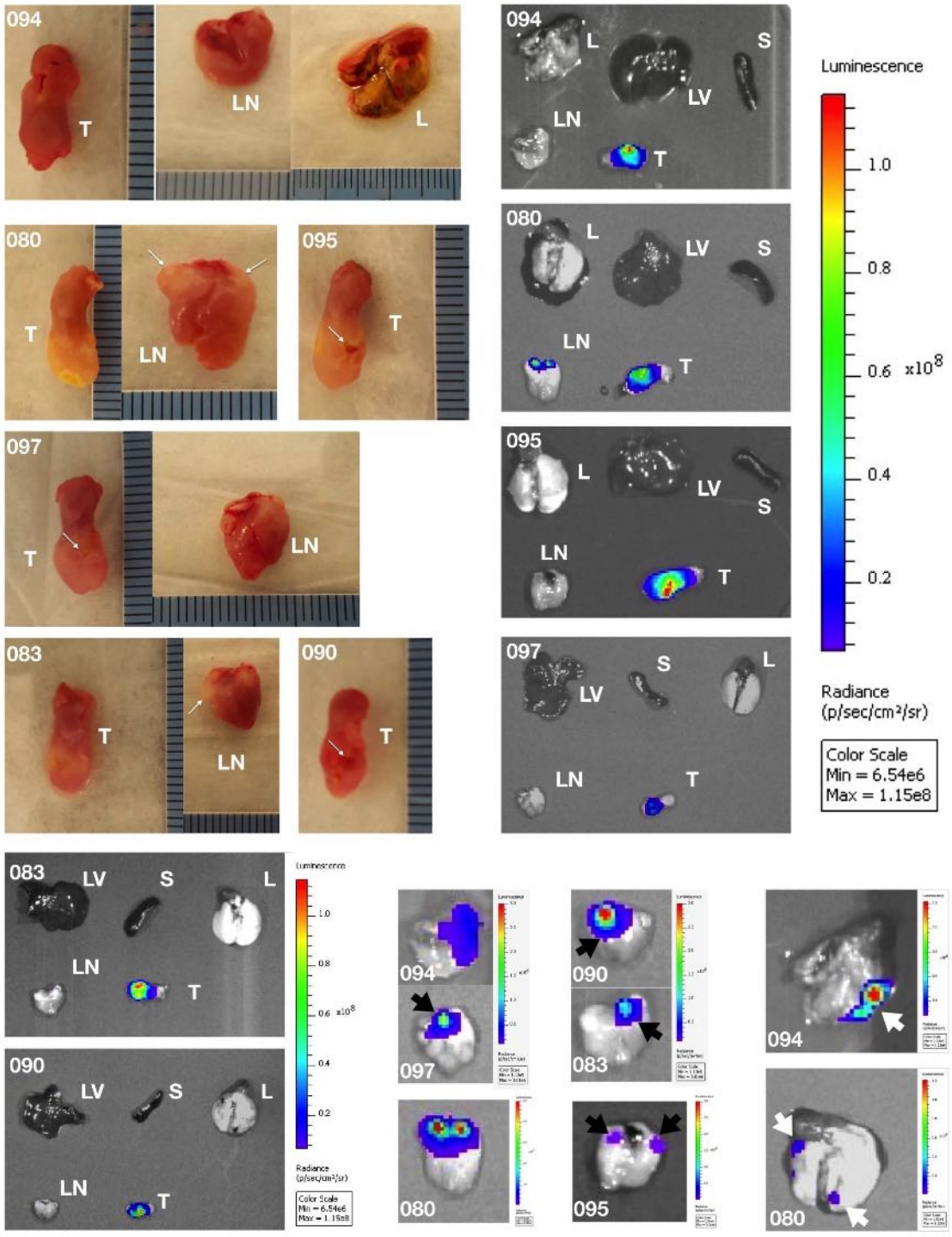

Figure 3.8: Necropsy and *ex vivo* IVIS of female mice tumor and organs. Representative pictures of the tongue (T), regional lymph nodes with salivary glands (LN) and lungs (L) of 6 mice. *Ex vivo* IVIS of the tongue (T), lymph node (LN), lungs (L), liver (LV), and spleen (S) of 6 mice. Black and white arrows indicate the presence of lymph node and lung metastases respectively. Lung metastases were observed in 2\7 mice. No liver metastases were observed.

3.2.6 Histology and immunohistochemistry

The presence of the tongue tumor and metastases was further confirmed by H&E and staining for human CK. Representative images of the tongue tumor, regional lymph node, and lung metastases are reported in Figg. 3.9 - 3.17.

Primary tumor

In the tongue, the tumor was mainly located in the middle portion. The anterior portion of the tongue was involved in some cases, especially in females (Fig. 3.10). The difference in the dimension and intensity of signal between the tongue tumors observed by *ex vivo* IVIS in male mice (Fig. 3.7) was histologically confirmed (Fig. 3.9). In the large tumors, the growth was highly infiltrative with the invasion of the deep muscular layers. In the mice sacrificed at late time points (507 and 509), the tumor was smaller and was located only in the superficial layers of the muscle (Fig. 3.9 a, b). Interestingly, the mouse 509, whose tumor signal was decreased by IVIS (Figg. 3.3 - 3.4) seemed to be capsulated (Fig. 3.9, g-h). In contrast, there was no difference between the tongue tumors in female athymic nude mice. As previously observed by IVIS, all the tumors extended from the middle to the anterior portion of the tongue. In some cases, histological analysis of the primary tumors showed infiltration of the deep muscular layers close to the ventral epithelium (Fig. 3.10).

The cellular architecture was similar among the tongue tumors developed in both male and female nude mice and it was typical of a moderate/poorly differentiated OSCC. Indeed, most tumor cells formed several islands and/or cellular cords surrounded by some stroma. Few keratinization areas were present (Fig. 3.9, a-d; Fig. 3.10, a, e). At a greater magnification, tumor cells exhibited several features of malignancy in both sexes of mice: round to spindle morphology (pleomorphism), altered nuclear-cytoplasmic ratio, anisocytosis, anisokaryosis, prominent and/or multiple nucleoli, and nuclear atypia (Figg. 3.9-3.10).

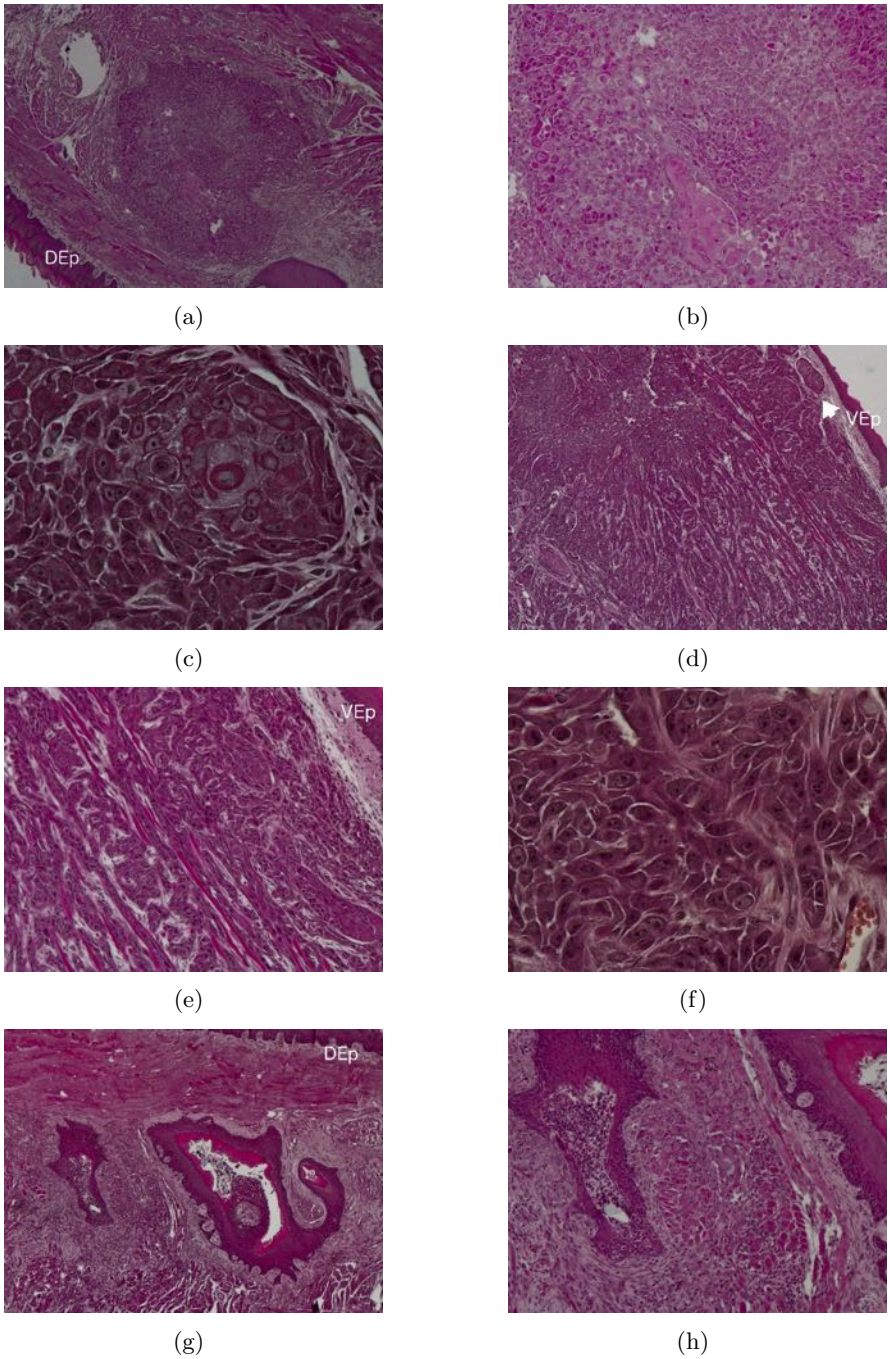

Figure 3.9: Representative pictures of tongue tumors in male athymic nude mice at different magnifications (40x, 100x, 400x): a-c represent a small tongue tumor, observed 11 weeks after the injection (40x, 100x, 400x). Tumor cells were organized in nests and presented keratinization. The tongue tumor at early time points (d-f) was highly invasive and it extended into the ventral portion of the tongue. Cancer cells were grouped in nests or in cord-like structures surrounded by abundant stroma. Atypia and keratinization (white arrows) were also present. In the mouse 509 (g-h), the tumor was located in the superficial layers of the muscle and displayed a high grade of keratinization. Some lymphocytes and fibrocytes were also present (40x, 100x). DEp= dorsal epithelium, VEp= ventral epithelium.

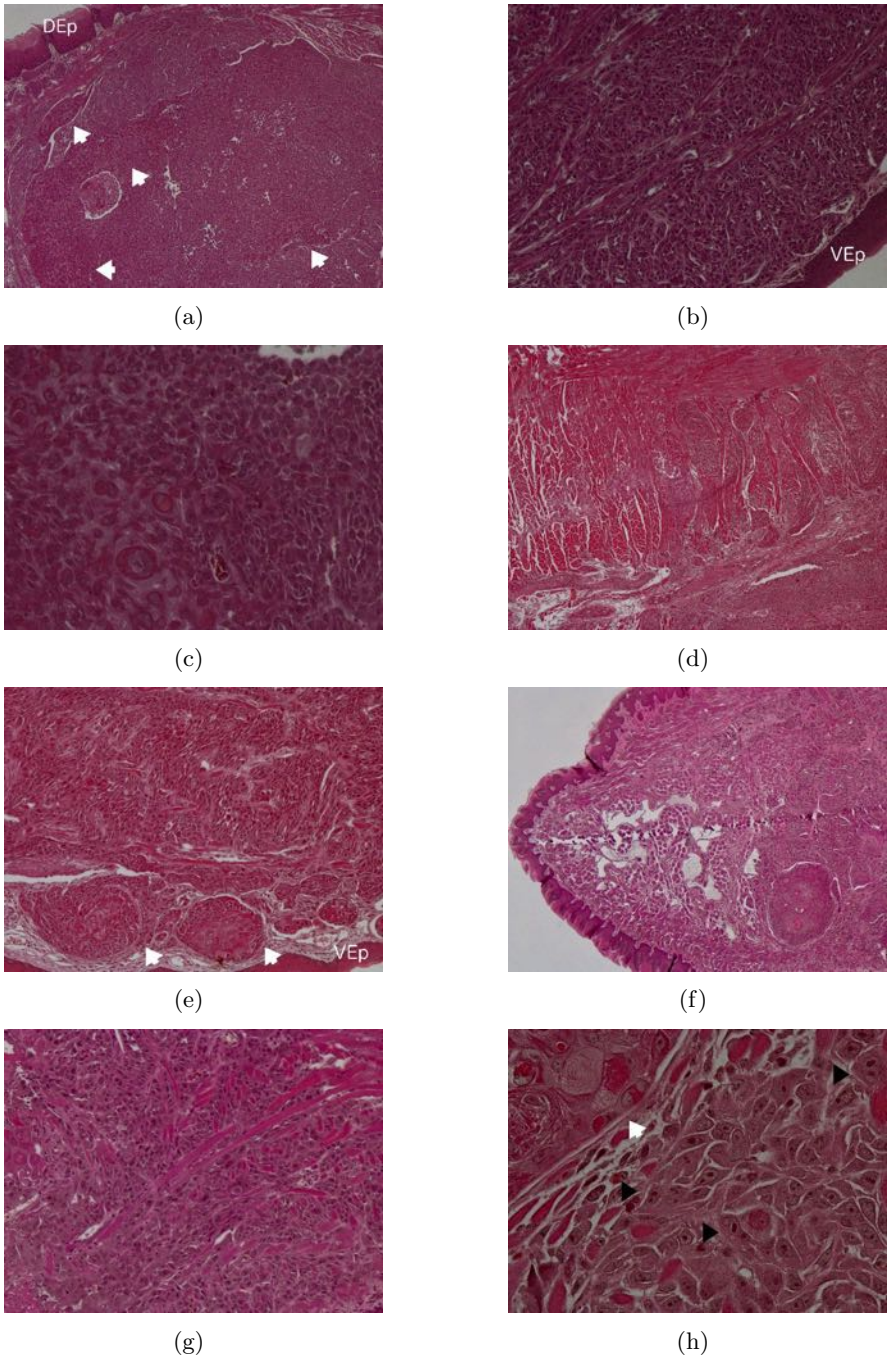

(a) (b) (c) (d) (e) (f) (g) (h)

Figure 3.10: Representative pictures of tongue tumors in female athymic nude mice: a-c represent a tongue tumor at 36 days after the injection (40x, 100x, 200x). The tumor presented a high cellularity and a deep infiltration of the muscle layer. Some keratinized areas were also present (white arrows). The same extensive growth and keratinization were also observed 44 days after the injection (d-e; 40x, 100x). In some cases, the apical portion of the tongue was also invaded by the tumor (g). Tumor cells formed several cellular islets and presented marked atypia, with pleomorphism and different nuclear size and shape (h, 400x). Some mitotic figures were also present (black arrows). DEp= dorsal epithelium, VEp= ventral epithelium.

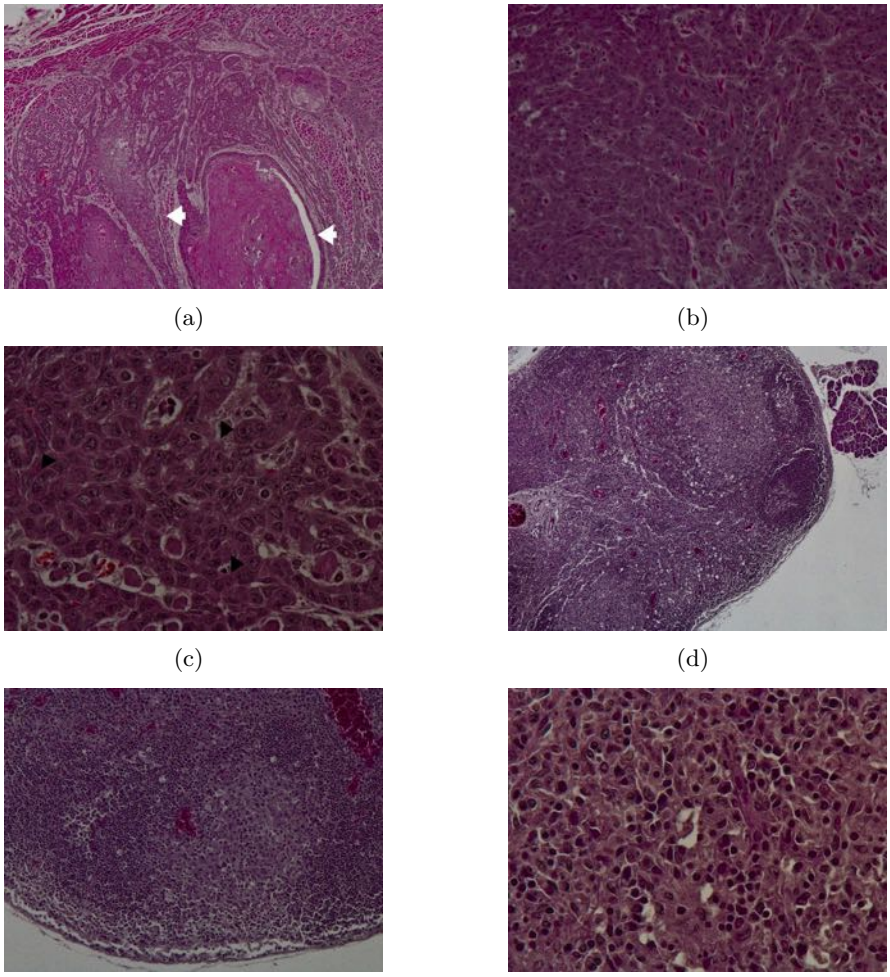

Figure 3.11: Representative pictures of the tongue tumor of mouse 510 at 40x, 100x, 400x (a-c): areas with a high cell density and high cellular keratinization (white arrows) were observed. At 400x, cells presented several features of malignancy, with a marked pleomorphism and severe nuclear atypia (black arrows). d-f regional lymph node (40x, 100x, 400x): tumor cells formed metastatic nodules in the lymph node cortex. At a greater magnification, tumor cells with large nuclei and prominent nucleoli between lymphocytes.

Lymph node and lung metastasis

The presence of lymph node metastases was first evaluated by H&E staining. Metastatic areas were located in the subcapsular sinus and/or in the cortex of the lymph nodes, especially in males (Figg 3.11-3-13). In some cases, tumor cells organized in cell nests formed large nodules surrounded by lymphocytes (Figg. 3.11-3.12). As in the tongue, nuclear atypia, prominent nucleoli and altered nuclear-cytoplasmic ratio were common features of the tumor cells in the lymph nodes.

Representative pictures of lung metastases in male (510, 508, 512) and female mice (094, 080) are reported in Fig. 3.14 and 3.15 respectively. In the mouse 510, tumor cells infiltrated diffusely the lung parenchyma, forming also keratin pearls (Fig. 3.14 a,b). In the other two males and in female nude mice, the cellular invasion of lung parenchyma was less diffuse, with the formation of metastatic nodules of different dimensions (Fig. 3.14 d-h; Fig. 3.15 a, b, d). As in the tongue and in the lymph nodes, cells formed islands in some cases (Fig. 3.14 a, b, e; Fig. 3.15 b) and presented altered nuclear-cytoplasmic ratio, pleomorphism, and atypia (Fig. 3.14 c, f; Fig. 3.15 d).

Cytokeratin expression

All tongue tumors were strongly positive to CK, with some tumor areas more positive than the others (Fig. 3.16 d, e). A lower expression of CK was found in the metastatic cells which invaded the subcapsular sinus and the cortex in the regional lymph nodes. The expression of pan-CK was cytoplasmic in the cells of the primary tumor, while metastatic cells expressed CK mostly on the membrane (Fig. 3.16 j-l).

Also in the lungs, not all tumor cells presented a high expression of CK, except for the mouse 510, in which several islands of metastatic cells were strongly positive for CK (Fig. 3.17 d-f). However, other tumor areas had a low expression of CK. In the other mice, the majority of the tumor cells presented a low or moderate expression of CK, with some tumor areas negative for CK (Fig. 3.17 j-l; m,n). The expression of CK was either cytoplasmic or on the membrane of metastatic cells. Small tumor areas expressing CK were found in some mice without visible lung metastases by IVIS (Fig. 3.17, o).

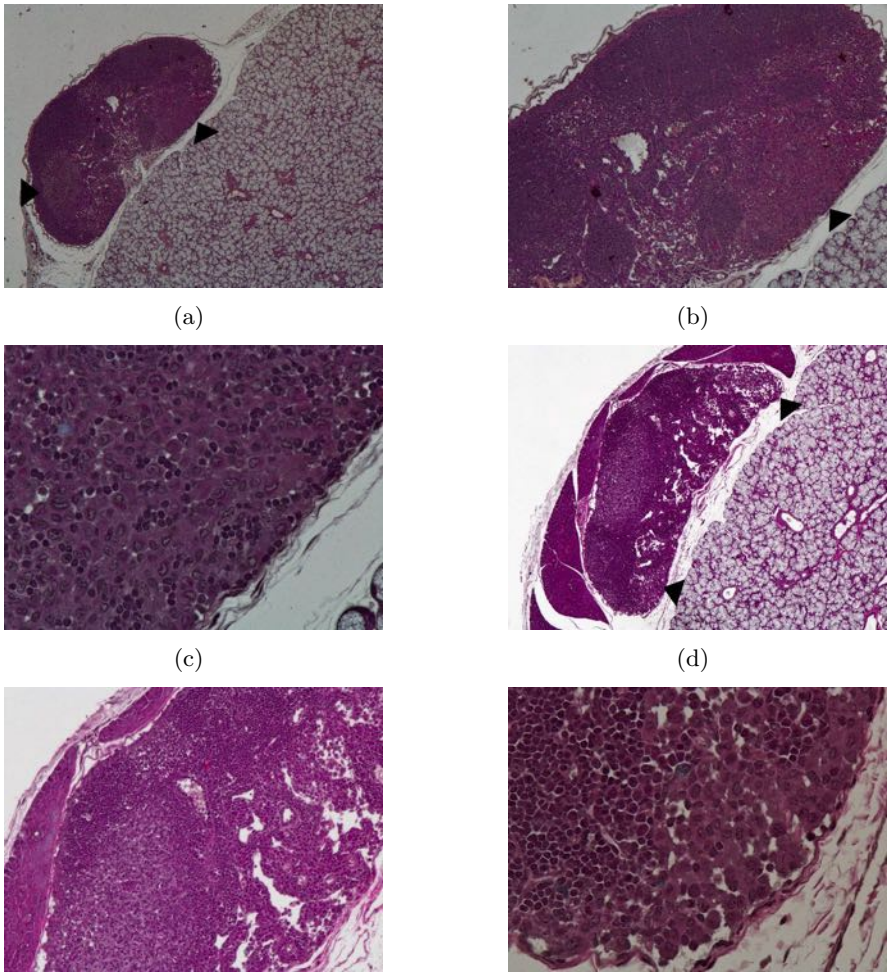

Figure 3.12: Representative pictures of regional lymph node metastasis in athymic nude male mice at different magnifications (40x, 100x, 400x): tumor cells were located into the subcapsular sinus and extended into the cortex 11 weeks (a-c) and 6 weeks (d-f) after the injection (black arrows). In both cases, metastatic cells had the same features of the primary tumor (cells grouped in nests with prominent nucleoli, nuclear atypia).

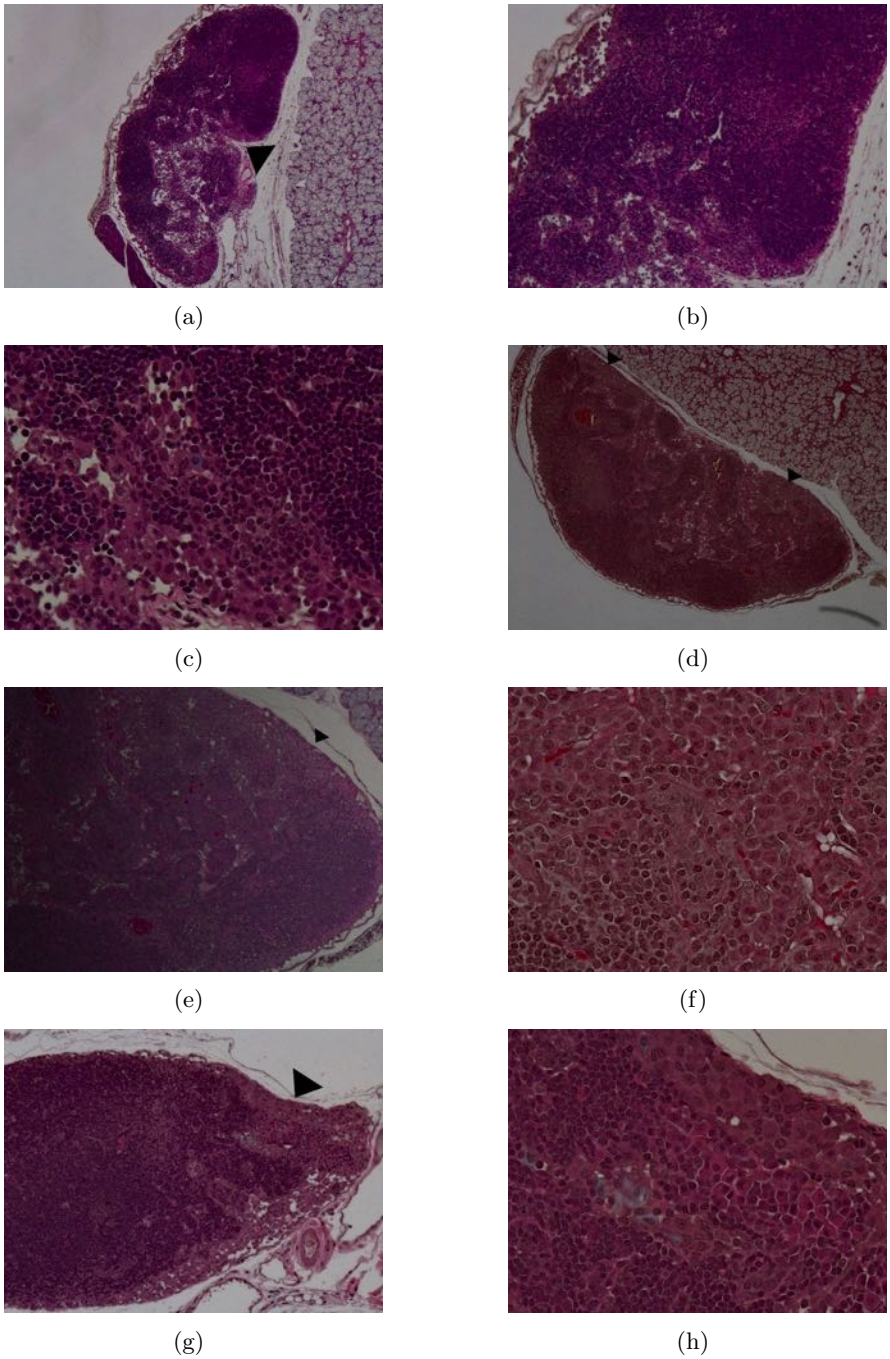

Figure 3.13: Representative pictures of regional lymph node metastasis in athymic nude female mice at 40x (a, d), 100x (b, g), 200x (e), and 400x (c, f, h): tumor cells were located into the subcapsular sinus and in some cases infiltrated into the cortex (arrows) (d-f). At a greater magnification, metastatic cells could be recognized by nuclear atypia and prominent nucleoli (c, f, h).

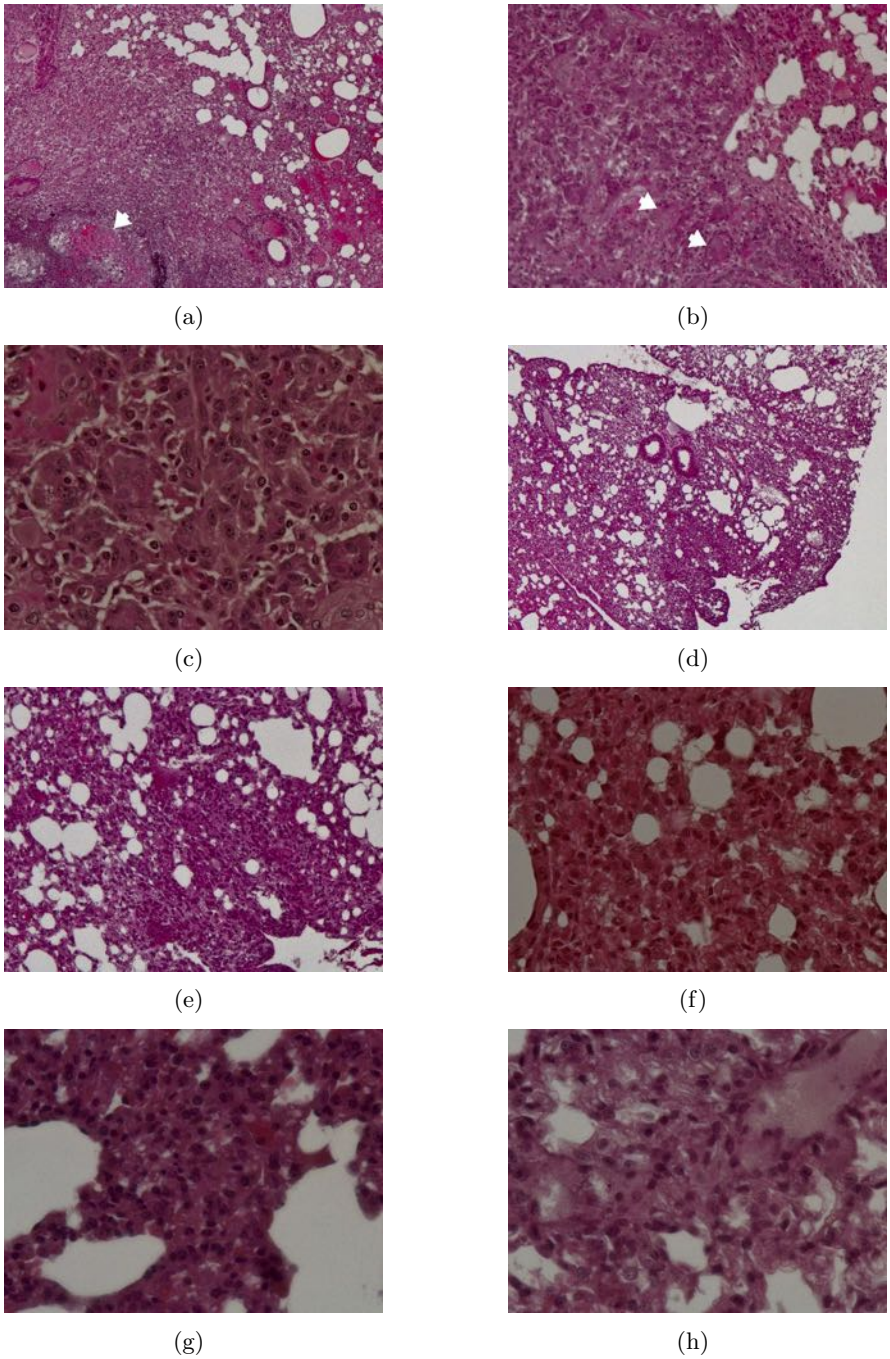

Figure 3.14: Representative pictures of lung metastasis in mice 510 (a-c), 508 (d-f), and 507-509 (g-h) at different magnifications (40x, 100x, 400x). In the first mouse, whose lung metastases were also macroscopically observed, tumor cells invaded the whole lung parenchyma. Cellular nests and areas of keratinization with pyknotic nuclei were also present (a, b, arrows). In the other mouse, metastatic nodules of different dimensions were present (d-e, g-h). Tumor cells displayed nuclear atypia, prominent nuclei and assumed various shapes (f), especially in mouse 510 (c). Interestingly, compact cellular aggregations were observed in the mice in which lung metastases were not detected by IVIS (g,h; 40x). At a greater magnification, these cells were atypic.

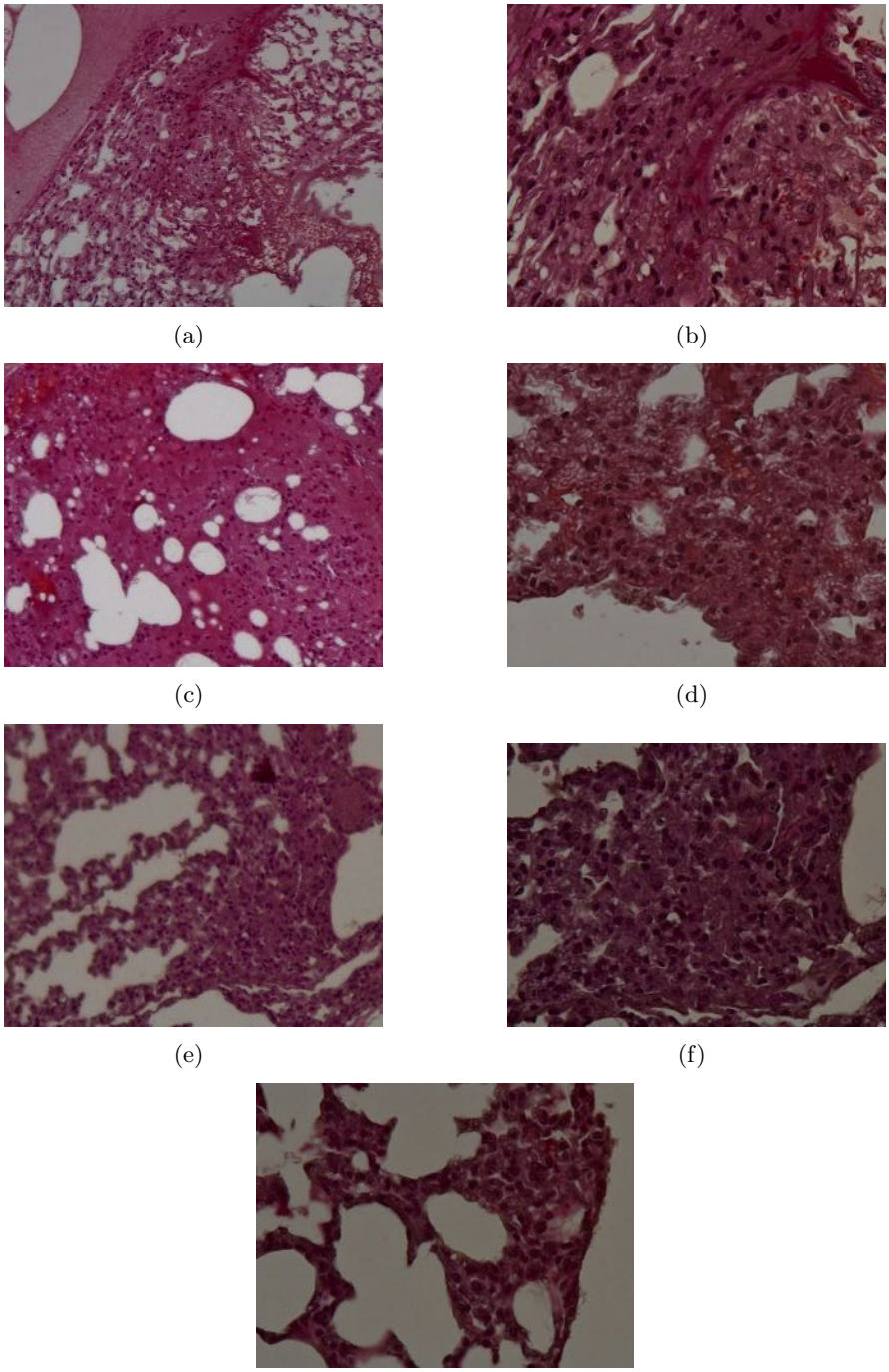

(a) (b) (c) (d) (e) (f) (g)

Figure 3.15: Representative pictures of lung metastasis in female mice at 100x (a, c), 200x (e), and 400x (b, d, e, f, g). Metastatic nodules were present within the lung parenchyma (a, c). At a greater magnification, tumor cells displayed atypia (nuclear atypia, pleomorphism). As in the male mice, cellular aggregations were present also in the lungs of the mice which did not present lung metastases by IVIS (e-g). Indeed, some atypic cells were observed in some areas of the lung.

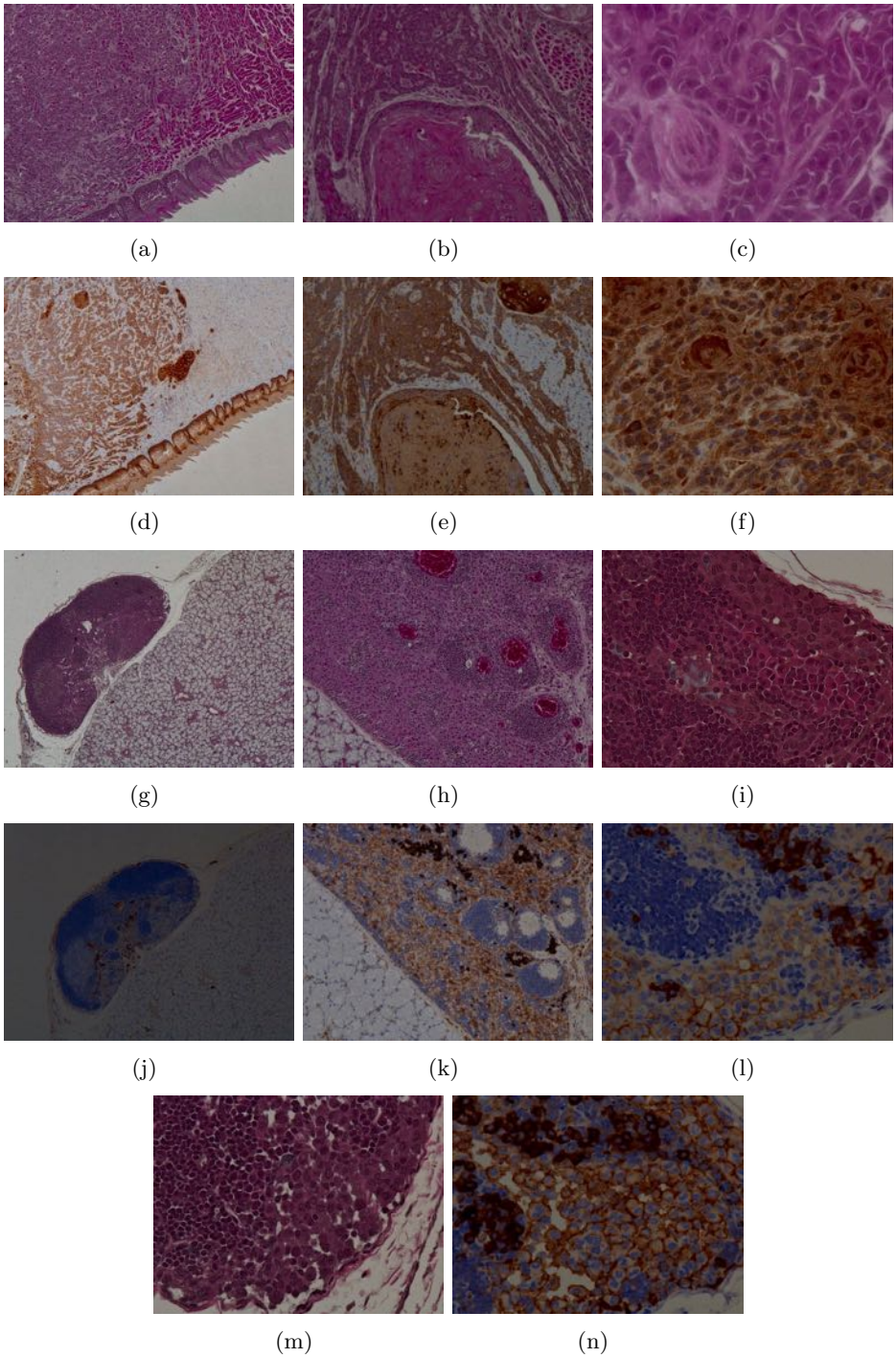

Figure 3.16: Representative pictures of H&E and IHC for cytokeratin (CK) of the primary tumor (a-f) and lymph node metastases (g-n) in athymic nude female and male mice at 40x, 100x and 400x. The tongue tumor was positive for CK. Some groups of tumor cells had a high expression of CK (d, e). CK-positive tumor cells were also located into the subcapsular sinus and in the cortex of the regional lymph nodes (j-l). The expression of CK was mostly on the membrane. Non-specific cytoplasmic staining of plasma cells. Various degree of CK expression was also observed in the metastatic cells (j-l, n).

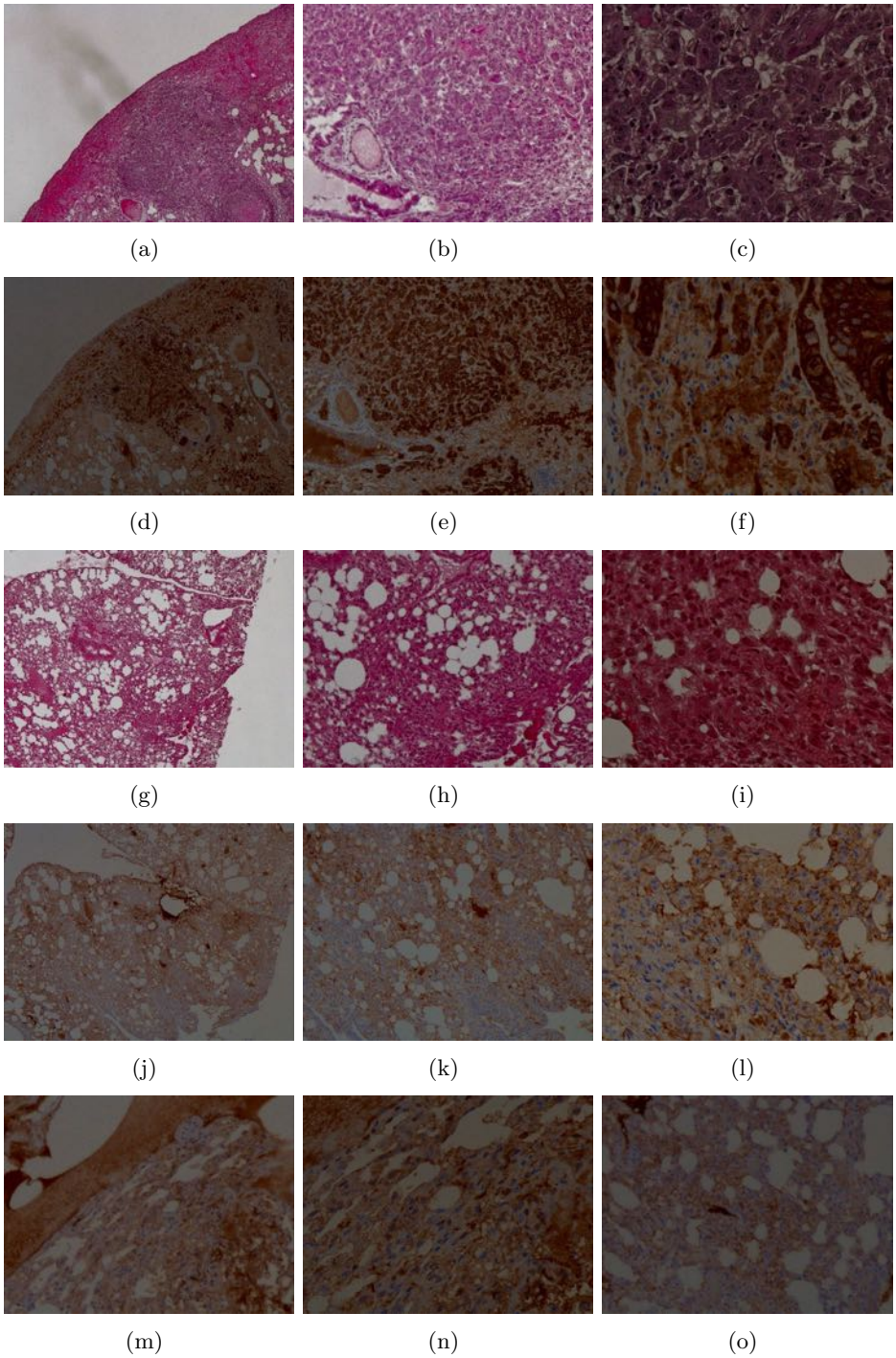

Figure 3.17: Representative pictures of H&E and IHC for CK of lung metastases in athymic nude female and male mice at 40x, 100x, and 400x. Tumor areas displayed various degrees of CK expression: in the mouse 510, several cells were strongly positive for CK, while a low or absent expression of CK was observed in other tumor areas. In the other mice, most of the tumor cells in the lungs presented a low-moderate expression of CK, with some tumor areas negative for CK. At a greater magnification, these cells displayed a marked atypia (f, l, n). A few areas positive for CK were also found in some mice, in which lung metastases were not observed by IVIS (o, 200x). Non-specific staining of plasma in blood vessels was present.

Chapter 4

Development of a model of OSCC lung metastasis

4.1 Materials and Methods

Generation of the HSC-3 GFP/Luc M1 cell line All animal experiments were approved by the IACUC at the Houston Methodist Research Institute in accordance to the National Institutes of Health Guide for the Care and Use of Laboratory Animals.

Five athymic nude-Foxn1nu mice (Envigo), male, 5-6 weeks old, weight 24.84 $\pm$ 2.15, were injected with 1 x 10^5 HSC-3 GFP/Luc cells in 100 μl of PBS into the tail vein (day 0). IVIS Spectrum In-Vivo Imaging System (Perkin Elmer Inc., Waltham, MA) was performed weekly to monitor the growth of lung metastases following the same procedure reported in the Material and Methods of Chapter 3.

Thirty-four days after the injection, one mouse with large lung metastases was sacrificed. Both lungs were removed and were minced into small pieces with scissors and scalpel. The minced tissue underwent enzymatic dissociation using collagenase IV at a concentration of 0.7 mg\ml in D-PBS and incubated at 37°C for 50-60 minutes. The digestion product was then filtered using a 70 μm cell strainer (Fisherbrand ^{TM}) and plated in a 10 cm Petri dish in DMEM 10 % FBS plus 2 % of PS for the first 3 days. The cells were then expanded *in vitro* in media 10% FBS plus 1% of PS .

After a few passages, the cells were sorted for GFP expression as described in the Material and Methods of Chapter 3 to select only the human tumor cells. After sorting, pure HSC-3 GFP/Luc M1 cells were obtained and were allowed to grow in the normal media. The Luc expression of HSC3 GFP/Luc

M1 cells was then confirmed by IVIS, using the same procedure described in the Material and Methods of Chapter 3.

Development of a model of OSCC lung metastasis with HSC-3 GFP/Luc M1 cells To evaluate the *in vivo* metastatic potential of HSC-3 GFP/Luc M1 cells, 5 athymic nude Foxn1nu mice (Envigo), female, 7-8 weeks old, weight 21.22 $\pm$ 0.70, were injected with 0.5 x 10^6 cells in 100 μl of PBS into the tail vein. The growth of lung metastases was monitored periodically by IVIS. All mice were humanely sacrificed through an overdose of isoflurane and cervical dislocation 46 days after the injection.

Ex vivo IVIS of the lungs, heart, liver, and spleen was then performed. The organs were fixed in Bouin′s solution (lungs) or in 10% buffered formalin solution (all other tissues) and embedded in paraffin as reported in the Material and Methods of Chapter 3. The presence of lung metastases was further confirmed by H&E staining. Pictures were taken using an upright microscope system (Nikon Eclipse 80i).

4.2 Results

The aim of the present study was to establish a lung metastasis model of OSCC by injection into the tail vein. Despite the limitations of this model, it is widely used to reproduce lung metastases of different type of cancers. In addition, it has been reported that lung metastases established through the tail vein injection of tumor cells may be similar to those obtained in orthotopic models[54]. In addition, several authors have reported an increased metastatic potential and a different gene expression between parental tumor cell lines and the same tumor cells isolated from metastases. These findings were reported regarding OSCC cells isolated from lymph node metastases by Masood et al.[49]. In addition, a few articles have been published on lung metastases of OSCC. For these reasons, a model of OSCC lung metastasis was established using HSC-3 cells isolated from lung metastases (HSC-3 GFP/Luc M1). In this new model, lung metastases were first observed 21 days after injection. Forty-six days after the injection, all five mice were sacrificed and the presence of lung metastases was evaluated by *ex vivo* IVIS and histology. The lung metastasis prevalence of this model was 60% (3\5) by *ex vivo* IVIS. The histological analysis confirmed the presence of the lung metastases and revealed compact cellular aggregations also in the lungs of the remaining 2 mice.

4.2.1 Isolation of HSC-3 GFP M1 cell line and cell sorting

One male mouse injected with 1 x 10^5 HSC-3 GFP/Luc cells started to develop lung metastases two weeks after the injection (Fig. 4.1 a). Lung

metastases continued to grow, developing a moderate bioluminescent signal 29 days after the injection. Thirty-four days after the injection, the mouse was sacrificed and the lungs with visible tumor masses were collected (Fig. 4.1 b, 1). At cell sorting, the cells isolated from the lungs had a good expression of GFP (FITC intensity between 10^4 and 10^5) and Luc (Fig. 4.1 b, 2, 3).

4.2.2 New model of lung metastasis with HSC-3 M1 GFP/Luc cell line

Evaluation of the lung metastases by IVIS

In this model, the development of lung metastases was not homogeneous among all the animals injected. Indeed, the first presence of lung metastases was observed 22 days after the injection in one mouse (Fig. 4.2 a, b). Two weeks later, two more mice presented large lung metastases, while no signal was observed in the remaining two mice (Fig. 4.2 c). All the mice were then sacrificed 46 days after the injection and *ex vivo* IVIS of the lungs, liver, and spleen was performed. Large lung metastases were detected in both lungs and the left lobe was more involved in two mice (Fig. 4.3) In the other mouse, the lung metastases occurred mainly in the right lobes. No lung abnormalities were observed in the remaining two mice.

Histology

Representative pictures of the H&E of the lungs are reported in Fig. 4.4. In the mice, in which lung metastases were already visible by IVIS, several coalescent metastatic nodules, which invaded a large section of the lungs were present. The cell density of the metastases was high, except for few areas where the cells seemed to be more scattered (a, b). The cell architecture consisted of nests with little (e) or abundant stroma (b, h). Few areas also presented keratinization (a, e, h, i). At a greater magnification, metastatic cells appeared pleomorphic, assuming a round, ovoid and spindle morphology. Other features of these cells included a prominent nucleolus, a marked anysokariosis, anysoanisocytosiscytosis, and nuclear atypia (f, i).

The histological analysis of the lungs of the remaining two mice revealed the presence of cellular aggregations in few areas (j-l). Such structures consisted of cells with a high variability in the nuclear size and shape and a prominent nucleolus. Therefore, they were identified as lung micrometastases. These histological findings also in the mice in which lung metastases were not previously detected by *ex vivo* IVIS revealed a high aggressivity of this new model of lung metastasis.

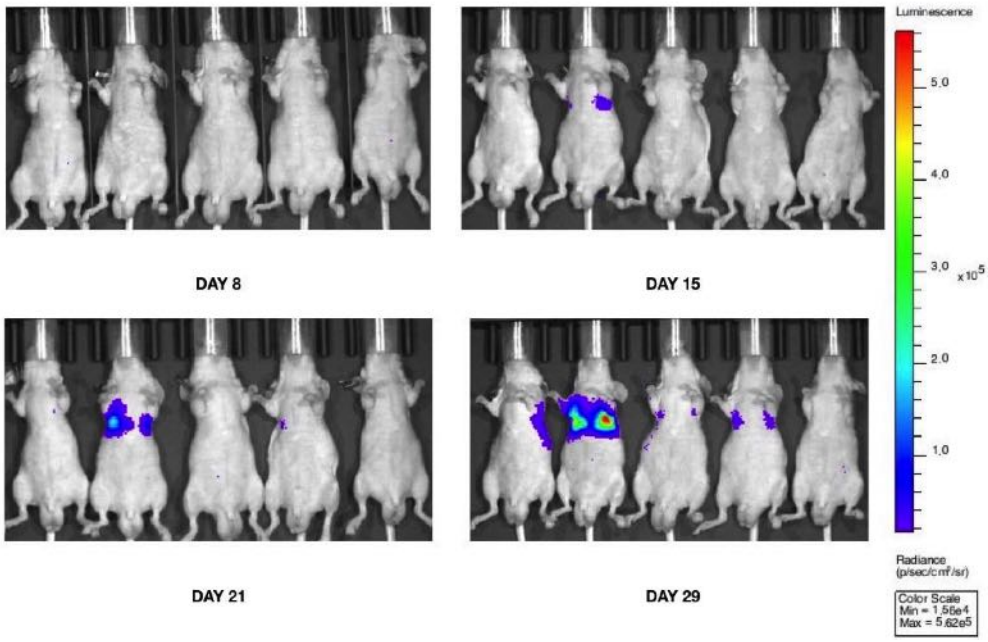

(a)

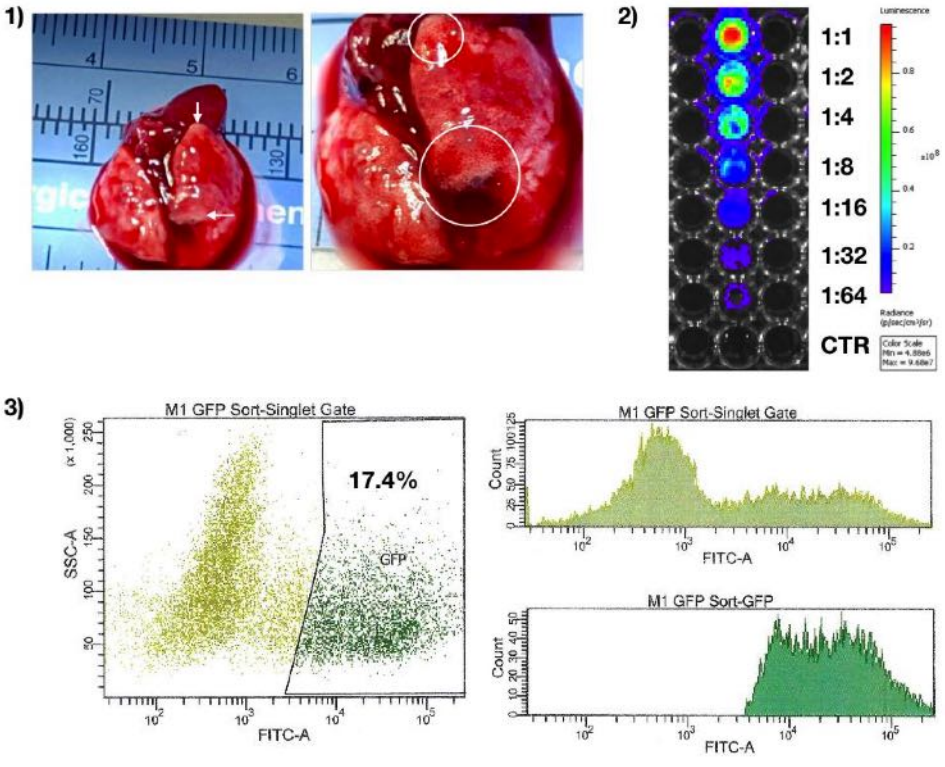

(b)

Figure 4.1: (a) IVIS for lung metastases: the mouse from which HSC-3 GFP M1 cell line was isolated developed already lung metastases from day 15. (b) 1. Pictures of the lungs at necropsy: macroscopic whitish tumor masses (arrows) 2. IVIS of HSC-3 GFP M1: initial concentration 0.5 x 10^6 cells/100μl. DMEM served as negative control. 3. Sorting of HSC-3 M1 cell line by GFP expression: positivity for GFP found in 17.4% of cells (BD FACSAria II Cell Sorter).

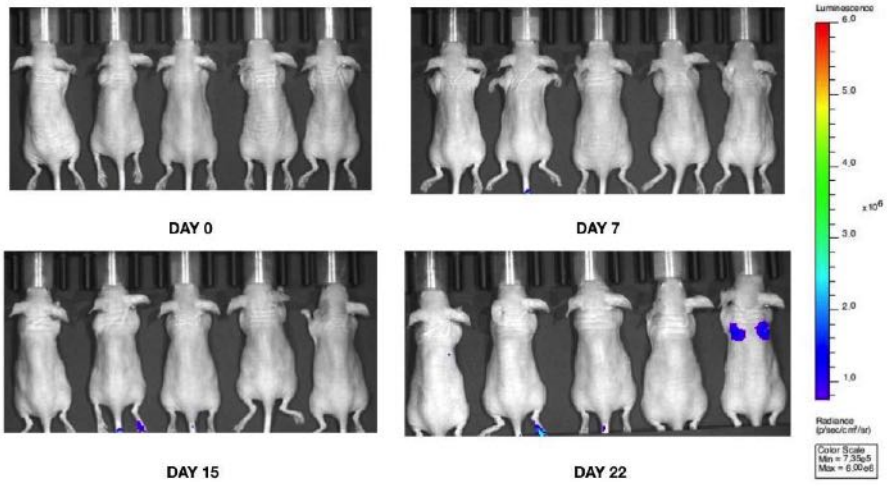

(a)

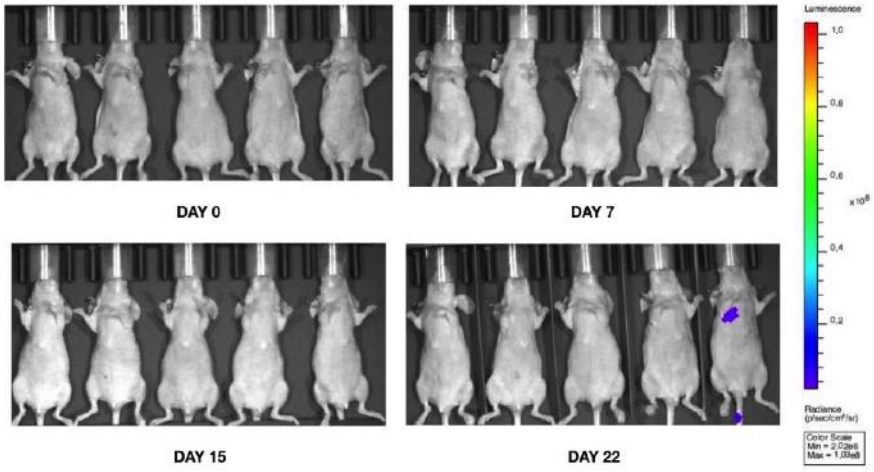

(b)

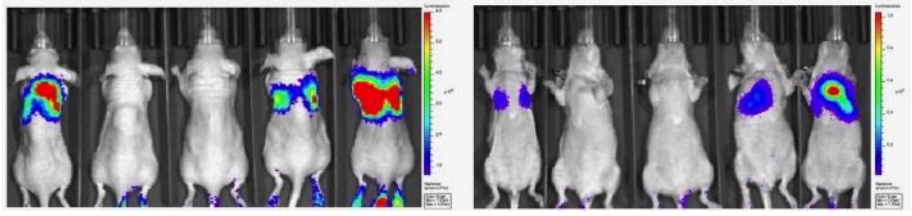

(c)

Figure 4.2: IVIS for lung metastases of the athymic nude mice faced on the back (a) and on the front (b): the first signal of moderate intensity from the lungs (10^6) was observed three weeks after the injection. (c) Five weeks after the injection, the signal was very intense in 3\5 mice (10^8), which developed large lung metastases.

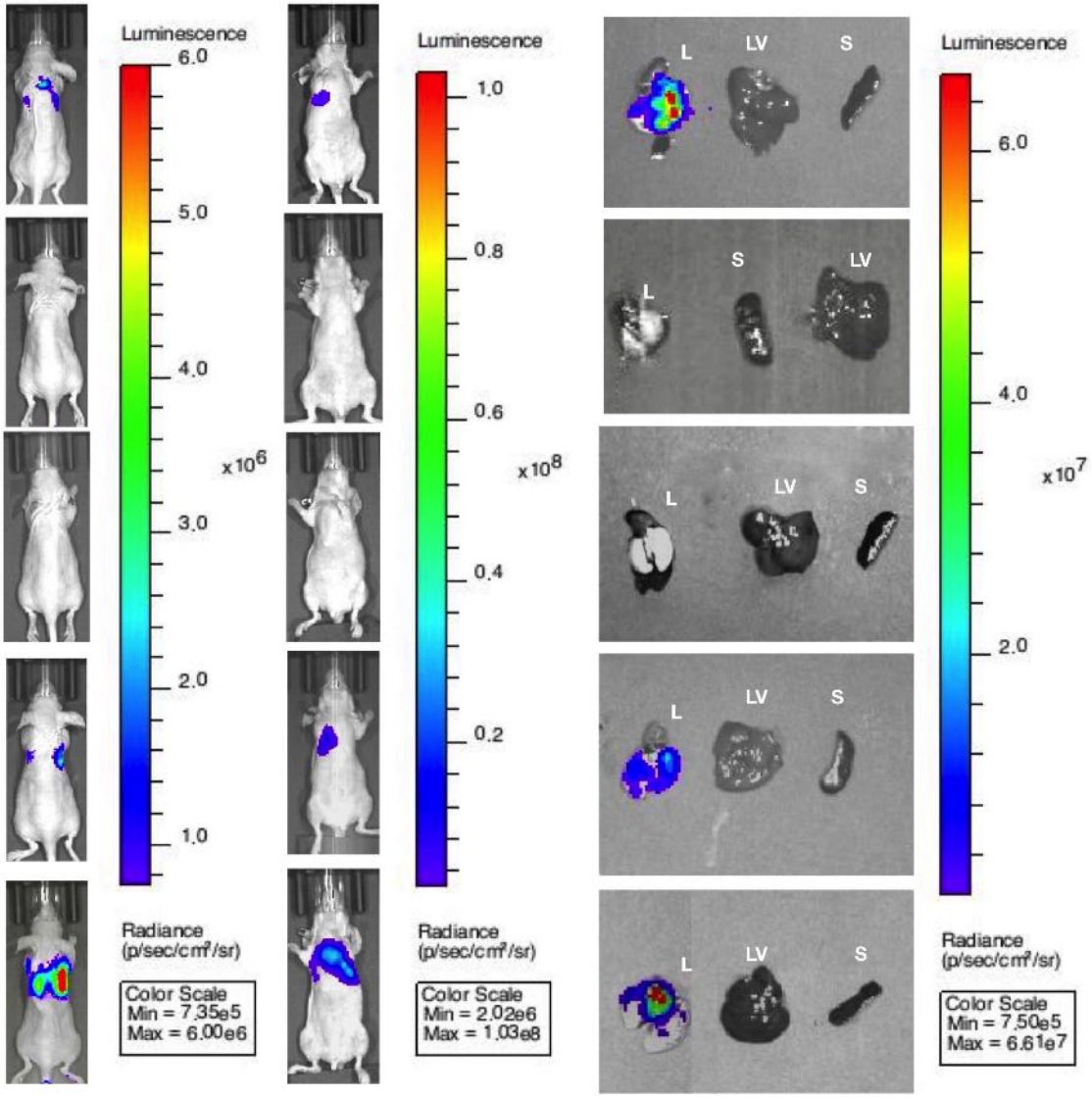

Figure 4.3: IVIS of the mice faced on the back and front 46 days after the injection (right). *Ex vivo* IVIS of the lung (L), liver (LV), and spleen (S) of all 5 mice (left). Large lung metastases were observed in 3/5 mice. No liver metastases were detected.

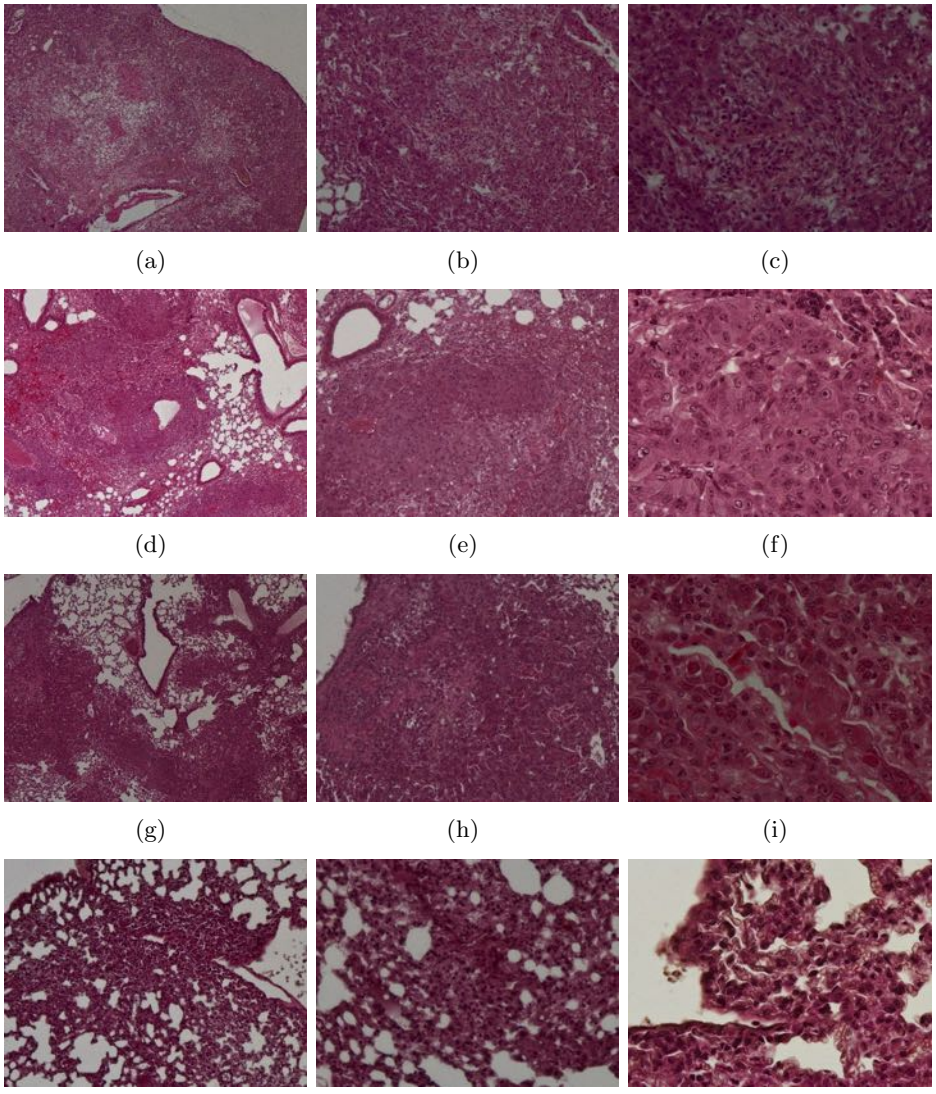

Figure 4.4: Representative pictures of lung metastases in the model with HSC3 GFP/Luc M1 at 40x, 100x, and 400x. (a)-(i): histology of the lung metastases already detected by *ex vivo* IVIS. A diffuse tumor cell infiltration was observed, with cell islands and keratinization areas. At a greater magnification, cell nuclei were different in size and shape (i, f). (j)-(l): histology of the lungs of the remaining two mice, in which micrometastases were observed. At a greater magnification, the tumor cells assumed a round to spindle morphology and had large nuclei with prominent/multiple nucleoli (l).

Chapter 5

Use of pDox on a new OSCC metastatic cell line

5.1 Materials and Methods

Cell line For the present experiment, the cell line HSC-3 GFP/Luc M1 was used. The procedure of cell isolation and the culture method are reported in the Material and Methods of Chapter 4.

Synthesis and preparation of pDox nanoparticles The procedures used to synthesize pDox and to form NPs are reported in the Material and Methods of Chapter 2.

MTS Assay HSC-3 GFP/Luc M1 cells were plated in a 96-well plate (3.5 x 10^3 cells per well) and incubated for 24 h to allow cell adhesion. After that, the cells were treated with different concentrations of doxorubicin and equimolar amounts of pDox NPs. After 72 and 96 h, cells viability was evaluated through MTS assay (Promega) according to the manufacturer′s protocol.

Uptake studies of pDox nanoparticles and free doxorubicin HSC-3 GFP/Luc M1 cells (2 x 10^4 cells per chamber) were seeded on 4-well chamber slides (BD Falcon) and incubated for 24 h. Cells were then treated with 5 μM of free doxorubicin and equimolar amounts of pDox NPs for 6 h and 24 h. When the endpoint was reached, cells were fixed and stained using the same procedure and reagents reported in the Material and Methods of Chapter 2. Z-stack images were then captured using a confocal microscope (Nikon A1 Confocal Imaging system) using the same method reported in the Material and Methods of Chapter 2.

Statistical analysis Statistical analyses were performed using one-way analysis of variance (ANOVA) with the GraphPad Prism software. Differences at $p < 0.05$ were considered to be statistically significant.

5.2 Results

After the isolation of the OSCC cell line HSC-3 GFP/Luc M1 and the development of a highly aggressive lung metastatic model *in vivo*, these cells were treated with the free form of doxorubicin and pDox NPs. The aim of the viability assay and the qualitative uptake study was to collect preliminary data on the response of the new cell line to these treatments. Indeed, some articles have been published, reporting a difference between parental tumor cells and tumor cells isolated from the metastases. In OSCC, little is known about lung metastases and the possible effective therapeutic strategies to adopt. Interestingly, the viability assay after 72 and 96 h of treatment with pDox NPs and doxorubicin and the cellular uptake study conducted on HSC-3 GFP/Luc M1 did not show different results from the ones reported for HSC-3 cells (see 2.2.1).

5.2.1 Viability assay for HSC-3 GFP/Luc M1 cells after treatment with doxorubicin and pDox NPs

Results obtained from MTS assay of HSC-3 GFP/Luc M1 cells treated with different concentrations of the free form of doxorubicin and the pDox NPs are summarized in Fig. 5.1. The treatment with high concentrations of the free form of doxorubicin (0.5 and 1 μM) resulted in a significantly lower cell viability than controls at both time points. However, there was no statistically significant difference between the cell treatment with 0.5 and 1 μM of doxorubicin. In addition, the cells treated for 96 hours had a lower viability than those of cells treated for 72 hours.

The measurements of the size of pDox NPs were performed using intensity average. The average size of pDox NPs was 129.1 $\pm$ 9.214 nm. After 72 h of treatment, no significant effect of pDox NPs on the cell viability was observed, while the treatment with 0.5 and 1 μM pDox NPs resulted in a significant cytotoxic effect after 96 h of treatment (Fig. 5.1 a, b).

Additionally, doxorubicin exerted significantly more cytotoxic effect than pDox NPs at 72 (a) and 96 h (b) in this metastatic cell line of OSCC. However, the difference between the treatment with the highest dosage of the free form of doxorubicin and pDox NPs was statistically significant after 72 h (P=0.028), but not after 96 h (P=0.189). This finding proved that both doxorubicin and pDox NPs may be effective in killing the metastatic

HSC-3 GFP/Luc M1 cell line, as well as the parental cells HSC-3 (see 2.2.1). No statistically significant difference was observed between the viability of the two cell lines treated with doxorubicin or pDox NPs.

5.2.2 Cellular uptake study of pDox NPs and free doxorubicin in HSC-3 GFP/Luc M1 cells

Fig. 5.2 reported the qualitative cellular uptake performed on HSC-3 GFP/Luc M1 after 6 and 24 h of treatment with pDox NPs and doxorubicin. After 6 h of treatment, doxorubicin was visible only within the nucleus of the cells treated for 24 h with pDox NPs. In contrast, doxorubicin was present in the cells treated with the free form after 6 and 24 h of treatment. This finding confirmed the delayed entry of pDox NPs which also occurred in HSC-3 GFP/Luc M1 cell line.

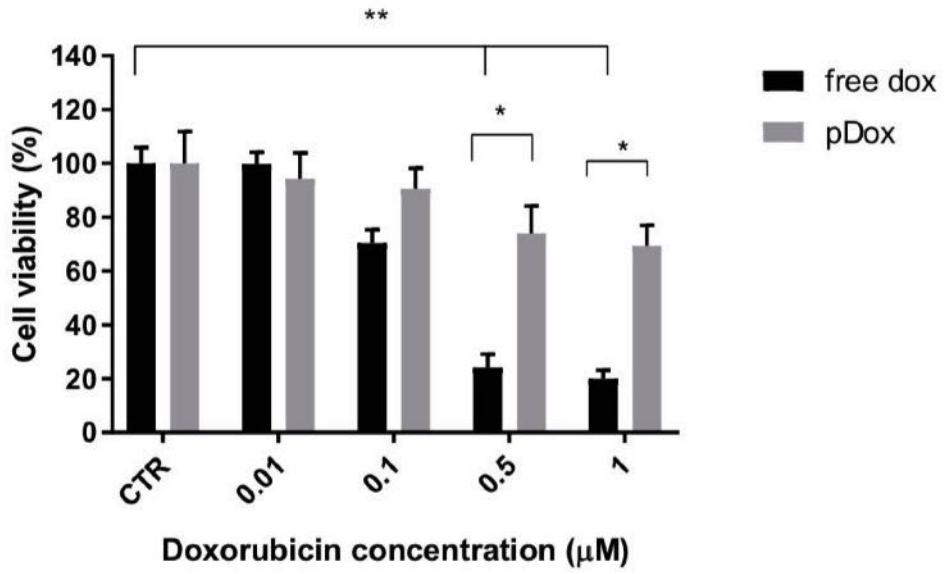

(a)

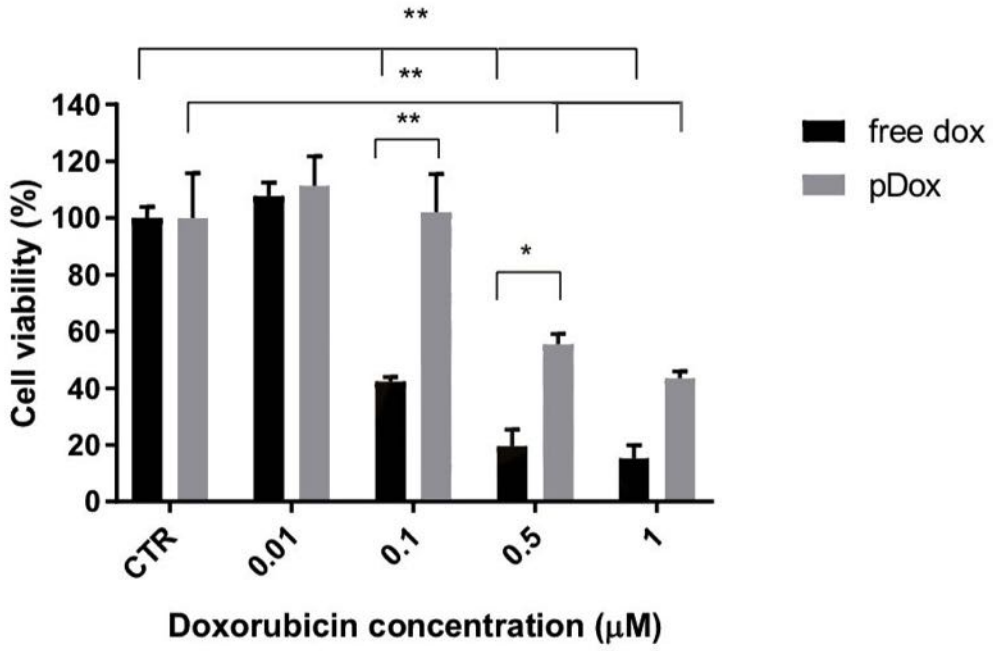

(b)

Figure 5.1: Viability assay results for HSC-3 M1 cell line after 72 (a) and 96 h (b) of treatment with different concentrations of pDox NPs and doxorubicin. Data are expressed as the mean ± SEM of three experiments. $^{*}P \leq 0.05$, ** P $\leq$0.01 by one-way ANOVA statistical analysis and the *post hoc* Tukey test.

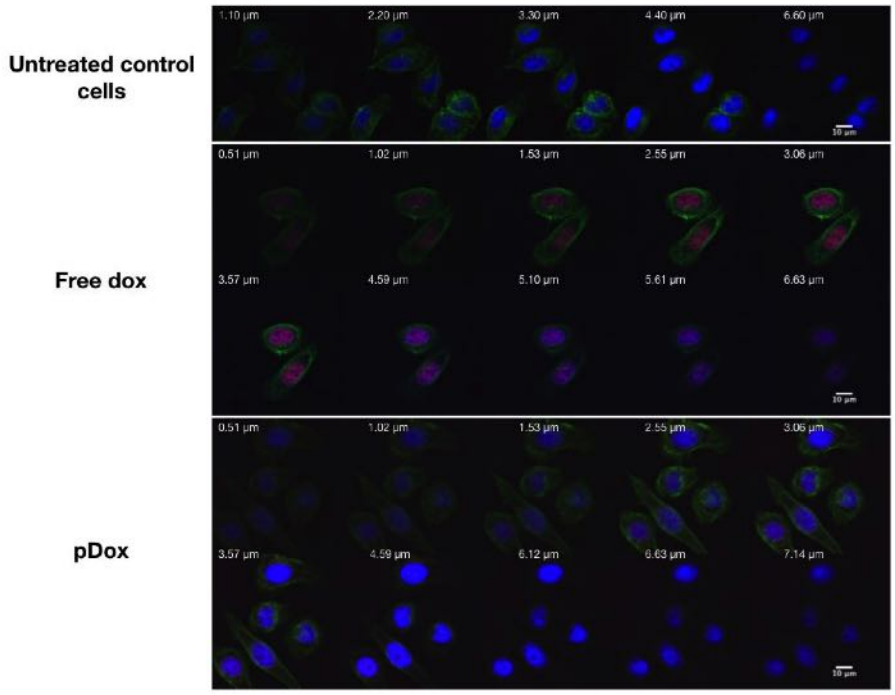

(a)

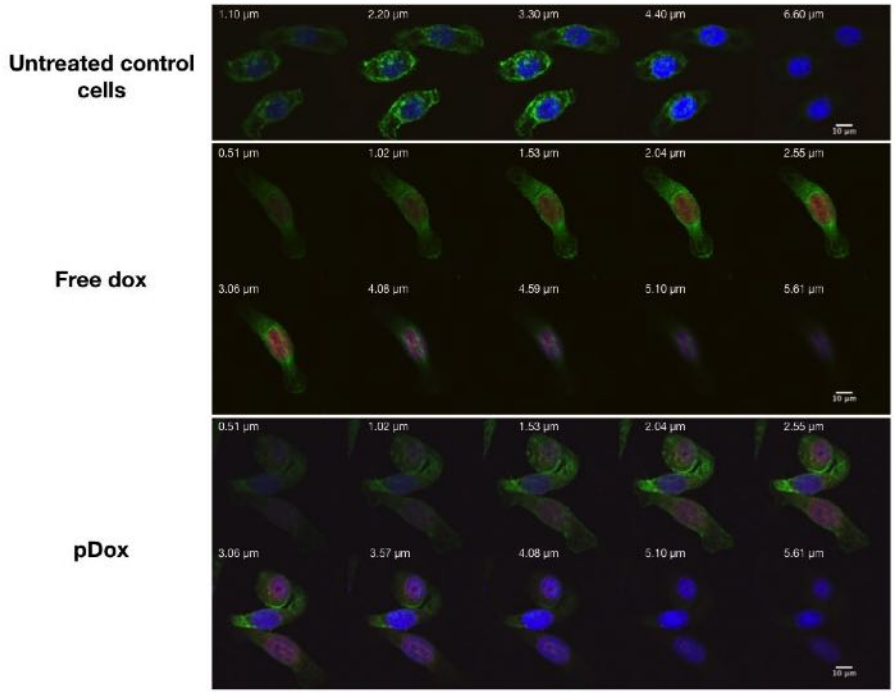

(b)

Figure 5.2: Z-stack confocal images after 6 (a) and 24 h (b) of treatment with doxorubicin and pDox NPs. DAPI (blue fluorescence) was used to stain the nuclei. Green fluorescence represents the cytoskeleton. Propidium iodide channel (red fluorescence) was used to detect doxorubicin in the free and polymeric form. The pink/purple fluorescence indicates a co-localization of PI and DAPI. This occurred in few cells after 24 h of treatment with pDox NPs. Scale bar represents 10 μm.

Chapter 6

Discussion and Conclusion

6.1 pDox NPs were significantly less cytotoxic than free doxorubicin on HSC-3 and HSC-3 M1 cells

A cell viability assay and a qualitative cellular uptake study of doxorubicin and pDox were performed on two cell lines: HSC-3 cells, which derives from a human metastatic tongue SCC and HSC-3 M1 cells, which were isolated from lung metastases developed in a mouse injected IV with HSC-3 cells. In both cell lines, doxorubicin was significantly more cytotoxic than pDox NPs. This may be owed to the fact that the cellular uptake of pDox was delayed compared to the free form of doxorubicin. Indeed, the co-localization of doxorubicin (PI) and DAPI occurred at later time points in the pDox NPs group than the free doxorubicin group (after 6 h in HSC-3 and after 24 h in HSC3 M1). The results obtained are in agreement with those obtained on the same compounds by Xu et al.[66]. For this study, the human triple-negative breast cancer cell lines MDA-MB-231 and MDA-MB-468 were used and doxorubicin was more cytotoxic than pDox at a concentration$\leq$ 1000 nM after 96 hours of treatment. In addition, the cellular entry of pDox was delayed also in the MDA-MB-231 cell line compared with the free form of doxorubicin[66]. Indeed, pDox co-localization with lysotracker reached a high level only 8 hours after the treatment.

In addition, other studies reported more cytotoxicity with doxorubicin or other drugs than with NPs encapsulating them[86, 106, 107]. Endo et al.[86] observed a 14-fold more potent cytotoxic effect of free cisplatin compared to 30 nm-sized-polymeric micelles loaded with cisplatin in HNSCC cell lines. Iafisco et al.[106] evaluated biomimetic apatite NPs loaded with doxorubicin and a targeting moiety on a human gastric carcinoma cell line. In this cell line, a minor toxicity and a slower cellular uptake of the NPs were observed than the free doxorubicin. The same findings were reported in a human breast cancer cell line treated with polymeric immuno-NPs loaded

with doxorubicin. In this study, the NPs loaded with doxorubicin presented also a slower nuclear transport inside the tumor cell than free doxorubicin, in addition to a slower internalization rate[107].

The minor cytotoxicity and the slow uptake of pDox in OSCC cell lines may represent the consequence of a slow intracellular transport and a slow release of the drug, as reported by other authors[86, 106, 107]. In addition, cell-type dependent differences may affect the cellular uptake of NPs. In a study by Poller et al.[108], the uptake and toxicity of iron oxide NPs in four breast cancer cell lines were influenced not only by the intrinsic properties of NPs but also by the cell type, which may exhibit a difference in the activity of the endocytic pathways[108]. To confirm this finding, further analysis of these pathways may be performed in our OSCC lines and the triple-negative breast cancer cell lines.

In conclusion, these findings on the OSCC cell lines do not represent a drawback of the compound, because it may be less toxic also *in vivo*, as reported by Endo et al.[86] in further experiments. In addition, the efficacy of pDox relies mostly on the targeting efficiency of iNPG[66]. The use of the platform iNPG-pDox seems promising as an anti-metastatic therapy for OSCC, also because pDox *in vitro* toxicity was not significantly different between HSC-3 M1 cells and the parental HSC-3 cell line.

6.2 The orthotopic model of OSCC metastasis reported a moderate prevalence of lung metastases

After demonstrating a significant cytotoxic effect of pDox on HSC-3 cells, an orthotopic model of metastatic tongue SCC was established using the same cell line. Fifty thousands of tumor cells were injected in the tongue of male and female athymic nude mice and the growth of the primary tumor and lung metastases was then evaluated by IVIS. Through this method, lung metastases were observed in one male mouse 30 days after the injection, while female mice did not present any visible lung metastasis. After the mice sacrifice, IVIS of the mice organs (tongue, mandibular lymph nodes, lungs, spleen, liver) revealed the presence of the primary tumor in 100% of male mice and 80% of female mice. Lymph node metastases were present in 80% and 67% in male and female mice respectively, while 60% of male mice presented lung metastases. In contrast, only 22% of female mice developed visible lung metastases by *ex vivo* IVIS. In addition, the histological evaluation of the lungs revealed some CK+ areas in the remaining two male mice, while cellular aggregations were observed also in the female mice, in which

metastases were not visible by *ex vivo* IVIS.

Interestingly, our orthotopic model reported a moderate-high prevalence of lung metastases. Other studies conducted with the same cell line did not obtain our same results[44, 45]. In such studies, a high number of cells (1.75-4x10^5) were injected in the tongue, in contrast with the minor number of cells injected in our study (5x10^4). In addition, the mice were sacrificed 3 weeks after the implantation[44, 45], while, in our study, the first signal of lung metastases was observed only 30 days after the injection. Therefore, the injection of a high number of cells may result in a faster growth of the primary tumor and the sacrifice of the animals before lung metastases become evident[44, 45].

Only a few studies[32, 50, 52] reported lung metastases in $\geq$ 40% of the mice. The orthotopic model of OSCC reported by Lou et al.[52] was a syngeneic one, while our model was a xenograft. Bais et al.[32] injected 0.5x10^6 of UM-SCC-2, a cell line derived from a recurrent tumor (T2N0M0) in the oral cavity. As stated in the 1.1.3, tumors with an aggressive behavior are also at high risk of local recurrence and present histological indicators of malignancy[7]. Finally, 83% of lung metastases were reported in an orthotopic model of OSCC with a human cell line isolated from lymph node metastases of the mice (USC-HN3-GFP-G1)[50].

Interestingly, the same procedure repeated three times with HSC-3 cell line did not result in an increase of the prevalence of lung metastases (10% vs 10% of the parental cells), in contrast to the lymph node metastases (90% vs 30% of the parental cells)[44]. Indeed, a different metastatic potential to lymph nodes and lungs was reported between the OSCC cell lines[49, 55]. Despite the metastatic potential to lungs was evaluated only by IV injection of OSCC cells, the study revealed a different gene expression between the metastatic and non-metastatic cell lines[55]. In particular, high levels of AP-1 family molecules such as c-Jun, FosL1 and JunB were found in metastatic cells compared to non-metastatic ones. A high expression of these genes and disruptive TP53 mutations were also observed in OSCC cell lines with the highest regional metastatic potential compared to less metastatic OSCC ones[49]. The presence of both lymph node and lung metastases in our study may be indicators of the high metastatic potential of the HSC-3 cell line, which deserves further investigation. In addition, these findings confirm the correlation between regional and distant metastases (DMs) observed in the clinical setting[23, 24]. However, the limitations of our study were the use of only one cell line (HSC-3) and the lack of a gene expression analysis of HSC-3 cells. To confirm and/or to discover novel genes involved in the metastatic process, an *in vitro* and *in vivo* evaluation of the gene expression

and the distant metastatic potential may be performed between HSC-3 cells and other OSCC cell lines.

6.3 Male and female athymic nude mice presented a different prevalence of lung metastases

Another interesting finding of the present study was the large difference observed in the prevalence of lung metastases between male and female mice. To date, our study is the first which established an orthotopic model of OSCC lung metastasis in both sexes of mice. Indeed, only male[44, 48] or female mice[32, 43, 45] were used in other studies. As stated in the 1.1.1, OSCC has a higher prevalence in men than in women, although this difference is now less marked[3]. Interestingly, a higher prevalence of DMs in men than in women was also reported by some clinical studies[26, 28, 109]. However, the sex of the patient was not reported as a significant indicator of DMs and it may be probably due to the higher frequency of OSCC in males than in females[28, 109, 110]. Nevertheless, further studies conducted on both sexes of mice may be needed in order to confirm this difference in the prevalence of OSCC lung metastases.

6.4 Lung metastases displayed similarities with the metastases reported in HNSCC patients

Finally, the localization of lung metastases in preferentially one lung (except for one male mouse, in which both lungs were involved) and the number of macrometastases (1-2) seem to be similar to the findings observed in the study by Osaki et al.[27]. In this study, the presence of DMs was evaluated in 636 HNSCC patients and lung metastases were found in 35 patients. One of the lungs was involved in the majority of the patients (right: 18\35; left: 5\35), while only 8 patients presented an involvement of both right and left lungs. In addition, 18 patients presented a single metastatic nodule in the lungs, while a diffuse tumor infiltration was reported only in 3 patients[27]. The similarity between the lung metastases obtained in our orthotopic model of OSCC and those reported in patients is encouraging. However, a limit of our study was the use of a xenograft model. Indeed, the nude mouse (nu/nu) lacks lymphocytes T, which are involved in the tumor progression[29, 31]. Despite this difference, further characterization of the mouse model and histological analyses of lung metastases from patients may be necessary to prove the correspondence between our orthotopic model and the OSCC in patients.

6.5 Lung metastases in the IV model of HSC-3 M1 cells presented a diffuse tumor cell infiltration

In addition to the orthotopic model of OSCC metastasis, another mouse model of OSCC lung metastasis was established through IV injection of OSCC cells. In order to acquire more significant results, the cell line HSC-3 M1 was used. This cell line was isolated from the lung metastases of a mouse, which was previously IV injected with HSC-3 cells. In this model, the lung prevalence was 60% (3\5) in female mice by *ex vivo* IVIS. In addition, the histological analysis of the remaining two mice revealed the presence of compact aggregations with atypic cells. To date, this is the first study in which a mouse model of metastatic OSCC was established using OSCC cells isolated from lung metastases. The prevalence of metastases observed in our study is similar to those reported in the other studies[55, 92]. Indeed, Hyakusoku reported a 90% of lung metastasis rate injecting $1x10^6$ of HSC-3 cells, while a 100% of lung metastasis rate was obtained injecting $2x10^6$ CAL-27 cells[92]. However, a pan-CK staining of the lungs was not performed to further confirm the metastatic nature of the cellular aggregations in the remaining 2 mice. In addition, the other studies assessed the presence of lung metastases only at the study endpoint by histology and pan-CK staining, while we used IVIS to track the growth of lung metastases during the experiment and histology was performed at the sacrifice of the animals. Indeed, *in vivo* imaging techniques have allowed researchers not only to follow the development of single metastatic nodule but also to follow the response of the therapy over time[29, 66]. The use of IVIS is emerging also in OSCC research. Therefore, few studies used *in vivo* imaging[32, 47].

Finally, several coalescent metastatic nodules and a diffuse tumor cell infiltration occurred in our model and other reported models of OSCC lung metastasis reported several metastatic nodules in the lungs[55, 92]. According to Osaki et al.[27], these findings were observed only in a few patients (3-6\35). Therefore, this mouse model may not be the best option to test future anti-metastatic therapies for OSCC.

6.6 Conclusions

Advanced-stage OSCC cases still present a 5-year survival rate of less than 50%, despite the multimodality therapy and the administration of molecular-targeted agents. In clinical studies, nanomedicine drugs proved to be effective in the treatment of some type of cancers, although a significant efficacy was not achieved against metastatic sites. Third-generation platforms and more elaborated ones have been developed to target more efficiently sites of metastases such as the lungs and liver. One of these platforms, iNPG-pDox

demonstrated to be effective against lung metastases in an orthotopic model of breast cancer.

From the results reported in the present dissertation, it can be concluded that pDox NPs were efficiently internalized and exerted their cytotoxic action also on HSC-3 M1 cells. Therefore, further *in vivo* studies may be necessary in order to evaluate the therapeutic efficacy of iNPG-pDox.

In vivo, lung metastases were successfully reproduced in two different mouse models of OSCC, with a moderate-high prevalence of lung metastases observed after the IV injection of HSC-3 M1 cells (non-orthotopic model) and the tongue injection of HSC-3 cells (orthotopic model). Interestingly, the lymph node and lung metastases obtained in the orthotopic model presented some features in common with the data reported on HNSCC patients. For these reasons, future efficacy studies of anti-metastatic therapies such as iNPG-pDox may offer a better contribution to clinical trials, if performed using an orthotopic model of lung metastasis OSCC. Moreover, an orthotopic model of OSCC lung metastasis may be a useful tool to investigate the mechanism of regional lymph node and lung metastases in OSCC.

Acknowledgments

I would like to express my sincere gratitude to my advisor Prof. Giovanni Lodi and my co-advisor Dr. Mauro Ferrari. I would like to thank Prof. Giovanni Lodi for his patient guidance, encouragement, suggestions, interest, and help in the planning of this research work and of this dissertation. I would like to thank Dr. Mauro Ferrari for giving me the opportunity to work at the Houston Methodist Research Institute and for providing funding, assistance, and suggestions for this research work. I would like to thank you for believing in me, for challenging me, for inspiring me to pursue great things and for your witness during the presentation of "Disarming Beauty". Your witness inspired me in doing the present research work for a greater aim.

I would like to thank Dr. Elena Varoni for her guidance, advice, and assistance in this research work and for her passion for research, which has been a great inspiration.

I would like to thank Dr. Haifa Shen and Dr. Kenji Yokoi for giving their time to discuss the present research work, for their questions, suggestions, and explanations. The advice given by Dr. Haifa Shen has been a great help in doing the present research work and in understanding the field of Nanomedicine.

I am grateful for the assistance and the welcome given by the Ph.D.Coordinator Elvin Blanco and the Lab Manager Maricela Ramirez. The meetings with Dr. Elvin Blanco have been a great help in doing the present research work and in the understanding that research includes success and failure.

I wish to acknowledge Guodong, Junhua, Giulia, Ali, Sara, Elvin Blanco, and Stefania for their contribution to this project. Advice and teachings provided by Giulia, Clara, Sara, Shreya, Stefania, and Carlotta were also greatly appreciated as well as the welcome they gave me in the lab. I would like to offer my special thanks to Giulia for her support and encouragement.

I would like to thank Prof. Massimo Del Fabbro for his guidance and for allowing me to do part of the Ph.D. in the US.

I would also like to extend my thanks to Dr. Ashley Holder, Dr. David Tinkey and the CMP staff of the Houston Methodist Research Institute.

I would like to express my gratitude to Lucia for making me think about the deep meaning of the present research work.

I would like to express my gratitude to Eveline, Marcia, Giulia M., Giulia S., David, Theresa, Paolo, Benedetto, Federico, Nino, Elisabetta, Tommaso, Marta, Ernesto, Margherita, Federica, Stefano, Sara, Tommaso, Chiara, Giulia, Chiara, Stefano Alberto, Alessandra, Linda, Cristina, and to my other Italian, American friends and professors for their presence and support.

Finally, I would like to thank my parents for their encouragement throughout the Ph.D.

Bibliography

[1] Hsu H-W, Wall NR, Hsueh C-T, Kim S, Ferris RL, Chen C-S et al. *Combination antiangiogenic therapy and radiation in head and neck cancers.* Oral Oncol 2014;50:19-26.

[2] Naruse T, Yanamoto S, Matsushita Y, Sakamoto Y, Morishita K, Ohba S et al. *Cetuximab for the treatment of locally advanced and recurrent/metastatic oral cancer: an investigation of distant metastasis.* Mol Clin Oncol 2016;5:246-252.

[3] Furness S, Glenny A-M, Worthington H V, Pavitt S, Oliver R, Clarkson JE et al. *Interventions for the treatment of oral cavity and oropharyngeal cancer: chemotherapy.* In: Furness S, editor. Cochrane Database Syst. Rev., Chichester, UK: John Wiley & Sons, Ltd; 2011, p. CD006386.

[4] Chi AC, Day TA, Neville BW. *Oral cavity and oropharyngeal squamous cell carcinoma: an update.* CA Cancer J Clin 2015;65:401-21.

[5] Iriti M, Varoni E. *Chemopreventive potential of flavonoids in oral squamous cell carcinoma in human studies.* Nutrients 2013;5:2564-76.

[6] Chan KK, Glenny AM, Weldon JC, Furness S, Worthington HV, Wakeford H. *Interventions for the treatment of oral and oropharyngeal cancers: targeted therapy and immunotherapy.* Cochrane Database Syst Rev. 2015;12:CD010341.

[7] Sutton D, Brown J, Rogers S, Vaughan E, Woolgar J. *The prognostic implications of the surgical margin in oral squamous cell carcinoma.* Int J Oral Maxillofac Surg. 2003;32:304.

[8] De Visscher SA, Melchers LJ, Dijkstra PU, Karakullukcu B, Tan IB, Hopper C et al. *mTHPC-mediated Photodynamic Therapy of Early Stage Oral Squamous Cell Carcinoma: A Comparison to Surgical Treatment.* Ann Surg Oncol. 2013;20:3076-82.

[9] Adelstein D, Gillison ML, Pfister DG, Spencer S, Adkins D, Brizel DM et al. *NCCN Guidelines Insights: Head and Neck Cancers, Version 2.2017.* J Natl Compr Canc Netw. 2017;15:761770.

[10] Wang Z-Q, Liu K, Huo Z-J, Li X-C, Wang M, Liu P et al. *A cell-targeted chemotherapeutic nanomedicine strategy for oral squamous cell carcinoma therapy.* J Nanobiotechnol 2015;13:63.

[11] Zhao H, Feng H, Liu D, Liu J, Ji N, Chen F et al. *Self-assembling monomeric nucleoside molecular nanoparticles loaded with 5-FU enhancing therapeutic efficacy against oral cancer.* ACS Nano 2015;9:9638-51.

[12] de Oliveira MG, Ramalho LMP, Gaião L, Pozza DH, de Mello RA. *Retinoblastoma and p53 protein expression in pre-malignant oral lesions and oral squamous cell carcinoma.* Mol Med Rep 2012;6:163-6.

[13] Wang C, Liu XQ, Hou JS, Wang JN, Huang HZ. *Molecular mechanisms of chemoresistance in oral cancer.* Chin J Dent Res 2016;19:25-33.

[14] Specenier P, Vermorken JB. *The role of taxanes and targeted therapies in locally advanced head and neck cancer.* Curr Opin Oncol. 2007;19:195-201.

[15] Blanco E, Shen H, Ferrari M. *Principles of nanoparticle design for overcoming biological barriers to drug delivery.* Nat Biotechnol 2015;33:941-51.

[16] Wutzl A, Ploder O, Kermer C, Millesi W, Ewers R, Klug C. *Mortality and causes of death after multimodality treatment for advanced oral and oropharyngeal cancer.* J Oral Maxillofac Surg. 2007;65:255-60.

[17] Baxi SS, Pinheiro LC, Patil SM, Pfister DG, Oeffinger KC, Elkin EB. *Causes of death in long-term survivors of head and neck cancer.* Cancer. 2014;120:1507-13.

[18] Shen W, Sakamoto N, Yang L. *Cancer-specific mortality and competing mortality in patients with head and neck squamous cell carcinoma: a competing risk analysis.* Ann Surg Oncol. 2015;22:264-71.

[19] Kirita T, Ohgi K, Shimooka H, Yamanaka Y, Tatebayashi S, Yamamoto K et al. *Preoperative concurrent chemoradiotherapy plus radical surgery for advanced squamous cell carcinoma of the oral cavity: an analysis of long-term results.*Oral Oncol. 1999;35:597-606.

[20] Bernier J, Domenge C, Ozsahin M, Matuszewska K, Lefèbvre JL, Greiner RH et al. *Postoperative irradiation with or without concomitant chemotherapy for locally advanced head and neck cancer.* N Engl J Med. 2004;350:1945-52.

[21] Kowalski LP, Carvalho AL, Martins Priante AV, Magrin J. *Predictive factors for distant metastasis from oral and oropharyngeal squamous cell carcinoma.* Oral Oncol. 2005;41:534-41.

[22] Noguti J, De Moura CF, De Jesus GP, Da Silva VH, Hossaka TA, Oshima CT et al. *Metastasis from oral cancer: an overview.* Cancer Genomics Proteomics. 2012;9:329-35.

[23] Hasegawa T, Shibuya Y, Takeda D, Iwata E, Saito I, Kakei Y et al. *Prognosis of oral squamous cell carcinoma patients with level IV/V metastasis: An observational study.* J Craniomaxillofac Surg. 2017;45:145-149.

[24] Steeg PS. *Targeting metastasis.*Nat Rev Cancer. 2016;16:201-18.

[25] Sugiura T, Inoue Y, Matsuki R, Ishii K, Takahashi M, Abe M et al. *VEGF-C and VEGF-D expression is correlated with lymphatic vessel density and lymph node metastasis in oral squamous cell carcinoma: implications for use as a prognostic marker.* Int J Oncol 2009;34:673-80.

[26] Irani S. *Distant metastasis from oral cancer: A review and molecular biologic aspects.* J Int Soc Prev Community Dent. 2016;6:265-71.

[27] Osaki T, Yoneda K, Yamamoto T, Kimura T, Matuoka H, Sakai H et al. *Clinical investigation on pulmonary metastasis of head and neck carcinomas.* (abstract only) Oncology. 2000;59:196-203.

[28] Takahashi M, Aoki T, Nakamura N, Carreras J, Kajiwara H, Kumaki N et al. *Clinicopathological analysis of 502 patients with oral squamous cell carcinoma with special interest to distant metastasis.* Tokai J Exp Clin Med 2014;39:178-85.

[29] Saxena M, Christofori G. *Rebuilding cancer metastasis in the mouse.* Mol Oncol. 2013;7:283-96.

[30] Laoui D, Van Overmeire E, De Baetselier P, Van Ginderachter JA, Raes G. *Functional Relationship between Tumor-Associated Macrophages and Macrophage Colony-Stimulating Factor as Contributors to Cancer Progression.* Front Immunol. 2014;5:489.

[31] Mognetti B, Di Carlo F, Berta GN. *Animal models in oral cancer research.* Oral Oncol 2006;42:448-60.

[32] Bais MV, Kukuruzinska M, Trackman PC. *Orthotopic non-metastatic and metastatic oral cancer mouse models.* Oral Oncol 2015;51:476-82.

[33] Vermeer DW, Coppock JD, Zeng E, Lee KM, Spanos WC, Onken MD et al. *Metastatic model of HPV+ oropharyngeal squamous cell carcinoma demonstrates heterogeneity in tumor metastasis.* Oncotarget. 2016;7:24194-207.

[34] Coppock JD, Vermeer PD, Vermeer DW, Lee KM, Miskimins WK, Spanos WC et al. *mTOR inhibition as an adjuvant therapy in a metastatic model of HPV+ HNSCC.* Oncotarget. 2016;7:24228-41.

[35] Cho JK, Hyun SH, Choi N, Kim MJ, Padera TP, Choi JY et al. *Significance of lymph node metastasis in cancer dissemination of head and neck cancer.* Transl Oncol. 2015;8:119-25.

[36] Patel V, Marsh CA, Dorsam RT, Mikelis CM, Masedunskas A, Amornphimoltham P et al. *Decreased lymphangiogenesis and lymph node metastasis by mTOR inhibition in head and neck cancer.* Cancer Res. 2011;71:7103-12.

[37] Atallah I, Milet C, Quatre R, Henry M, Reyt E, Coll JL et al. *Role of near-infrared fluorescence imaging in the resection of metastatic lymph nodes in an optimized orthotopic animal model of HNSCC.* Eur Ann Otorhinolaryngol Head Neck Dis. 2015;132:337-42.

[38] Atallah I, Milet C, Henry M, Josserand V, Reyt E, Coll JL et al. *Near-infrared fluorescence imaging-guided surgery improves recurrence-free survival rate in novel orthotopic animal model of head and neck squamous cell carcinoma.*Head Neck. 2016;38 Suppl 1:E246-55.

[39] Shigeta T, Umeda M, Komatsubara H, Komori T . *Lymph node and pulmonary metastases after transplantation of oral squamous cell carcinoma cell line (HSC-3) into the subcutaneous tissue of nude mouse: detection of metastases by genetic methods using beta-globin and mutant p53 genes.* Oral Surg Oral Med Oral Pathol Oral Radiol Endod 2008;105:486-90.

[40] Kawashiri S, Kumagai S, Kojima K, Harada H, Nakagawa K, Yamamoto E. *Reproduction of occult metastasis of head and neck cancer in nude mice.* Clin Exp Metastasis. 1999;17:277-82.

[41] Noguchi N, Kawashiri S, Tanaka A, Kato K, Nakaya H. *Effects of fibroblast growth inhibitor on proliferation and metastasis of oral squamous cell carcinoma.* Oral Oncol 2003;39:240-7.

[42] Kawashiri S, Noguchi N, Tanaka A, Nakaya H, Kato K, Yamamoto E. *Inhibitory effect of neoadjuvant chemotherapy on metastasis of oral squamous cell carcinoma in a mouse model.* Oral Oncol.2009;45:794-7.

[43] Shirako Y, Taya Y, Sato K, Chiba T, Imai K, Shimazu Y et al. *Heterogeneous tumor stromal microenvironments of oral squamous cell carcinoma cells in tongue and nodal metastatic lesions in a xenograft mouse model.* J Oral Pathol Med. 2015;44:656-68.

[44] Matsui T, Ota T, Ueda Y, Tanino M, Odashima S. *Isolation of a highly metastatic cell line to lymph node in human oral squamous cell carcinoma by orthotopic implantation in nude mice.* Oral Oncol.1998;34:253-6.

[45] Umeda M, Yokoo S, Komori T, Nishimatsu N, Shibuya Y, Fujioka M. *Experimental model of invasion and metastasis by orthotopic transplantation of oral squamous and adenoid cystic carcinomas into the tongue of nude mice.* Br J Oral Maxillofac Surg. 39:376-80.

[46] Kamide D, Yamashita T, Araki K, Tomifuji M, Tanaka Y, Tanaka S et al. *Selective activator protein-1 inhibitor T-5224 prevents lymph node metastasis in an oral cancer model.* Cancer Sci. 2016;107:666-73.

[47] Braks JA, Spiegelberg L, Koljenovic S, Ridwan Y, Keereweer S, Kanaar R et al. *Optical Imaging of Tumor Response to Hyperbaric Oxygen Treatment and Irradiation in an Orthotopic Mouse Model of Head and Neck Squamous Cell Carcinoma.* Mol Imaging Biol. 2015;17:633-42.

[48] Myers JN, Holsinger FC, Jasser SA, Bekele BN, Fidler IJ. *An orthotopic nude mouse model of oral tongue squamous cell carcinoma.* Clin Cancer Res. 2002;8:293-8.

[49] Sano D, Xie TX, Ow TJ, Zhao M, Pickering CR, Zhou G et al. *Disruptive TP53 mutation is associated with aggressive disease characteristics in an orthotopic murine model of oral tongue cancer.* Clin. Cancer Res. 2011;17:6658-70.

[50] Masood R, Hochstim C, Cervenka B, Zu S, Baniwal SK, Patel V. *A novel orthotopic mouse model of head and neck cancer and lymph node metastasis.* Oncogenesis. 2013;2:e68.

[51] Wu TF, Chen L, Bu LL, Gao J, Zhang WF, Jia J. *CD44+ cancer cell-induced metastasis: A feasible neck metastasis model.* Eur J Pharm Sci. 2017;101:243-250.

[52] Lou E, Kellman RM, Hutchison R, Shillitoe EJ. *Clinical and pathological features of the murine AT-84 orthotopic model of oral cancer.* Oral Dis. 2003;9:305-12.

[53] Paolini F, Massa S, Manni I, Franconi R, Venuti A. *Immunotherapy in new pre-clinical models of HPV-associated oral cancers.* Hum Vaccin Immunother. 2013;9:534-43.

[54] Vigneswaran N, Wu J, Song A, Annapragada A, Zacharias W. *Hypoxia-induced autophagic response is associated with aggressive phenotype and elevated incidence of metastasis in orthotopic immunocompetent murine*

models of head and neck squamous cell carcinomas (HNSCC). Exp Mol Pathol. 2011;90:215-25.

[55] Hyakusoku H, Sano D, Takahashi H, Hatano T, Isono Y, Shimada S et al. *JunB promotes cell invasion, migration and distant metastasis of head and neck squamous cell carcinoma.* J Exp Clin Cancer Res. 2016;35:6.

[56] Hier MP, Black MJ, Shenouda G, Sadeghi N, Karp SE. *A murine model for the immunotherapy of head and neck squamous cell carcinoma.* Laryngoscope. 1995;105:1077-80.

[57] Li HM, Yang JG, Liu ZJ, Wang WM, Yu ZL, Ren JG et al. *Blockage of glycolysis by targeting PFKFB3 suppresses tumor growth and metastasis in head and neck squamous cell carcinoma.* J Exp Clin Cancer Res. 2017;36:7.

[58] Sano D, Myers JN. *Xenograft models of head and neck cancers.*Head Neck Oncol. 2009;1:32.

[59] Marcazzan S, Varoni EM, Blanco E, Lodi G, Ferrari M. *Nanomedicine, an emerging therapeutic strategy for oral cancer therapy.* Oral Oncol. 2018;76:1-7.

[60] Godin B, Tasciotti E, Liu X, Serda RE, Ferrari M. *Multistage nanovectors: from concept to novel imaging contrast agents and therapeutics.* Acc Chem Res 2011;44:979-89.

[61] Anselmo AC, Mitragotri S. *Nanoparticles in the clinic.* Bioeng Transl Med 2016;1:10-29.

[62] Wicki A, Witzigmann D, Balasubramanian V, Huwyler J. *Nanomedicine in cancer therapy: challenges, opportunities, and clinical applications.* J Control Release 2015;200:138-57.

[63] Caponigro F, Comella P, Budillon A, Bryce J, Avallone A, De Rosa V et al. *Phase I study of Caelyx (doxorubicin HCL, pegylated liposomal) in recurrent or metastatic head and neck cancer.* Ann Oncol Off J Eur Soc Med Oncol 2000;11:339-42.

[64] Prabhakar U, Maeda H, Jain RK, Sevick-Muraca EM, Zamboni W, Farokhzad OC et al. *Challenges and key considerations of the enhanced permeability and retention effect for nanomedicine drug delivery in oncology.* Cancer Res 2013;73:2412-7.

[65] Jain S, Hirst DG, O' Sullivan JM. *Gold nanoparticles as novel agents for cancer therapy.* Br J Radiol 2012;85:101-13.

[66] Xu R, Zhang G, Mai J, Deng X, Segura-Ibarra V, Wu S et al. *An injectable nanoparticle generator enhances delivery of cancer therapeutics.* Nat Biotechnol 2016;34:414-8.

[67] Wolfram J, Shen H, Ferrari M. *Multistage vector (MSV) therapeutics.* J Control Release. 2015;219:406-415.

[68] Mi Y, Wolfram J, Mu C, Liu X, Blanco E, Shen H et al. *Enzyme-responsive multi- stage vector for drug delivery to tumor tissue.* Pharmacol Res 2016;113:92-9.

[69] Mi Y, Mu C, Wolfram J, Deng Z, Hu TY, Liu X et al. *A micro/nano composite for combination treatment of melanoma lung metastasis.* Adv Healthc Mater 2016;5:936-46.

[70] Harrington KJ, Lewanski C, Northcote AD, Whittaker J, Peters AM, Vile RGet al. *Phase II study of pegylated liposomal doxorubicin (Caelyx) as induction chemotherapy for patients with squamous cell cancer of the head and neck.*Eur J Cancer 2001;37:2015-22.

[71] Faivre S, Alsabe H, Djafari L, Janot F, Julieron M, Domenge C et al. *Locoregional effects of pegylated liposomal doxorubicin (Caelyx) in irradiated area: a phase I-II study in patients with recurrent squamous cell carcinoma of the head and neck.* Eur J Cancer 2004;40:1517-21.

[72] Fountzilas G, Papakostas P, Dafni U, Makatsoris T, Karina M, Kalogera-Fountzila A et al. *Paclitaxel and gemcitabine vs. paclitaxel and pegylated liposomal doxorubicin in advanced non-nasopharyngeal head and neck cancer. An efficacy and cost analysis randomized study conducted by the Hellenic Cooperative Oncology Group.* Ann Oncol. 2006;17:1560-7.

[73] Rosenthal DI, Yom SS, Liu L, Machtay M, Algazy K, Weber RS et al. *A phase I study of SPI-077 (Stealth liposomal cisplatin) concurrent with radiation therapy for locally advanced head and neck cancer.* Invest New Drugs. 2002;20:343-9.

[74] Jehn CF, Boulikas T, Kourvetaris A, Kofla G, Possinger K, Lüftner D. *First safety and response results of a randomized phase III study with liposomal platin in the treatment of advanced squamous cell carcinoma of the head and neck (SCCHN).* Anticancer Res. 2008;28:3961-4.

[75] Jehn CF, Boulikas T, Kourvetaris A, Possinger K, Lüftner D. *Pharmacokinetics of liposomal cisplatin (lipoplatin) in combination with 5-FU in patients with advanced head and neck cancer: first results of a phase III study.* Anticancer Res. 2007;27:471-5.

[76] Damascelli B, Cantù G, Mattavelli F, Tamplenizza P, Bidoli P, Leo E et al. *Intraarterial chemotherapy with polyoxyethylated castor oil free paclitaxel, incorporated in albumin nanoparticles (ABI-007): Phase I study of patients with squamous cell carcinoma of the head and neck and anal canal: preliminary evidence of clinical activity.* Cancer. 2001;92:2592-602.

[77] Damascelli B, Patelli GL, Lanocita R, Di Tolla G, Frigerio LF, Marchianò A, et al. *A novel intraarterial chemotherapy using paclitaxel in albumin nanoparticles to treat advanced squamous cell carcinoma of the tongue: preliminary findings.* AJR Am J Roentgenol. 2003;181:253-60.

[78] Strieth S, Dunau C, Michaelis U, Jäger L, Gellrich D, Wollenberg B et al. *Phase I/II clinical study on safety and antivascular effects of paclitaxel encapsulated in cationic liposomes for targeted therapy in advanced head and neck cancer.* Head Neck. 2014;36:976-84.

[79] Adkins D, Ley J, Trinkaus K, Thorstad W, Lewis J Jr, Wildes T et al. *A phase 2 trial of induction nab-paclitaxel and cetuximab given with cisplatin and 5-fluorouracil followed by concurrent cisplatin and radiation for locally advanced squamous cell carcinoma of the head and neck.* Cancer. 2013;119:766-73.

[80] Mohan A, Narayanan S, Balasubramanian G, Sethuraman S, Krishnan UM. *Dual drug loaded nanoliposomal chemotherapy: a promising strategy for treatment of head and neck squamous cell carcinoma.* Eur J Pharm Biopharm 2016;99:73-83.

[81] Abbasi MM, Jahanban-Esfahlan R, Monfaredan A, Seidi K, Hamishehkar H, Khiavi MM. *Oral and IV dosages of doxorubicin-methotrexate loaded- nanoparticles inhibit progression of oral cancer by down- regulation of matrix Methaloproteinase 2 ex- pression in vivo.* Asian Pac J Cancer Prev 2014;15:10705-11.

[82] Abbasi MM, Monfaredan A, Hamishehkar H, Jahanban-Esfahlan R. *New formulated DOX-MTX-loaded nanoparticles down- regulate HER2 gene expression and improve the clinical outcome in OSCCs model in rat: the effect of IV and oral modalities.* Asian Pac J Cancer Prev 2014;15:9355-60.

[83] Abbasi MM, Monfaredan A, Hamishehkar H, Seidi K, Jahanban- Esfahlan R. *Novel DOX-MTX nanoparticles improve oral SCC clinical outcome by down regulation of lymph dissemination factor VEGF-C expression in vivo: oral and IV modalities.* Asian Pac J Cancer Prev 2014;15:6227-32.

[84] Saiyin W, Wang D, Li L, Zhu L, Liu B, Sheng L et al. *Sequential release of autophagy inhibitor and chemotherapeutic drug with polymeric delivery system for oral squamous cell carcinoma therapy.* Mol Pharm 2014;11:1662-75.

[85] Wang Z-Q, Liu K, Huo Z-J, Li X-C, Wang M, Liu P et al. *A cell-targeted chemotherapeutic nanomedicine strategy for oral squamous cell carcinoma therapy.* J Nanobiotechnol 2015;13:63.

[86] Endo K, Ueno T, Kondo S, Wakisaka N, Murono S, Ito M et al. *Tumor-targeted chemotherapy with the nanopolymer-based drug NC-6004 for oral squamous cell carcinoma.* Cancer Sci 2013;104:369-74.

[87] Zhao H, Feng H, Liu D, Liu J, Ji N, Chen F et al. *Self-assembling monomeric nucleoside molecular nanoparticles loaded with 5-FU enhancing therapeutic efficacy against oral cancer.* ACS Nano 2015;9:9638-51.

[88] Afifi MM, El Sheikh SM, Abdelsalam MM, Ramadan H, Omar TA, El Tantawi M et al. *Therapeutic efficacy of plasmonic photothermal nanoparticles in hamster buccal pouch carcinoma.* Oral Surg Oral Med Oral Pathol Oral Radiol 2013;115:743-51.

[89] Melancon MP, Lu W, Zhong M, Zhou M, Liang G, Elliott AM, et al. *Targeted multifunctional gold-based nanoshells for magnetic resonance-guided laser ablation of head and neck cancer.* Biomaterials 2011;32:7600-8.

[90] Hackenberg S, Scherzed A, Harnisch W, Froelich K, Ginzkey C, Koehler C et al. *Antitumor activity of photo-stimulated zinc oxide nanoparticles combined with paclitaxel or cisplatin in HNSCC cell lines.* J Photochem Photobiol B Biol 2012;114:87-93.

[91] Lin M, Wang D, Liu S, Huang T, Sun B, Cui Y, et al. *Cupreous complex-loaded chitosan nanoparticles for photothermal therapy and chemotherapy of oral epithelial carcinoma.* ACS Appl Mater Interfaces 2015;7:20801-12.

[92] Li P, Zhou G, Zhu X, Li G, Yan P, Shen L, et al. *Photodynamic therapy with hyperbranched poly(ether-ester) chlorin(e6) nanoparticles on human tongue carcinoma CAL-27 cells.* Photodiag Photodyn Ther 2012;9:76-82.

[93] Lucky SS, Idris NM, Huang K, Kim J, Li Z, Thong PSP et al. *In vivo biocompatibility, biodistribution and therapeutic efficiency of titania coated upconversion nano- particles for photodynamic therapy of solid oral cancers.* Theranostics 2016;6:1844-65.

[94] Moosavi Nejad S, Takahashi H, Hosseini H, Watanabe A, Endo H, Narihira K et al. *Acute effects of sono-activated photocatalytic titanium dioxide nanoparticles on oral squamous cell carcinoma.* Ultrason Sonochem 2016;32:95-101.

[95] Satapathy SR, Siddharth S, Das D, Nayak A, Kundu CN. *Enhancement of cytotoxicity and inhibition of angiogenesis in oral cancer stem cells by a hybrid nanoparticle of bioactive quinacrine and silver: implication of base excision repair cascade.* Mol Pharm 2015;12:4011-25.

[96] Miao L, Liu C, Ge J, Yang W, Liu J, Sun W, et al. *Antitumor effect of TRAIL on oral squamous cell carcinoma using magnetic nanoparticle-mediated gene expression.* Cell Biochem Biophys 2014;69:663-72.

[97] Lecaros RLG, Huang L, Lee T-C, Hsu Y-C. *Nanoparticle delivered VEGF-A siRNA enhances photodynamic therapy for head and neck cancer treatment.* Mol Ther 2016;24:106-16.

[98] Chen W-H, Lecaros RLG, Tseng Y-C, Huang L, Hsu Y-C. *Nanoparticle delivery of HIF1α siRNA combined with photodynamic therapy as a potential treatment strategy for head-and-neck cancer.* Cancer Lett 2015;359:65-74.

[99] Chang P-Y, Peng S-F, Lee C-Y, Lu C-C, Tsai S-C, Shieh T-M, et al. *Curcumin-loaded nanoparticles induce apoptotic cell death through regulation of the function of MDR1 and reactive oxygen species in cisplatin-resistant CAR human oral cancer cells.* Int J Oncol 2013;43:1141-50.

[100] Singh SP, Sharma M, Gupta PK. *Enhancement of phototoxicity of curcumin in human oral cancer cells using silica nanoparticles as delivery vehicle.* Lasers Med Sci 2014;29:645-52.

[101] Lee M-H, Lin JL, Thomas H-W, Chen C-M, Shen W-J, Yang M-H et al. *In vitro suppression of oral squamous cell carcinoma growth by ultrasound-mediated delivery of curcumin microemulsions.* Int J Nanomed 2012;7:941.

[102] Mazzarino L, Loch-Neckel G, Bubniak LDS, Mazzucco S, Santos-Silva MC, Borsali R et al. *Curcumin-loaded chitosan-coated nanoparticles as a new approach for the local treatment of oral cavity cancer.* J Nanosci Nanotechnol 2015;15:781-91.

[103] Gavin A, Pham JT, Wang D, Brownlow B, Elbayoumi TA. *Layered nanoemulsions as mucoadhesive buccal systems for controlled delivery of oral cancer therapeutics.* Int J Nanomed 2015;10:1569-84.

[104] Sulfikkarali N, Krishnakumar N, Manoharan S, Nirmal RM. *Chemopreventive efficacy of naringenin-loaded nanoparticles in 7,12-dimethylbenz(a)anthracene induced experimental oral carcinogenesis.* Pathol Oncol Res 2013;19:287-96.

[105] Li H, Shi L, Wei J, Zhang C, Zhou Z, Wu L et al. *Cellular uptake and anticancer activity of salvianolic acid B phospholipid complex loaded nanoparticles in head and neck cancer and precancer cells.* Colloids Surf B Biointerfaces 2016;147:65-72.

[106] Iafisco M, Delgado-Lopez JM, Varoni EM, Tampieri A, Rimondini L, Gomez-Morales J et al. *Cell surface receptor targeted biomimetic apatite nanocrystals for cancer.* Small 2013;9:3834-44.

[107] Shi M, Ho K, Keating A and Shoichet M. *Doxorubicin-Conjugated Immuno-Nanoparticles for Intracellular Anticancer Drug Delivery.* Advanced Functional Materials 2009;19:1689-1696.

[108] Poller JM, Zaloga J, Schreiber E, Unterweger H, Janko C, Radon P et al. *Selection of potential iron oxide nanoparticles for breast cancer treatment based on in vitro cytotoxicity and cellular uptake.* Int J Nanomedicine. 2017;12:3207-3220.

[109] Shingaki S, Suzuki I, Kobayashi T, Nakajima T. *Predicting factors for distant metastases in head and neck carcinomas: an analysis of 103 patients with locoregional control.* J Oral Maxillofac Surg. 1996;54:853-7.

[110] Gumusay O, Ozet A, Buyukberber S, Baykara M, Coskun U, Cetin B et al. *Factors predicting the development of distant metastases in patients with head and neck squamous cell carcinoma: A retrospective study from a single centre.* J BUON. 2015;20:521-6.

[111] https://www.nature.com/subjects/nanoparticles (last visit: 20 September 2018)

[112] https://clinicaltrials.gov (last visit: 22 September 2018)

[113] https://www.nccn.org (last visit: 20 November 2018)

[114] https://cancerstaging.org (last visit: 20 November 2018)